

This document downloaded from  
vulcanhammer.net vulcanhammer.info  
Chet Aero Marine



Don't forget to visit our companion site  
<http://www.vulcanhammer.org>

Use subject to the terms and conditions of the respective websites.

SCHOOL OF  
CIVIL ENGINEERING

INDIANA

DEPARTMENT OF TRANSPORTATION

JOINT HIGHWAY RESEARCH PROJECT  
JHRP-91/9  
Final Report

DRIVING OF THIN SHELLS FOR STEEL  
ENCASED CONCRETE PILES

Girish Agrawal  
Jean-Lou A. Chameau



PURDUE UNIVERSITY



**JOINT HIGHWAY RESEARCH PROJECT  
JHRP-91/9  
Final Report**

**DRIVING OF THIN SHELLS FOR STEEL  
ENCASED CONCRETE PILES**

**Girish Agrawal  
Jean-Lou A. Chameau**

## Final Report

### DRIVING OF THIN SHELLS FOR STEEL ENCASED CONCRETE PILES

To: Vincent P. Drnevich  
Joint Highway Research Project

March 6, 1991

From: Girish Agrawal

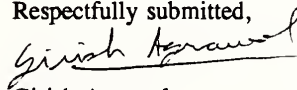
Project: C-36-36S  
File: 6-14-19

Attached is the final report of the INDOT study entitled "Driving of Thin Shells for Steel Encased Concrete Piles", prepared by G. Agrawal and J.L. Chameau. This report outlines a set of procedures to enable INDOT engineers to make use of available dynamic analysis technology to estimate stresses developed, and mitigate driving difficulties, during driving of thin shells used for cast-in-situ concrete piles that support bridge approaches on Indiana highways.

The purpose of this study was to identify the causes for the driving difficulties and consequent damage to shells, and suggest appropriate changes in the design, construction and contract specification procedures to improve identification and correction of problems at the earliest possible stage. Chapter 1 of the report discusses the motivation for the study and presents the general background of the problem. Chapter 2 outlines, and contains a detailed example of, the procedures followed in the analysis. Chapter 3 contains examples of the procedures outlined in Chapter 2 as applied to data from three actual highway projects in Indiana where thin shells were driven. Chapter 4 contains conclusions and recommendations, including general guidelines for modifying specification requirements as well as some suggestions for further work involving dynamic measurements during driving. A set of appendices contains technical information, references and copies of published charts and graphs used for analysis in the report.

The draft final report for this project, dated March 6, 1991, was approved as is and hence no changes have been made in preparing the body of the final report. This final report is presented for approval by INDOT.

Respectfully submitted,

  
Girish Agrawal

cc:	A.G. Altschaeffl	G. Henneke	P. Owens
	J.L. Chameau	K.R. Hoover	B.K. Partridge
	W.F. Chen	C.W. Letts	C.F. Scholer
	W.L. Dolch	C.W. Lovell	G.B. Shoener
	A.R. Fendrick	D.W. Lucas	K.C. Sinha
	J.D. Fricker	J. McLaughlin	C.A. Venable
	D.W. Halpin	D.C. Nelson	T.D. White

**Final Report**

**DRIVING OF THIN SHELLS FOR STEEL ENCASED CONCRETE PILES**

by

**Girish Agrawal  
and  
Jean-Lou A. Chameau**

**Joint Highway Research Project**

**Project No.: C-36-36S  
File No.: 6-14-19**

**Prepared for an Investigation**

**Conducted by the**

**Joint Highway Research Project  
Engineering Experiment Station  
Purdue University**

**in cooperation with the**

**Indiana Department of Transportation**

**Purdue University  
West Lafayette, Indiana 47907**

**March 6, 1991**



1. Report No. <b>JHRP-91/9</b>		2. Government Accession No.		3. Recipient's Catalog No.	
4. Title and Subtitle  <b>Driving of Thin Shells for Steel Encased Concrete Piles</b>				5. Report Date <b>March 6, 1991</b>	
				6. Performing Organization Code	
7. Author(s)  <b>G. Agrawal and J.L. Chameau</b>				8. Performing Organization Report No.  <b>JHRP-91/9</b>	
9. Performing Organization Name and Address <b>Joint Highway Research Project Civil Engineering Building Purdue University West Lafayette, IN 47907</b>				10. Work Unit No.	
				11. Contract or Grant No.	
12. Sponsoring Agency Name and Address <b>Indiana Department of Transportation State Office Building 100 North Senate Avenue Indianapolis, IN 46204</b>				13. Type of Report and Period Covered  <b>Final Report</b>	
				14. Sponsoring Agency Code	
15. Supplementary Notes					
16. Abstract <p>The major purpose of this study was to identify the causes for the driving difficulties often given experienced on highway projects where thin shells are used for cast-in-situ concrete piles that support bridge approaches, and to develop a set of recommendations and procedures to enable INDOT engineers to (a) make use of available technology for dynamic analysis of pile driving; and (b) make appropriate changes in the design, construction and contract specification procedures to improve identification and correction of problems at the earliest possible stage</p> <p>This study indicates that the parameter of greatest importance for most projects is the hammer and driving train used in the piling operations. Hence, it is suggested that INDOT Geotechnical engineers provide specifications based on detailed analysis of the anticipated effect of various hammer sizes. This analysis is done using the wave equation analysis program, WEAP87, available with the INDOT, as opposed to the usual design procedure where the 'set' is obtained using energy formulae which are generally inaccurate and do not predict driving resistance. The results of the analysis can be summarized with a family of curves - usable in the field. Development of these charts and plots for various parameters is explained in the report with detailed examples and case studies.</p> <p>The suggestions contained in the study can be implemented by the INDOT and would result in savings, both in terms of mitigating damage to the shells, and reducing the time spent on driving of piles.</p>					
17. Key Words  <b>thin steel shells, cast-in-place, wave equation, pile driving</b>			18. Distribution Statement  <b>No restrictions. This document is available to the public through the National Technical Information Service, Springfield, Virginia 22161</b>		
19. Security Classif. (of this report) <b>Unclassified</b>		20. Security Classif. (of this page) <b>Unclassified</b>		21. No. of Pages <b>166</b>	22. Price



Digitized by the Internet Archive  
in 2011 with funding from

LYRASIS members and Sloan Foundation; Indiana Department of Transportation



## TABLE OF CONTENTS

	Page
LIST OF TABLES .....	vii
LIST OF FIGURES .....	viii
<b>Chapter 1:</b>	
INTRODUCTION .....	1
1.1 Motivation.....	1
1.2 General Background .....	2
1.3 Outline of Approach Followed in the Project.....	3
1.4 Residual Stress Considerations.....	4
1.5 Summary, Benefits and Implementation.....	6
1.6 Thrust of Report and Organization.....	6
<b>Chapter 2:</b>	
PROCEDURE .....	9
2.1 Assumptions .....	9
2.2 Estimation of Parameters for WEAP87 - Narrative.....	9
2.3 Application of WEAP87 to Driving of Thin Shells, Numerical Example .....	12
2.3.1 Shaft Capacity .....	15
2.3.2 Capacity at Pile Toe .....	18
2.3.3 Stiffness and Damping .....	20
2.3.4 Driving System .....	20
2.3.5 Residual Stresses .....	22
2.3.6 Ultimate Capacity .....	22
2.3.7 Other Parameters .....	23
2.3.8 Parametric Study and Results .....	23
2.3.9 Adjustment Factors, $AF_S$ and $AF_B$ , and Conclusions .....	28

	Page
2.4 Drivability Study .....	50
2.4.1 Discussion of Results .....	50
2.4.2 Three-dimensional representation of results .....	51
<b>Chapter 3:</b>	
<b>EXAMPLES</b> .....	57
3.1 State Road 26 over Coffee Run Creek .....	57
3.1.1 Pile at bent number 4 (End bent) .....	57
3.1.1.1 Drivability study and comparison with field observations ....	61
3.1.2 Pile at bent number 3 (interior bent) .....	74
3.1.2.1 Drivability study and comparison with field observations ....	77
3.2 East 206th Street over White River .....	90
3.2.1 Pile at bent number 1 (end bent) .....	90
3.2.2 Pile at bent number 2 (interior bent) .....	104
3.3 State Road 14 over Beal Taylor Ditch .....	118
3.3.1 Pile at bent number 1 (End bent) .....	121
3.3.2 Pile at bent number 3 (interior bent) .....	132
<b>Chapter 4:</b>	
<b>CONCLUSIONS AND RECOMMENDATIONS</b> .....	145
4.1 Conclusions and Synopsis of Results .....	145
4.2 Suggestions and General Recommendations .....	146
4.3 Suggestions for Future Work .....	148
<b>APPENDICES</b>	
Appendix A: Charts, Plots and Tables used .....	149
Appendix B: List of References .....	161
Appendix C: Explanation of the WEAP87 input variable, IPERCS .....	165

## LIST OF TABLES

Table	Page
2.1 Data and results for example calculation .....	17
2.2 Hammer Properties .....	21
2.3 Material Properties of Hammer Cushions .....	22
2.4 Range of $R_{ult}$ : IPERCS = 80% .....	23
2.5 Residual variables at end of analysis .....	49
2.6 $R_{ult}$ for drivability study .....	50
3.1 Range of $R_{ult}$ : IPERCS = 20% .....	59
3.2 $R_{ult}$ for drivability study .....	62
3.3 Range of $R_{ult}$ : IPERCS = 12% .....	74
3.4 $R_{ult}$ for drivability study .....	78
3.5 Range of $R_{ult}$ : IPERCS = 29% .....	90
3.6 Range of $R_{ult}$ : IPERCS = 26% .....	104
3.7 Range of $R_{ult}$ : IPERCS = -60% .....	121
3.8 Range of $R_{ult}$ : IPERCS = -25% .....	132
Appendix	
Table	
A.1 Values of the angle of pile to soil friction for various interface conditions .....	156
A.2 Values of the coefficient of horizontal stress, $K_o$ .....	156
A.3 Penetration Resistance and Soil Properties on Basis of the Standard Penetration Test (after Table 5.3, pp. 114, <i>Peck, Hanson and Thornburn, 1974</i> ) .....	157
A.4 Relation of Consistency of Clay, Number of Blows $N$ on Sampling Spoon, and Unconfined Compressive Strength (after Table 45.2, <i>Terzaghi and Peck, 1967</i> ) .....	157
A.5 Empirical values for $\phi$ , $D_r$ , and unit weight of granular soils based on the standard penetration number with corrections for depth and for fine saturated sands (after Table 3-2, Bowles, 1982) .....	158
A.6 Empirical values for $q_n$ and consistency of cohesive soils based on the standard penetration number (after Table 3-3, Bowles, 1982) .....	158
A.7 Influence of various parameters on ultimate driving resistance from wave equation analysis .....	159
A.8 Case damping factor $J_c$ for different soils at the pile toe .....	159

## LIST OF FIGURES

Figure	Page
1.1 Thin steel shell with flat plate butt-welded at toe .....	2
2.1 Boring location plan for bridge over Cabin Creek .....	13
2.2 Minimum pile toe elevations - bridge over Cabin Creek .....	14
2.3 Log of test boring no. 2 (TB-2) for bridge over Cabin Creek .....	13
2.4 Shaft friction distribution for bent no. 2 State Road 1 over Cabin Creek .....	19
2.5 Variation in thin shell gage .....	30
2.6 Comparison of different hammers .....	32
2.7 Variation in hammer efficiency .....	34
2.8 Comparison of different hammer cushions .....	36
2.9 Variation in helmet weights .....	38
2.10 Variation in quake .....	40
2.11 Effect of variation in damping .....	42
2.12 Variation in skin friction distribution .....	44
2.13 Residual stress analysis .....	46
2.14 Residual stress/force at end of analysis - (a) Residual pile stress distribution; (b) Residual shaft friction resistance distribution .....	48
2.15 Bearing curves for drivability study (best fit lines) .....	52
2.16 Maximum compressive stresses in drivability study .....	52
2.17 Drivability study - three-dimensional representation of variation in ultimate capacity .....	54
2.18 Drivability study - three-dimensional representation of variation in max. comp. stress .....	55
3.1 Boring plan and bent location for the SR26 bridge over Coffee Run Creek .....	58
3.2 Shaft friction distribution for bent no. 4 at State Road 26 .....	59
3.3 Variation in thin shell gage (SR26/TB-4) .....	64
3.4 Effect of heavier hammer (SR26/TB-4) .....	66
3.5 Variation in damping at toe (SR26/TB-4) .....	68
3.6 Variation in quake (SR26/TB-4) .....	70
3.7 Bearing curves for drivability study at SR26/TB-4 .....	72
3.8 Maximum compressive stresses in drivability study at SR26/TB-4 .....	72

Figure	Page
3.9 Shaft friction distribution for bent no. 3, State Road 26 over Coffee Run Creek .....	75
3.10 Variation in thin shell gage (SR26/TB-3) .....	80
3.11 Effect of heavier hammer (SR26/TB-3) .....	82
3.12 Variation in damping at toe (SR26/TB-3) .....	84
3.13 Variation in quake (SR26/TB-3) .....	86
3.14 Bearing curves for drivability study at SR26/TB-3 .....	88
3.15 Maximum compressive stresses in drivability study at SR26/TB-3 .....	88
3.16 Plan layout of the six test borings (TB-1 to TB-6) used to obtain the soil profiles for the East 206th street bridge over White river .....	91
3.17 Generalized subsurface conditions at site of bridge structure (East 206th street bridge over White river) .....	92
3.18 Shaft friction distribution for bent no. 1, East 206th Street over White River .....	93
3.19 Variation in thin shell gage (E206/TB-1) .....	96
3.20 Effect of heavier hammer (E206/TB-1) .....	98
3.21 Variation in damping at toe (E206/TB-1) .....	100
3.22 Variation in quake (E206/TB-1) .....	102
3.23 Shaft friction distribution for bent no. 2, East 206th Street over White River .....	105
3.24 Variation in thin shell gage (E206/TB-2) .....	108
3.25 Effect of heavier hammer (SR26/TB-3) .....	110
3.26 Variation in damping at toe (SR26/TB-3) .....	112
3.27 Variation in quake (SR26/TB-3) .....	114
3.28 Effect of jetting/preboring (E206/TB-2) .....	116
3.29 Boring plan and bent location for the SR14 bridge over Beal Taylor Ditch - (a) Plan layout of the three test borings (TB-1, TB-3 and TB-4); (b) Minimum pile toe elevations at each bent .....	119
3.30 Generalized subsurface conditions at site of bridge structure (SR14 over Beal Taylor Ditch) .....	120
3.31 Shaft friction distribution for bent no. 1 at SR14 over Beal Taylor Ditch ..	123
3.32 Variation in thin shell gage (SR14/TB-1) .....	124
3.33 Effect of heavier hammer (SR14/TB-1) .....	126
3.34 Variation in damping at toe (SR14/TB-1) .....	128
3.35 Variation in quake (SR14/TB-1) .....	130
3.36 Shaft friction distribution for bent no. 3 at SR14 over Beal Taylor Ditch ..	135
3.37 Variation in thin shell gage (SR14/TB-3) .....	136
3.38 Effect of heavier hammer (SR14/TB-3) .....	138
3.39 Variation in damping at toe (SR14/TB-3) .....	140
3.40 Variation in quake (SR14/TB-3) .....	142

Appendix  
Figure

Page

A.1	Adhesion factors for piles driven to deep penetration into clays (after <i>Semple and Rigden</i> , 1984) - (a) Peak adhesion factor vs. shear strength/effective overburden pressure; (b) Length factor .....	149
A.2	Determination of angle of shearing resistance of granular soils from in-situ tests - (a) relationship between standard penetration test $N$ values and angle of shearing resistance (after <i>Peck, Hanson and Thornburn</i> , 1974); (b) relationship between static cone resistance and angle of shearing resistance (after <i>Meyerhof</i> , 1956) .....	150
A.3	(a) Approximate ultimate base resistance for foundations in sand (after <i>Kulwaly</i> , 1984); (b) Bearing capacity factors (after <i>Berezantsev, et al.</i> , 1961) .....	151
A.4	Bearing-capacity factors for deep foundations (Fig. 16-14, <i>Bowles</i> , 1982)	152
A.5	Curves showing the relationship between bearing-capacity factors and $\phi$ , as determined by theory, and rough empirical relationship between bearing capacity factors or $\phi$ and values of standard penetration resistance $N$ (Fig. 19.5, pp. 310, <i>Peck, Hanson and Thornburn</i> , 1974) ...	153
A.6	Chart for correction of $N$ -values in sand for influence of overburden pressure; reference value of effective overburden pressure is 1 tsf (Fig. 19.6, pp. 312, <i>Peck, Hanson and Thornburn</i> , 1974) .....	154
A.7	Relationship between mass shear strength, modulus of volume compressibility, plasticity index and standard penetration test $N$ -values (after <i>Stroud</i> , 1975) .....	155

# INTRODUCTION

## 1.1 Motivation

"Thin shells used for cast-in-place concrete piles are often damaged during driving, usually in the upper portion of the shell, and, in some cases, in the lower portion. Since these piles are commonly selected for highway structures in Indiana, the driving difficulties and resulting damage affect the construction of many projects."

"Reliable methods for the prediction of pile stresses are necessary because of the ever increasing damage and financial loss incurred on many piling projects due to improper selection of driving hammer. There is a delicate balance between pile stress, driving resistance, and hammer-to-pile weight ratio. Too large a hammer may destroy the pile whereas too small may not be adequate to drive the piles effectively."

The former statement, from the original research proposal leading to this study, describes the problem being considered; while the latter, taken from the abstract of a paper by Sandhu (1982), focuses on the physical cause of the problem, and suggests the most probable reasons for the occurrence of damaging stress levels in the shells.

These two statements together outline the *raison d'être* for this study whose major objective has been to develop procedures for estimating stresses developed during driving of thin shells used for cast-in-situ concrete piles that support bridge approaches on Indiana highways. There is an existing dynamic pile analysis technology base, however it is not implemented to its full potential within INDOT because the different offices involved look only at parts of the problem or are not familiar enough with the technology.

This study outlines a set of procedures to enable INDOT engineers to make use of available technology, and suggests appropriate changes in the design, construction and



contract specification procedures to improve identification and correction of problems at the earliest possible stage.<sup>1</sup>

## 1.2 General Background

Cast-in-place concrete piles are subdivided in two types: those which are encased in a thin shell, and those which are not (i.e. "uncased" concrete pile). The shell-type concrete piles are most commonly used on highway projects in Indiana. Most of these shells are thin (seven gage - a thickness of 0.179 inch - is most common), and can be easily damaged when high stresses are generated during driving.

Most highway projects involve seven gage steel shells of medium length (25-40 ft. long), with a typical outside diameter of 14 inches, driven into medium dense to dense sands. These piles are driven with a one inch thick steel plate, usually with a diameter slightly greater than that of the shell (Fig. 1.1), butt-welded to the toe. Local contractors, usually small size firms, are employed on these jobs, and the construction practices can differ widely. However, most contractors use conventional hammers of small to medium size, often Vulcan or Delmag hammers, with wood and/or commercial cushions. Often, driving will start with a small size hammer, followed by heavier equipment when driving difficulties are encountered. On a job of medium size (of the order of 30 piles), it is not uncommon to have as many as 50% of the piles being damaged at the top, and in some cases damage also occurs along the embedded length of the piles. This latter damage is more significant than fractures at the top, however, it is usually limited to a small number of piles. There have been instances where contractors have decided to use a heavier gage of steel to reduce/avoid these driving problems.

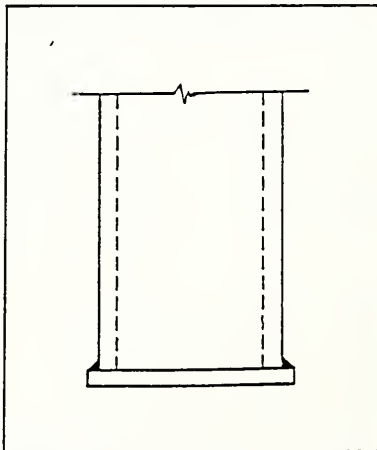


Figure 1.1 Thin steel shell with flat plate butt-welded at toe

<sup>1</sup> As an aside it is noted that this would also require improvement of the exchange of information between the various INDOT offices involved with different aspects of piling jobs.

When problems occur, the selection of a heavier hammer and/or a shell with a heavier gage of steel often reduces the problems as mentioned above. However, there are no specific guidelines to help the engineer make the best possible choice to avoid or minimize the possibility of these problems before they occur or as early as possible after construction begins. The analyses in this report show that selection of the pile-hammer (driving train) system for a given set of site conditions is the most critical parameter. Another important factor is the hard driving conditions often encountered when driving through unaccounted for material. This problem is explained next.

Not using jetting (or pre-drilling) to get past the scour depth (or embankment fill) can result in piles being driven through material which was not considered for the purpose of providing support, and hence also not included as providing any dynamic resistance when specifying driving criteria. Article 701.03 in Sec. 700 of the 1985 Indiana Specifications requires that for end bents the shells must be driven before embankment fill is placed and, in interior bents, jetting must be used to get past material which is likely to be washed away by scouring. Such criteria should be explicitly stated in the driving specifications provided to the contractors. If the designers implicitly assume that the contractors would follow these guidelines, then driving of shells may be attempted based solely on provided target penetration depth and minimum acceptable blow-count. If construction personnel are not made aware of the need for jetting/pre-drilling, there can be an increase in the resistance to driving over what was expected, by as much as 50%, and the resultant hard driving can lead to excessive stresses which damage the pile.

Since the use of thin-shell cast-in-place piles is common on highway projects, and driving difficulties are apparently widely spread, this study was initiated to develop the means to limit the occurrence of these problems. It is believed that they can be mitigated by use of the suggestions contained in this report, which emphasize efficient application of prediction techniques to estimate stresses and select driving systems.

### **1.3 Outline of Approach Followed in the Project**

Rausche and Goble (1972), based on actual measurements, demonstrated that the driving ability of a hammer depends on the impact velocity at the pile top and the pile cross-sectional area ( $c/s$  area). The velocity at the pile top is a function of the cushion, energy losses in the hammer, the ratio of ram mass to anvil plus cap mass and, in the case of diesel hammers, of the hammer combustion chamber pressure before impact.

The wave equation analysis is the best available technique to compare driving trains and select the one most suited to a particular situation. Starting with the available bore-hole data (such as standard penetration, SPT, or cone penetration, CPT, measurements and visual observation of retrieved samples), a bore-hole profile is obtained from which parameters are estimated for input to the soil model of the wave equation package (WEAP87 in this report). This information combined with the wave equation analysis produces an estimate of the expected penetration resistance (in terms of blows per foot, bpf) that the pile will face during driving. These results, together with estimates from static analyses, are used to predict the pile capacity, and to specify the required blow count and final penetration depths in design recommendations.

The results of the wave equation analysis are also used to estimate the driving stresses in the pile. Towards this end, charts called bearing curves are prepared for each bent varying the parameters known to influence the wave equation analyses. These calculations are repeated for various driving train combinations and gages of shells (e.g. 7 gage and the thicker 5 gage). An appropriate range of quake,  $Q$ , and damping factor,  $J$ , is used along with several shapes of side resistance distribution. Plots of stress-time history can be generated for various locations in the pile, peak stresses identified and noted on the charts as guidelines to check if excessive stresses would be generated while driving with a particular combination of elements.

If such charts are developed for several depths (drivability study) at each bent, then the field engineer can use the values of blows per foot (bpf) obtained for each bench mark depth to select the best fitting bearing curve from the available set generated at the initial design stage. The current driving criteria (speed, fall height, cushion thickness, etc.) can thus be adjusted to keep the stresses within acceptable limits while achieving the target penetration and bearing capacity.<sup>2</sup>

#### 1.4 Residual Stress Considerations

Wave equation analyses performed by Hery (1983) indicated that the driving stresses are slightly higher if residual stresses are considered. Residual stresses are most likely to occur when the shell penetrates deep into a cohesionless stratum and ignoring them in

---

<sup>2</sup> See related comments in Chapter 3 of Darrag, 1987.

the analyses can lead to an underestimation of the maximum driving stresses. This was confirmed by Darrag (1987).

Residual stresses can also accumulate in the pile when driving through fill. These residual stresses have a very important effect on the pile capacity prediction and the interpretation of static load test results. Hence, residual stress analysis must be used in cases where piles are driven through fill or whenever the presence of some considerable residual stresses is expected.

The residual stresses are caused by the load/rebound cycles occurring during the driving process and thus are mainly affected by the relative pile-soil stiffness, rather than by the driving elements as the change in range of magnitude of residual stresses is very narrow over a wide range of hammer energies (Table 17 of Darrag, 1987). Results also indicate that the type of cap or cushion used in the driving procedure has almost no effect on the magnitude of the residual stresses at the pile toe (Table 18 of Darrag, 1987). Thus, the residual stresses do not vary to any considerable extent when different driving trains are used.

Skin friction (as a percent of total bearing capacity) has a major influence on residual stresses and has to be accounted for carefully to get a correct estimate of stresses in pile material. For larger  $c/s$  area the residual stress percentage is lower (Figure 59 of Darrag, 1987). This effect may be important when the shell penetrates deep into a cohesionless stratum as evidenced by the work on monotube piles reported by Goble and Hauge (1978).

In conclusion, it will be stressed again in this report that wherever appreciable residual stresses are expected, they must be taken into account for accurate estimation of stresses in the pile material. This is because residual stresses due to driving have considerable effect on the stresses generated in shells, especially when driving in sandy soils. In such cases it is suggested that at least one set of dynamic analyses be always performed to estimate the effect of residual stresses on the drivability of the pile. This option is provided by the package available at the INDOT (WEAP87) and does not involve any extra effort if dynamic analyses are done routinely.

## **1.5 Summary, Benefits and Implementation**

The overall design process needs to be modified to incorporate dynamic analyses on a routine basis at the initial design stage using the suggested procedures. This will lead to better estimates of stresses developed in shells during driving, and the development of suitable driving criteria. This report includes recommendations and guidelines for accomplishing this. It can be done primarily by using the software available to the INDOT (WEAP87). Towards this end the report is formatted somewhat like a help manual which contains complete examples. Complete analysis/design evaluations of a number of projects have been performed, starting with the preliminary site investigation report. One example of comparisons with, and adjustments based on, field observations is also presented. This is done in a manner which can be used as a guideline by INDOT engineers without excessive investment of time and physical resources on the part of INDOT.

It is clear that the scope of this project is limited and the small data base which was available for evaluation is not sufficient to cover all possible conditions, e.g. soil types, driving systems, pile types that INDOT can encounter. However, it can serve as a pilot study and the recommended procedures can serve as a model to INDOT engineers and promote the use of available dynamic analysis software during the design of piles.

## **1.6 Thrust of Report and Organization**

No theoretical or technical details are included beyond what is absolutely necessary for following the report and making use of the procedures and suggestions contained therein. The reader interested in acquiring a more thorough knowledge of the applications of stress-wave theory to piles and related work on prediction and performance of piles is referred to the publications listed in Appendix B.

Chapter 2 explains the procedure followed in the analyses. The assumptions are outlined and the estimation process to develop input parameters to WEAP87 is explained. The generation of charts/plots, for use in design as discussed in Section 1.3, is explained with a complete example in Section 2.3.

Chapter 3 contains examples of application of the procedures outlined in Chapter 2. The examples in Chapter 3 are based on actual highway projects in Indiana where thin-

shells were driven and information on these projects was provided by INDOT personnel. Charts and plots as mentioned in Section 1.3 are developed and their usage explained.

Chapter 4 contains conclusions and recommendations, including further work involving dynamic measurements during driving.





## PROCEDURE

### 2.1 Assumptions

The purpose of this report is to suggest procedures for mitigating pile driving difficulties on highway projects in Indiana. In an actual project, these procedures will take effect after the following steps have been taken by the INDOT:

- 1) The site investigation has been completed and a subsurface investigation and foundation recommendations report is available.
- 2) It has been decided to use cast-in-place concrete piles encased in thin steel shells,<sup>3</sup> and the shells are driven with a flat plate butt-welded to the toe.
- 3) The location and number of piles at each bent has been decided and plan drawings are available.
- 4) The required static capacity for the piles has been specified for each bent.
- 5) The depth of scour has been evaluated for each bent where scour may occur.
- 6) The design static capacity along with scour depth information has been used to tentatively specify the final toe elevation of the pile.

### 2.2 Estimation of Parameters for WEAP87 - Narrative

The first step is the generation of a soil profile representing the results of exploratory borings. This profile provides the information required to estimate parameters for input to the numerical wave equation program WEAP87. To make very accurate estimates of soil parameters at each pile location requires an extensive soil exploration program. However, this is usually not economically feasible for routine highway projects, and the

---

<sup>3</sup> All references to pile or tube from here on are to be understood to be for thin steel shells.

information from a few well placed bore-holes serves to create an approximate picture of the soil profile. Each bent is represented by a typical pile and the bore-hole record(s) from the test boring(s) closest to the bent is(are) used for the analyses.

The standard penetration test (SPT) is performed as a matter of routine in all granular soils and is used almost exclusively in Indiana for site characterization on bridge projects. Penetration tests can give unreliable results in soils containing occasional stones or rock fragments, hence it is important to carefully inspect the bore-hole records for any sudden changes or apparent anomalies. The  $N$  values reported on the boring logs are corrected based on the relationships recommended by various experts (Appendix B<sup>4</sup> contains a complete list of references). The appropriate corrections are selected based on prevailing conditions and available data. Corrected  $N$  values versus depth plots are developed for each location to be used in bearing capacity calculations and for generating shaft friction distributions for input to WEAP87. From available charts and tables, these corrected  $N$  values can be correlated with parameters such as the angle of shearing resistance and relative density of the soil. Once the necessary parameters are obtained, as shown in the example in Section 2.3, the shaft friction and toe bearing resistance of a pile can be estimated.

Since the wave equation program is not very sensitive to minor changes in the shape of the shaft friction distribution, the initial distribution profiles are smoothed by evening out the small irregularities. This also follows physical reality because a pile driven into soil tends to smear the effect of soil friction variations along its side.

Example calculations for shaft friction resistance are conducted in Section 2.3 using the charts and tables developed for cohesionless soils (as well as some for cohesive soils) in the work of Nordlund (1965), Broms (1966), Vesic (1970) and Kulwahy (1984). These procedures are also suggested by Tomlinson (1987). The charts and tables used are collected in Appendix A of this report. A value equal to about 75% of the static shaft friction estimated from the above procedure is input to WEAP87. As pointed out by Tomlinson (1987):

“... This is because a hammer blow acting on top of the pile causes the tube to expand and push out the soil at the instant of striking, followed by a contraction

---

<sup>4</sup> Appendix A has the charts and relationships used, to estimate soil parameters, in this report. Examples in the report refer to Appendix A which contains citations to the original sources listed in Appendix B.

of the tube. This frees the tube from some of the skin friction as it moves downward under the momentum of the hammer. The flexure of the pile acting as a long strut also releases the skin friction at the moment of impact.”

To calculate the capacity at the pile toe, the steps suggested by Tomlinson (1987) are followed with charts for bearing capacity coefficients taken from Berezantsev et al. (1961). For high end-bearing in sand, the load carrying capacity at the toe of the pile is limited by the crushing strength of the sand particles.

The static capacities thus obtained are used as the input ultimate values to the wave equation program. A check is done to assure that the toe capacity plus the shaft capacity (beyond scour depth for bents where scour is expected to occur) is at least as much as the required static capacity times the specified factor of safety.<sup>5</sup>

The estimated shaft friction distribution profile, along with information on the hammer and other components of the driving train, is input to WEAP87. Since multiple values of the ultimate capacity ( $R_{ult}$ ) can be input during one run of WEAP87, the distribution profile is normalized. It is reasonable to assume that the shape of the shaft friction distribution, for a given depth of embedment, does not change (a) with change in  $R_{ult}$  for a fixed value of the percentage of  $R_{ult}$  that is provided by skin friction resistance along the shaft; or (b) with change in percentage of load in skin friction for a fixed  $R_{ult}$ . The program simply distributes the available skin friction resistance along the length of the pile shaft, based on the specified shape of skin friction distribution.

The pile is specified by (a) its area in cross section<sup>6</sup>; (b) the modulus of elasticity,  $E$ , of the pile material (29000 ksi for steel); and (c) the unit weight,  $\gamma$ , of the pile material (492 pcf for steel). It is important to remember that WEAP87 (like other similar programs) does not look at any other information about the pile cross section besides its area. For instance the area of steel in a seven gage, 14"  $\phi$  shell is 7.77 in.<sup>2</sup>, which is the same as that of a five gage, 12.4"  $\phi$  shell. As far as WEAP87 is concerned, both

---

<sup>5</sup> Factor of Safety is usually taken as 2 unless very extensive subsoil testing has been done and the data is considered extremely reliable.

<sup>6</sup> Only the area of the pile material is considered. For a shell with an outer diameter of 14 in. (14"  $\phi$ ), this area is 7.77 in.<sup>2</sup> and 8.8 in.<sup>2</sup> for shell wall thicknesses of 0.18 in. (7 gage) and 0.203 in. (5 gage), respectively.

of these are identical and the pile parameters for input to WEAP87 would be the same in both cases. This behavior is a function of the algorithm used for the dynamic analysis and is mentioned here to avoid any confusion when comparing results, obtained using WEAP87 or similar analyses, for shells with different outer diameters and thicknesses but which have the same area in cross-section for the shell material. This is not really a problem in the cases studied here and in the situations commonly encountered by the INDOT since all the shells considered, almost exclusively have an outer diameter of 14 inches and a shell thickness of seven or five gage. With change in area, the stress generated in the pile material during driving varies. Since an excess of stress is what causes damage, it is the parameter of most concern.

Besides the parameters describing the estimated shaft friction distribution, driving train and pile properties, a few other parameters need to be specified as input to WEAP87. Estimated values for the soil quake along the pile shaft and at the pile toe as well as a damping factor for the soil. If residual analysis is to be performed, that also needs to be specified as input to WEAP87.

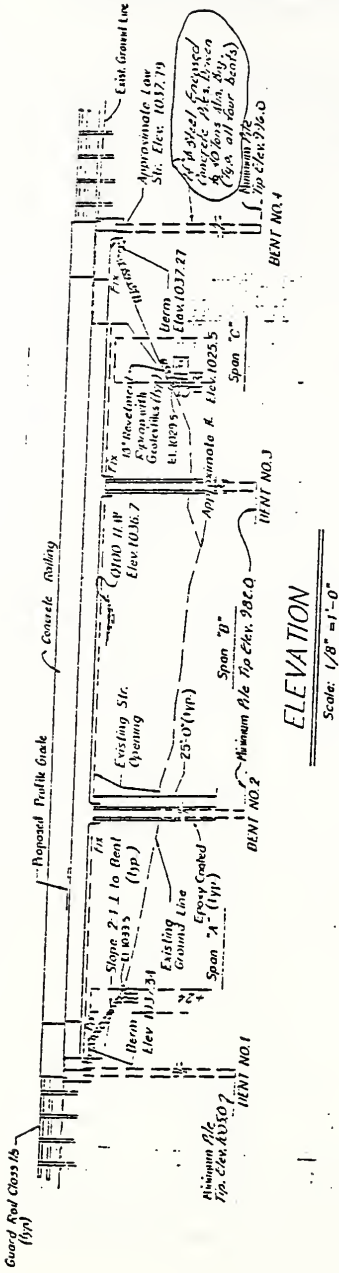
The wave equation program can generate force/stress/velocity *versus* time histories. WEAP87 also produces a summary of peak stresses for several locations along the length of the pile. This helps in identifying the most vulnerable section(s) of the shell. A value of bpf for each  $R_{ult}$  specified is also identified. Bearing curves are plotted based on these bpf values. A set of bearing curves can be generated by changing the various parameters one at a time.

The results of a wave equation analysis are only valid for the particular depth of embedment specified. To model the behavior of the pile as it is being driven to the final depth of embedment requires that WEAP87 be used to develop bearing graphs, and other plots if needed, for several depths. An example of this is presented at the end of this chapter (Sec. 2.4).

### 2.3 Application of WEAP87 to Driving of Thin Shells, Numerical Example

The following is a complete example of the application of dynamic wave equation analysis to the driving of a thin shell on a bridge project in Indiana. Since the effects of variations in different input parameters will follow similar trends, the results obtained





**ELEVATION**  
Scale: 1/8" = 1'-0"

**GENERAL PLAN**  
 CONTINUOUS R.C. SLAB BRIDGE  
 3 SPANS AT 33'-0", 41'-6", 33'-0"  
 40'-0" CLEAR ROADWAY SKETCH SQUARE  
 STATE ROAD 1 OVER CABIN CREEK

INDIANA DEPARTMENT OF HIGHWAYS  
 RANDOLPH COUNTY  
 SCALE: AS NOTED  
 DRAWN FOR APPROVAL

119  
 SHEET NO. 17192  
 PROJECT: STATE ROAD 1 BRIDGE  
 BRIDGE CONTRACT NO. 81005  
 DRAWING: CR 517 OF 52  
 SHEET NO. 17192  
 BRIDGE FILE: 1-66-7195

Figure 2.2 Minimum pile toe elevations - bridge over Cabin Creek



### 2.3.1 Shaft Capacity

The first step is the generation of an idealized soil profile. The  $N$  values reported on the boring log (Figure 2.3) are corrected for the effect of overburden (Bowles, 1982). For driven displacement piles, the skin friction resistance, per unit length, in each soil layer is estimated by the following expressions:

$$Q_s = (K_s \sigma_{vo} \tan \delta) A_s \quad (2.1)$$

for cohesionless soils; and,

$$Q_s = (F \alpha_p \bar{c}_u) A_s \quad (2.2)$$

for cohesive soils.  $K_s$  is the coefficient of horizontal stress which depends on the relative density and state of consolidation of the soil, the volume displacement of the pile, the material of the pile, and its shape;  $\sigma_{vo}$  is the average existing effective overburden pressure within the soil layer;  $\delta$  is the angle of friction between pile and soil;  $F$  is a length factor obtained using Fig. A.1(b);  $\alpha_p$  is the peak adhesion factor obtained using Fig. A.1(a); and  $\bar{c}_u$  is the average undisturbed undrained cohesion of the soil surrounding the pile shaft. The undisturbed undrained cohesion,  $c_u$ , can be estimated from testing of soil samples in the laboratory. Since testing can usually be done only for a limited number of samples,  $c_u$  often needs to be estimated from available relations such as those presented in Tables A.4 and A.6 or by establishing a relationship such as  $c_u = CN$ , where  $C$  is a constant determined by testing local cohesive samples, as proposed by Bowles (1982).  $A_s$  is the surface area of the pile shaft (per unit length of the shaft) contributing to the support of the pile in skin friction.

Eqn. 2.1 is based on work by Broms (1966), Peck, Hanson and Thornburn (1974), Vesic (1977) and Kulwaha (1984). Eqn. 2.2 is based on work by Burland (1973), Meyerhof (1976), Randolph and Wroth (1982) and, Semple and Rigden (1984). Eqn. 2.2 is usually applicable for moderately loaded piles driven into a bearing stratum of firm to stiff clay.



Table 2.1 lists the results obtained for the present example using Eq. 2.1 for the cohesionless strata (layers 1, 2 and 4 in column 1 of Table 2.1) and Eq. 2.2 for the cohesive strata (layers 3 and 5 in column 1 of Table 2.1). The values listed in columns 5 through 15 are average values for each layer.

For the layers of cohesionless soil, the following steps are taken. First  $\sigma'_{vo}$  (column 5) is obtained. Soil unit weight is 120 pcf and water table is 7 ft below ground surface, so  $\sigma'_{vo} = (120h - 64(h-7))/2000$  or  $[0.028h + 0.224]$  tsf, where  $h$  is the depth to the middle of the layer under consideration. The boring log of Fig. 2.3 is used to obtain average SPT  $N$  values (column 6). These are corrected for overburden pressure using a correction factor,  $C_N$ , obtained from Fig. A.6 (e.g.,  $C_N = 1.15$  for stratum no. 1) and listed in column 7. Next,  $\phi$  (column 8) is obtained from Fig. A.2(a) and this is used to estimate  $\delta$  (column 9) by selecting  $\delta = 0.8 \phi$ , as suggested from Table A.1. Column 10 lists the  $K_o$  values selected using Table A.2. Table A.2 is also used to obtain the relationship  $K_s = 1.5 K_o$ .  $K_s$  values are listed in column 11.

For the cohesive layers the steps taken are as follows.  $\sigma'_{vo}$  is obtained as above. No corrections for overburden need to be made for  $N$ .  $\bar{c}_u$  is obtained using the procedure suggested by Stroud (1975), where  $\bar{c}_u = f_i N / 96$  tsf.  $f_i$  is an empirical parameter related to the plasticity index,  $PI$ , as shown in Fig. A.7. Laboratory tests indicate  $PI = 14$  for stratum no. 3 and the same is assumed for stratum no. 5. This results in  $f_i = 7$  so  $\bar{c}_u = 0.073N$  tsf, listed in column 12. Since  $\bar{c}_u / \sigma'_{vo}$  is greater than 0.8 and the ratio of embedded length of shell to its diameter is less than 50 for both cohesive layers, the values of  $\alpha_p$  (column 13), and  $F$  (column 14) are estimated from Fig. A.1 to be 0.5 and 1.0, respectively.

$Q_s$  (column 15 of Table 2.1) can now be obtained by using Eqs. 2.1 and 2.2. The total load capacity in shaft-soil resistance,  $Q_{st}$ , is obtained by multiplying  $Q_s$  by the thickness,  $\Delta h$ , of each strata. For the current case, it is obtained as follows:

$$Q_{st} = \Sigma Q_s \Delta h = 0.94 \times 7.7 + 1.17 \times 5 + 1.34 \times 1.5 + 1.44 \times 3.5 + 2.14 \times 22.3 = 67.86$$

Which is  $\approx 70$ , and hence  $Q_{st} = 70$  tons can be used as a reasonable estimate.

As a final step, normalization of the side resistance is done by dividing each  $Q_s$  value by the largest value of  $Q_s$  ( $=2.14$ ) to obtain the values in column 16. These are then used as input values to WEAP87 for defining the shaft friction distribution profile. The profile obtained for the example under consideration is shown in Fig. 2.4(a).

Table 2.1

Elev (ft) (1)	Layer No. (2)	Below top of		$\sigma'_{vo}$ (tsf) (5)	SPT N-value		$\phi$ (deg) (8)	$\delta$ (deg) (9)	$K_o$ (10)	$K_B$ (11)	$C_u$ (tsf) (12)	$\alpha_p$ (13)	F (14)	$Q_B$ (tsf) (15)	NORM (16)
		Bore (ft) (3)	Pile (ft) (4)		Obs. (6)	Corr. (7)									
1032.3 to 1022.0	Scour	00.0 to 10.3	05.2 to 15.5	-----	--	--	-----	-----	-----	---	-----	---	---	---	----
1022.0 to 1014.3	1	10.3 to 18.0	15.5 to 23.2	0.62	33	38	38.0	30.5	0.45	0.7	-----	----	---	0.94	0.44
1014.3 to 1009.3	2	18.0 to 23.0	23.2 to 28.2	0.94	34	34	37.0	29.5	0.40	0.6	-----	----	---	1.17	0.55
1009.3 to 1007.8	3	23.0 to 24.5	28.2 to 29.7	1.03	10	10	-----	-----	-----	---	0.73	0.5	1.0	1.34	0.63
1007.8 to 1004.3	4	24.5 to 28.0	29.7 to 33.2	1.10	10	10	30.0	24.0	0.50	0.8	-----	----	---	1.44	0.67
1004.3 to 982.0	5	28.0 to 50.3	33.2 to 55.5	1.47	16	16	-----	-----	-----	---	1.17	0.5	1.0	2.14	1.00

Three profiles are used for this example. The first is the original profile of Fig. 2.4(a) as developed above. A smoother version (Fig. 2.4(b)) obtained by averaging the stepped portion of Fig. 2.4(a) and a simplified distribution, Fig. 2.4(c)<sup>7</sup>, are used as alternate distributions.

### 2.3.2 Capacity at Pile Toe

The next step is to estimate the bearing capacity of the pile toe. For most situations in cohesionless soils this can be calculated as:

$$Q_b = N_q \sigma_{vo} A_b \quad (2.3)$$

where  $A_b$  is the c/s area of the pile toe<sup>8</sup>, and  $N_q$  is the bearing capacity factor which depends on the ratio of depth of penetration of the pile to its diameter and on the angle of shearing resistance  $\phi$  of the soil ( $N_q$  can be estimated using the most appropriate of the available semi-empirical relationships such as those presented in Figs. A.3 to A.5). For cohesive soils the capacity is:

$$Q_b = N_c c_b A_b \quad (2.4)$$

where  $N_c$  is the bearing capacity factor, and  $c_b$  is the undisturbed undrained cohesion at the pile toe<sup>9</sup>.  $c_b$  is obtained in a similar manner as for the side friction resistance by using  $c_b = f_i N/96$  tsf. For the current case,  $c_b = 1.4$  tsf and  $N_c = 9$ <sup>10</sup>, hence a value of  $Q_b = 9 \times 1.4 \times 1.11 = 14$  tons is obtained. This results in a total estimated static resistance of 84 tons. This is more than twice the load carrying capacity called for in the specification (working load of 40 tons).

---

<sup>7</sup> Typically a triangular distribution is assumed for granular soil and a uniform distribution for cohesive soil.

<sup>8</sup> The base plate usually projects about 0.125 inch around the pile to enable welding so  $A_b$  for a 14"  $\phi$  pile would be about 1.11 ft<sup>2</sup>.

<sup>9</sup> It is not strictly correct to use the undisturbed cohesion for  $c_b$  since remolding has taken place beneath the toe. However, the greater part of the failure surface in end bearing is only partly disturbed.

<sup>10</sup> Meyerhof (1951) has shown theoretically that the bearing capacity factor  $N_c$  is approximately equal to 9 provided that the pile has been driven at least to a depth of five diameters into the bearing stratum.

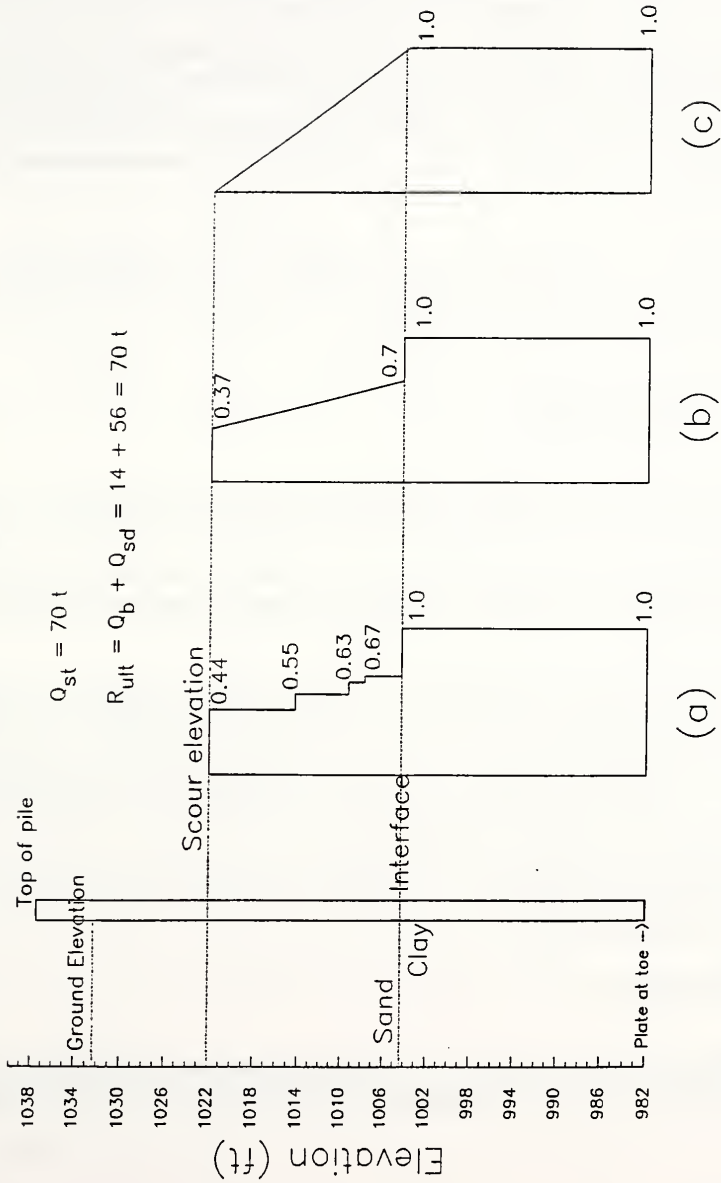


Figure 2.4 Shaft friction distribution for bent no. 2  
State Road 1 over Cabin Creek

The calculations have been presented in detail to enable the reader to duplicate the procedures for other situations. It is not suggested that the particular charts and tables used are the only ones available in the literature for estimating the skin friction resistance and toe bearing capacity of driven shells, however the steps taken and the approach will always be similar, irrespective of the charts, or empirical relationships being used.

For the examples in Chapter 3, most of the foregoing details are not presented since attention is primarily focused on wave equation analysis. Hence it is understood that the skin friction distribution has been obtained by procedures such as those described above and a profile is available in a form similar to Figure 2.4, before the wave equation analysis begins.

A standard case is used as the basis for comparison when different parameters are varied. The parameters of the standard case are described in Sec. 2.3.8. Table A.7 is used as a guideline for parameter variation.

### 2.3.3 Stiffness and Damping

The quake and damping parameters required for wave equation analysis are the most difficult ones to define as emphasized by Poulos (1987) in the following:

“These parameters may have a significant influence on the results of the analysis and the success or otherwise of predictions based on this approach rely to a large extent on judicious selection of  $Q$  and  $J$ .”

For a closed end pipe normal quakes of 0.1 inch are recommended and the damping factor,  $J$ , is suggested as 0.05 and 0.15 s/ft for skin and toe, respectively. These are the values most commonly cited in the literature and used in the current example, however parametric studies are also conducted. Table A.7 suggests that the damping factor has a greater influence on wave equation analysis results, so  $J$  is varied from 0.1 to 0.2 for the toe and 0.03 to 0.08 for the skin. Two sample runs are also performed to assess the effect of variation in quake.

### 2.3.4 Driving System

The hammer used for the standard case is a Mc Kiernan-Terry MKT DE 30, open-end diesel (OED) hammer. Two alternate hammers are considered, MKT 33 and a Delmag

D 22. All three hammers are open-end diesels with an assumed efficiency rating of 80%. The energy ratings and other parameters of the hammers are listed in Tab. 2.2.

**Table 2.2**  
Hammer Properties

Hammer Type	MKT DE 30	MKT 33	D 22
WEAP87 ID #	148	143	6
Maxm. Rated Energy kips-ft [kJ]	22.4 [30.5]	33.0 [44.9]	40.6 [55.2]
Weight of Ram kips [kN]	2.8 [12.5]	3.3 [14.7]	4.9 [21.9]
Maxm. Stroke ft [m]	8.0 [2.44]	10.0 [3.05]	8.3 [2.52]

Hammer efficiency has considerable effect on the results. A default value of 0.8 (80%) is used in the standard case. One run is done with a lower efficiency of 0.6 in Section 2.3.8 to demonstrate the degradation in drivability due to a lowering of the efficiency. Experience and data from the field must be used in choosing alternate efficiencies.

Helmet and hammer cushion parameters were estimated as suggested in the User's Manuals for WEAP87. A helmet weight of 1.01 kips is used. Helmet weight can have a considerable influence on the bearing curve. To assess this effect the standard case was reanalyzed with a heavier helmet which has a weight of 3.03 kips.

The hammer cushion information required is its area, thickness and elastic modulus. The cushion area used is 283.5 in<sup>2</sup> for all cases.<sup>11</sup> The thickness and elastic modulus of the cushion depend on the material used. Plywood, aluminum conbest, and nylon are the three most common materials used for hammer cushions. Four cushions are

---

<sup>11</sup> Variation in this area has little influence on the blow count. Also, in practice the area of cushions used for steel piles with a diameter up to 16 inches is usually the same.

evaluated for illustration, 1/2" and 1" plywood, 2" aluminum conbest, and 2" nylon. The material properties are taken from Table 3 of Vol. II of the WEAP87 user's manual and are presented here as Table 2.3. *For the cases in Chap. 3 only plywood is considered since that is the material most commonly used on INDOT projects.*

**Table 2.3**  
Material Properties of Hammer Cushions

Cushion Material	Elastic Modulus (ksi)	Coefficient of Restitution
Plywood	30	0.50
Alum. Conbest	280	0.80
Nylon (MC-904)	175	0.92

### 2.3.5 Residual Stresses

A residual stress analysis (RSA) is conducted with the same parameters as those for the standard case (parameters defined in Sec. 2.3.8). It is best to use Viscous damping when conducting a residual stress analysis so the type of damping used is Viscous Smith damping (option ISMITH = 2 in WEAP87). Since residual stresses are most likely to occur when the shell penetrates deep into a cohesionless stratum and a residual stress analysis (RSA) is quite sensitive to the skin friction (as a percent of total bearing capacity), an extensive RSA might not be necessary when the shell penetrates deep into a cohesive stratum. Details of the residual stress analysis and interpretation of the results are given in Section 2.3.8.

### 2.3.6 Ultimate Capacity

$R_{ult}$ , the ultimate capacity, is the sum of  $Q_{sd}$ , the dynamic capacity<sup>12</sup> in shaft friction

---

<sup>12</sup> The dynamic capacity is usually defined as the sum of the static capacity  $Q_s$ , and a dynamic component  $Q_d$  coming from damping and velocity terms in the wave equation. But in this report,  $Q_{sd}$  represents



resistance, and  $Q_b$ , the static capacity at the toe. A value of  $Q_{sd} = 56$  tons and  $Q_b = 14$  tons (from Sec 2.3.3) results in  $R_{ult} = 70$  tons for the standard case. A range of  $R_{ult}$  values around this best estimate are considered to obtain bearing plots. In WEAP87 this is achieved by the variable IPERCS which specifies how the value of  $R_{ult}$  is divided between shaft and toe. Appendix C contains an explanation of the role and usage of IPERCS. Table 2.4 lists the range of  $R_{ult}$  for the standard case.

Table 2.4  
Range of  $R_{ult}$  : IPERCS = 80%

$R_{ult}$ (tons)	40	60	70	80	100	120
$R_{ult}$ (kips)	88	132	154	176	220	264
$Q_b$ (tons)	8	12	14	16	20	24
$Q_{sd}$ (tons)	32	48	56	64	80	96

### 2.3.7 Other Parameters

A pile cushion is normally used only with concrete piles so no pile cushion is considered for any of the cases in this study.

The number of pile segments is not varied. WEAP87 uses a default length of about 5 ft for each segment which results in 11 segments for the current example.

### 2.3.8 Parametric Study and Results

Based upon the above considerations, the following parameters are used for the standard case (Case00):

Pile	Type	Thin steel shell
	Gage	7 (wall thickness = 0.179"; c/s area = 7.77in <sup>2</sup> )
	$\phi$	14"
	Length	55.5 ft

---

the total capacity in shaft friction resistance, *while driving*, and is obtained by reducing the value of  $Q$  (obtained in Sec. 2.3.1) by about 25%. The reason for this reduction is explained in Sec. 2.2 of this report.

Hammer	Type	MKT DE-30	
	Efficiency	0.8	
	Cushion	Area	283.5 in <sup>2</sup>
		Material	Plywood
	Thickness	1.0"	
	Helmet	Weight	2.02 kips
Soil Parameters	Quake	Shaft	0.1"
		Toe	0.1"
	Damping	Type	Smith (Normal)
		Shaft	0.05 s/ft
		Toe	0.15 s/ft
$R_{ult}$	Table 2.4		
Shaft Friction	As a % of $R_{ult}$ Distribution used	80 (IPERCS = 80) Fig. 2.4(a)	

A number of parametric studies are conducted next. Only one parameter is varied at a time, with the remainder of the data identical to that of the standard case:

Pile	Gage	Case15	5 (wall thickness = 0.203"; c/s area = 8.8in <sup>2</sup> )	
Hammer	Type	Case01	MKT 33	
		Case02	Delmag D 22	
	Efficiency	Case20	0.6	
		Cushion	Case03	0.5" Plywood
			Case04	2.0" Alum. Conbest
	Case05	2.0" Nylon (MC-904)		
Hammer	Helmet wt.	Case21	1.01 kips	
		Case22	3.03 kips	
Damping	Toe	Case08	0.10 s/ft	
		Case09	0.20 s/ft	
	Shaft	Case10	0.03 s/ft	
		Case11	0.08 s/ft	
Quake	Toe	Case14	0.12"	
	Shaft	Case13	0.08"	
Shaft Friction Distribution		Case07	Figure 2.4(c)	
		Case06	Figure 2.4(b)	

Residual  
Stress Analysis

Case12

Damping is Viscous Smith damping  
(ISMITH = 2)

The results for the above variations are compared to the reference case (Case00) in Figs. 2.5 to 2.14. A tabular summary of WEAP87 results follows each figure.

Using a thicker gage of steel results in significant reduction (10 to 20%) in stresses without an increase in the required blow count (Fig. 2.5) for ultimate capacities in the range of interest (50 to 90 tons). This implies that in cases where the expected stresses in the shell are close to the maximum allowable limit, the use of a shell with a greater wall thickness can mitigate the problem with limited increase in driving effort.

Fig. 2.6(a) shows that using heavier hammers results in considerable reduction in the number of blows required to achieve comparable bearing capacity. The hammer with the highest rated energy, the Delmag D 22, required only 17 bpf to drive the shell to a capacity of 70 tons, whereas the standard MKT DE 30 required 35 bpf. However, using a heavier hammer results in an increase in stresses induced in the shell (Fig. 2.6). Using the D 22 causes a 25% increase in the maximum stress as compared to the MKT DE 30. Using the MKT 33 instead of the MKT DE 30 reduces the required blow count by 25% while the increase in stress is only about 6%. This indicates that a MKT 33 would have been a good choice at this site. *This analysis also shows that if several hammers are to be evaluated for the conditions at a site, results from an initial wave equation analysis can be of considerable assistance.*

The efficiency of the hammer has also a significant effect on the driving effort (Fig. 2.7(a)). A lower efficiency implies that a hammer is operating at a lower than rated energy capacity and is in effect behaving like a lighter hammer. This conclusion is borne out by the similarity between Figs. 2.7 and 2.6. When specifications call for a particular blow count to be achieved as an indicator of the required capacity being reached, a lower efficiency can lead to the pile being driven to a lesser capacity than expected. For the present case this would lead to an attained  $R_{ult}$  of 60 t at 35 bpf if the hammer operates at 60% efficiency whereas the target was 70 t assuming the hammer was operating at 80% efficiency. These effects get considerably more pronounced as the target  $R_{ult}$  increases (Fig. 2.7).

The  $R_{ult}$  increases when stiffer hammer cushions with high coefficients of restitution are used. This increase gets larger at higher capacities. Fig. 2.8(c) shows that at  $R_{ult} = 70$  tons, the use of a Nylon or Aluminum Conbest cushion (properties given in Table 2.2) results in a 10% decrease in the required blow count when compared to driving with a 1" thick plywood cushion. The difference between a 0.5" and 1" plywood cushion is marginal for this case. As seen from Figs. 2.8 (a) & (b) the bearing curves for the plywood cushions are identical and the differences in maximum stress for the two cushions are negligible for the range of interest ( $R_{ult} = 60$  to 90 tons).

The standard helmet for the supplied hammer weighs 2.02 kips and is most appropriate as far as drivability of the shell is concerned (Fig. 2.9(a)). Non-standard helmet weights result in a little degradation but they follow a consistent trend in that the lighter helmet, 1.01 kips, requires the highest blow count to achieve comparable capacity. The pattern of induced stresses is more complex. At low capacities the heaviest helmet causes the least stress but a crossover occurs between 60 and 70 tons with the stresses falling with reduction in helmet weight. The lighter helmet reduces the stresses, however the drivability is reduced significantly. This shows that changing helmets must be careful decision that can be made only if the effects of various helmets have been evaluated by a wave equation analysis.

Changing the quake from the recommended values, 0.1" for both toe and shaft, has little or no effect on the drivability (Fig. 2.10(a)) and only marginal effect on the induced maximum compressive stresses (Fig. 2.10(b)).

WEAP87 is more sensitive to the value of the parameter specified for damping along the shaft than it is for that at the toe. An increase or decrease in the shaft damping results in a proportional increase or decrease in the induced stresses. This variance follows a smooth pattern as shown in Fig. 2.11(b). A similar but less pronounced effect is seen for the damping at the toe. The bearing curves in Figs. 2.11 (a) & (c) also vary in a smooth, proportional manner for the range studied. This implies that such curves can be generated for an appropriate range in damping parameters by using WEAP87 to get the extremes and the median and then interpolating other curves in between if necessary.

Variation in the assumed/estimated shape of the shaft friction distribution has negligible effect on the drivability (Figs. 2.12 (a) & (b)). Using a simplified (idealized) distribution

as in Fig. 2.4(c), instead of the actual estimated distribution from Fig. 2.4(a), results in WEAP87 estimating a slight increase in the maximum induced compressive stress in the shell. This increase is small for the range of interest. This apparent lack of response to simplifying the distribution is consistent with the fact that it is more important, *at least as far as wave equation analysis is concerned*, to accurately assess the load carried along the shaft, through resistance at the soil-shaft interface, as a fraction of the total load capacity rather than minor differences in the distribution of this friction load along the length of the shaft.

The last variation studied is the effect of considering residual stresses in the dynamic analysis. Fig. 2.13(a) indicates that the shell is easier to drive if residual stresses are included. As Darrag (1987) pointed out this is logical since “the accumulation of compressive residual stresses below the pile tip, as driving proceeds, facilitates the driving process”. This reduction in the blow count due to residual stress consideration is directly related to the magnitude of these and as  $R_{ult}$  increases this effect becomes more pronounced. In some cases refusal may be indicated by the results of wave equation analysis if residual stresses are not considered. That the situation is not really that of refusal becomes apparent when one looks at the results for Case00 and Case12, tabulated after Fig. 2.13, where the blow count at  $R_{ult} = 264$  kips (120 t) is almost 500 for the analysis without taking residual stresses into account whereas with residual stresses accounted for, the blow count is only about 140. Fig. 2.13(b) shows that the driving stresses, indicated by WEAP87, are higher if residual stresses are considered. Both of these effects are important. They could result in unnecessary hard driving and in some other case the stress could cause yielding of the shell material. For example, if no residual stress analysis were done in the present case, and an ultimate capacity of 100 tons was desired; then the specifications would call for a final blow-count of 92 bpf and the maximum compressive stress expected would be 32 ksi. However, the residual stress analysis shows that the specified blow-count would in fact result in an ultimate capacity of 115 tons and a maximum stress of 37 ksi. Accordingly, it is suggested that, whenever INDOT engineers use WEAP87 to assess suitability of driving system components - and other parameters - as presented in this report, at least one residual stress analysis should also be performed.

Fig. 2.14(b) shows the distribution of residual skin friction along the pile shaft for Case12 and Fig. 2.14(a) that of the residual stress in the pile segments. The residual

load at the toe is 4.23 t (9.31 kips) when  $R_{ult} = 70$  t and the peak residual stress in the shell is close to 3 ksi. Table 2.5 presents the same data numerically.<sup>13</sup>

### 2.3.9 Adjustment Factors, $AF_s$ and $AF_b$ , and Conclusions

The results of the parametric study may be directly used by generating a so-called *adjustment factor*. This factor can be used as a convenient tool to account for the variations (from the standard case) in the parameters obtained while driving, over the entire range of interest of  $R_{ult}$  values. Since the variations are usually smooth, the adjustment is the average over - and is thus applicable over - the entire range of interest of  $R_{ult}$  values studied. This factor is calculated as the coefficient of the blow count (or stress) in the case with variation *versus* that in the standard case. It can be interpreted as a measure of the amount of degradation/improvement (increase/decrease in number of blows per foot required to drive the shell; or increase/decrease in the peak stress in the shell) occurring due to the likely variation in a parameter.

Two such factors are defined:  $AF_s$  = adjustment factor for stress;  $AF_b$  = adjustment factor for blow count. These factors are used for estimated parameters such as quake, damping and efficiency; as well as to account for the effects of variation in shell gage, type of hammer etc. They may also be used to account for the effect of residual stresses.

The basic assumption behind the use of these factors is that the effect of variation in parameters can be accounted for independent of one another. Once the  $AF$  are estimated for each parameter, a cumulative  $AF$  can be calculated by multiplication of the individual adjustment factors. This cumulative  $AF$  can then be used with the standard case plots to develop an 'envelop' within which the field observations will lie. For the current example the adjustment factors are calculated and listed at the top of the next page.

Cumulative adjustment factors may now be calculated for cases with different sets of parameter variations. For example, a case with a Delmag D 22 hammer, toe damping of 0.20 s/ft and shaft damping of 0.08 s/ft, would have an  $AF_b = 0.55$  ( $= 0.45 \times 1.06 \times 1.15$ ) and  $AF_s = 1.31$  ( $= 1.25 \times 1.01 \times 1.04$ ). Hence, the expected blow count

---

<sup>13</sup> Since the pile is in equilibrium at the end of a hammer blow, the sum of the upward residual toe load, upward (positive) residual shaft friction and downward (negative) residual shaft friction must be zero. Adding the numbers in the columns in Table 2.5 confirms this.



Parameter	$AF_B$	$AF_S$
Shell gage (5 vs. 7)	1.00	0.88
Hammer (Delmag D 22 vs. MKT DE 30)	0.45	1.25
Hammer efficiency (0.6 vs. 0.8)	1.50	0.95
Toe Quake (0.12" vs. 0.10")	1.00	1.00
Shaft Quake (0.08" vs. 0.10")	1.00	0.98
Toe Damping (0.20s/ft vs. 0.10s/ft)	1.06	1.01
Shaft Damping (0.08s/ft vs. 0.05s/ft)	1.15	1.04
Residual stress analysis	0.80	1.07

would be 55% of the blow count in the standard case and peak stress would be 31% greater than the peak stress in the standard case.

Plots similar to those discussed in the preceding section can be generated for a series of depths (driveability study: Section 2.4) using only the parameters for the standard case. These plots can then be used in conjunction with the adjustment factors, for the parameters of interest, for comparison with the blow-count *versus* depth data being recorded on the driving logs. Such a comparison would enable the engineer in the field to assess the parameters being obtained, at several stages during the driving, by selecting the bearing curves which most closely match the field bearing curves. This would help in estimating when the shell has reached required capacity and provide information about the stresses occurring in the shell. This would also indicate the potential for any problems such as excessively high stresses, which might occur at a later stage in the driving, so that they might be avoided or at least partially mitigated by adjusting driving criteria.



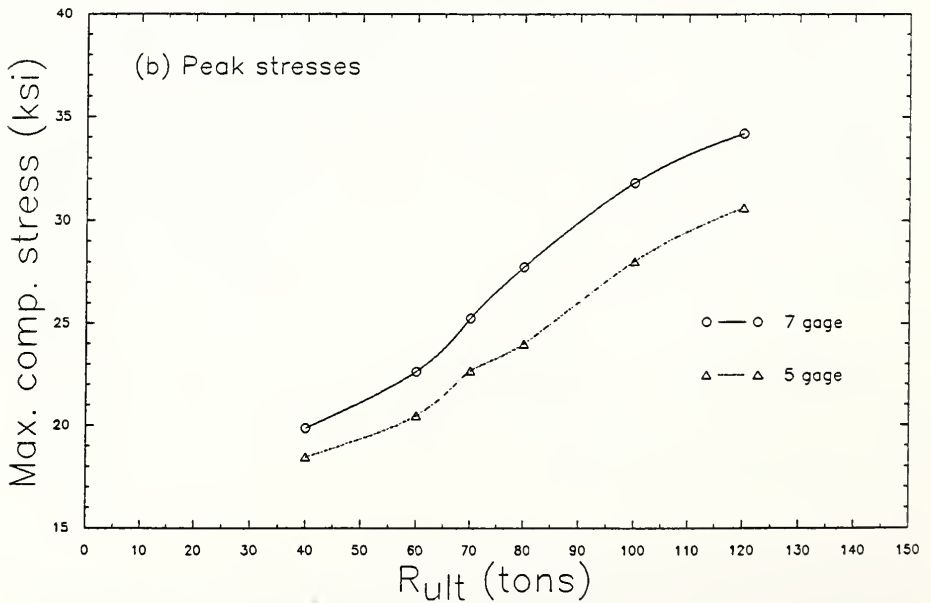
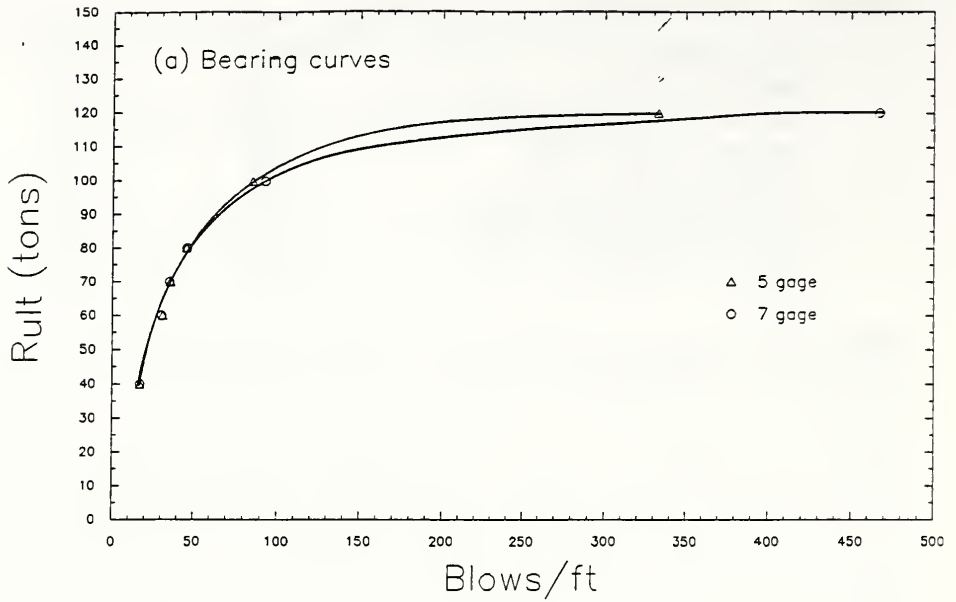


Figure 2.5 Variation in thin shell gage

Section 2.3 Example - SR1 (TB-2) Case00

R ULT	BL CT	STROKE (FT)		MINSTR	I,J	MAXSTR	I,J	ENTHRU	BL RT
KIPS	BPF	DOWN	UP	KSI		KSI		FT-KIP	BPM
88.0	16.9	4.3	4.3	-0.74	( 4,380)	19.85	( 2,102)	8.1	56.1
132.0	30.3	4.7	4.9	-1.43	( 4,337)	22.61	( 4,106)	7.5	53.5
154.0	35.3	5.2	5.0	-1.69	( 4,294)	25.23	( 4,120)	8.2	51.8
176.0	45.7	5.5	5.4	-1.61	( 4,275)	27.75	( 4,122)	8.4	50.3
220.0	92.4	6.0	5.9	-2.69	( 4,253)	31.82	( 4,122)	8.8	48.3
264.0	467.0	6.2	6.3	-3.33	( 4,246)	34.19	( 4,121)	8.9	47.0

Sec. 2.3 Example-SR1(TB-2) 5-gage Case15

R ULT	BL CT	STROKE (FT)		MINSTR	I,J	MAXSTR	I,J	ENTHRU	BL RT
KIPS	BPF	DOWN	UP	KSI		KSI		FT-KIP	BPM
88.0	17.0	4.4	4.4	-0.71	( 4,374)	18.46	( 3,101)	7.9	56.1
132.0	30.9	4.7	4.9	-1.36	( 4,337)	20.45	( 4,101)	7.2	53.3
154.0	35.7	5.2	5.1	-1.60	( 4,294)	22.65	( 4,101)	7.8	51.5
176.0	45.5	5.5	5.4	-1.26	( 4,268)	23.99	( 4,102)	8.0	50.3
220.0	85.1	5.9	5.9	-2.56	( 4,248)	28.03	( 4,122)	8.3	48.4
264.0	332.6	6.1	6.4	-3.18	( 4,238)	30.61	( 4,122)	8.4	47.0

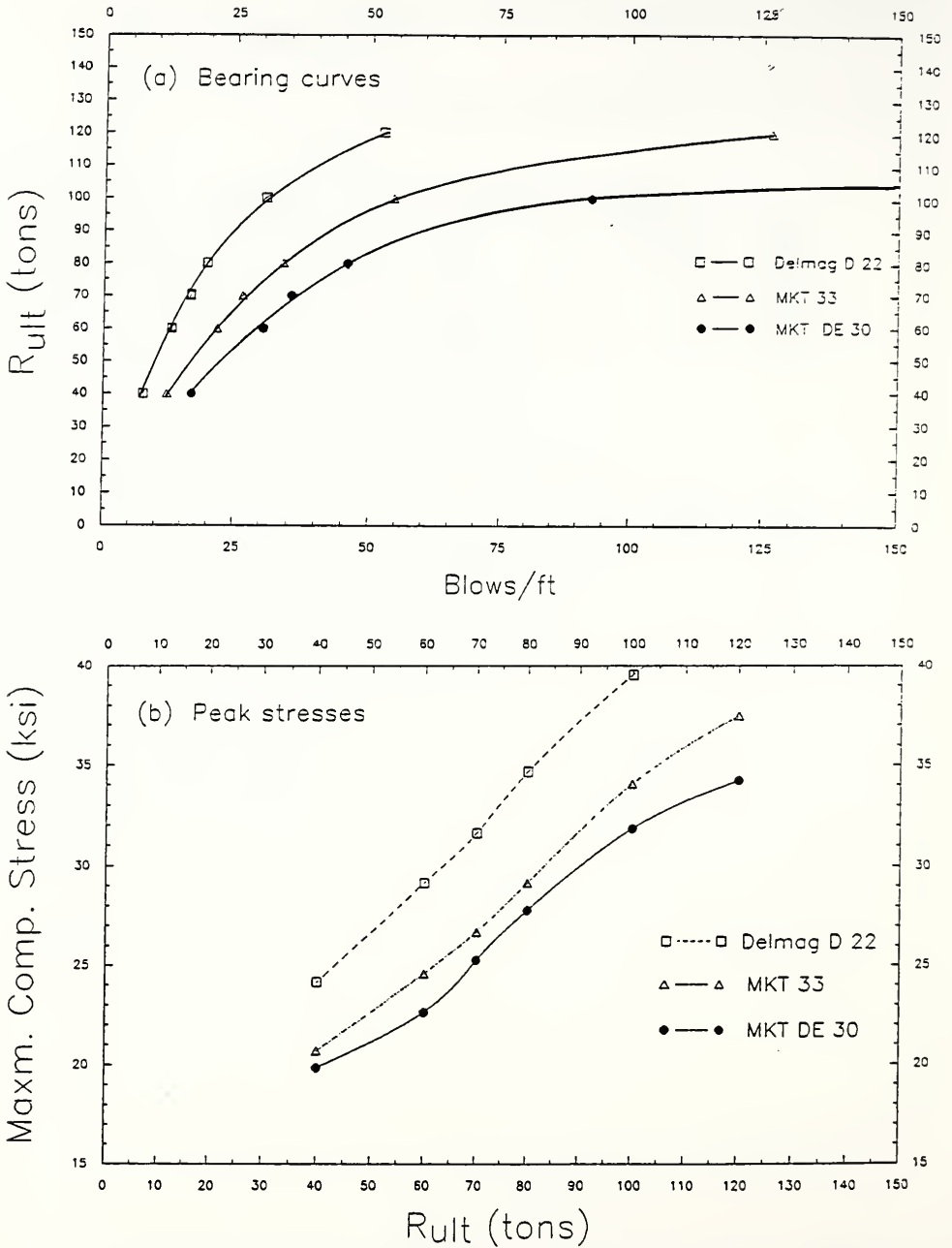


Figure 2.6 Comparison of different hammers

Section 2.3 Example - SR1 (TB-2) Case00

R ULT	BL CT	STROKE	(FT)	MINSTR	I,J	MAXSTR	I,J	ENTHRU	BL RT
KIPS	BPF	DOWN	UP	KSI		KSI		FT-KIP	BPM
88.0	16.9	4.3	4.3	-.74	( 4,380)	19.85	( 2,102)	8.1	56.1
132.0	30.3	4.7	4.9	-1.43	( 4,337)	22.61	( 4,106)	7.5	53.5
154.0	35.3	5.2	5.0	-1.69	( 4,294)	25.23	( 4,120)	8.2	51.8
176.0	45.7	5.5	5.4	-1.61	( 4,275)	27.75	( 4,122)	8.4	50.3
220.0	92.4	6.0	5.9	-2.69	( 4,253)	31.82	( 4,122)	8.8	48.3
264.0	467.0	6.2	6.3	-3.33	( 4,246)	34.19	( 4,121)	8.9	47.0

Section 2.3 Example - SR1 (TB-2) Case01

R ULT	BL CT	STROKE	(FT)	MINSTR	I,J	MAXSTR	I,J	ENTHRU	BL RT
KIPS	BPF	DOWN	UP	KSI		KSI		FT-KIP	BPM
88.0	12.2	5.3	5.4	-.52	( 4,340)	20.69	( 4, 80)	10.9	50.5
132.0	21.7	6.0	6.1	-1.41	( 4,285)	24.56	( 4, 78)	10.3	47.7
154.0	26.5	6.3	6.3	-1.59	( 4,265)	26.67	( 4, 96)	10.4	46.7
176.0	33.9	6.5	6.6	-1.47	( 4,243)	29.12	( 4, 97)	10.3	45.9
220.0	54.2	7.2	7.1	-2.00	( 4,215)	34.04	( 4, 98)	10.9	44.0
264.0	126.5	7.5	7.7	-2.99	( 4,204)	37.44	( 4, 97)	11.1	42.8

Section 2.3 Example - SR1 (TB-2) Case02

R ULT	BL CT	STROKE	(FT)	MINSTR	I,J	MAXSTR	I,J	ENTHRU	BL RT
KIPS	BPF	DOWN	UP	KSI		KSI		FT-KIP	BPM
88.0	7.6	3.2	3.2	.00	( 1, 0)	24.15	( 1,100)	17.7	64.8
132.0	13.0	3.9	3.7	-.60	( 4,352)	29.13	( 1,100)	16.8	59.6
154.0	16.6	4.0	4.1	.00	( 1, 0)	31.59	( 4,109)	15.7	58.0
176.0	19.7	4.3	4.2	-1.34	( 4,320)	34.65	( 4,109)	15.6	56.6
220.0	30.7	4.6	4.6	-1.66	( 4,289)	39.53	( 4,111)	15.0	54.5
264.0	52.3	5.0	5.0	-2.58	( 4,268)	43.56	( 4,110)	15.0	52.2

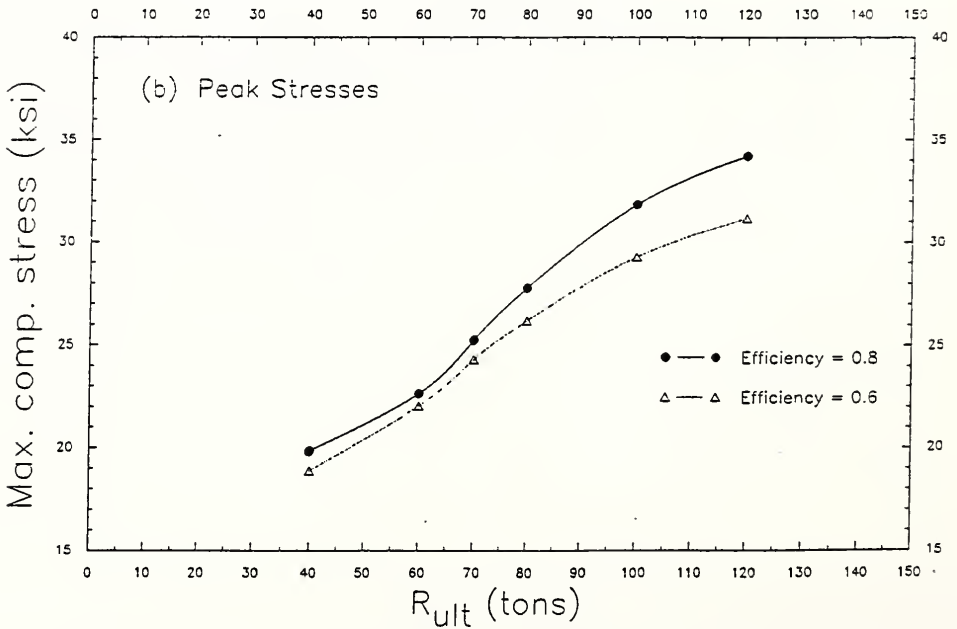
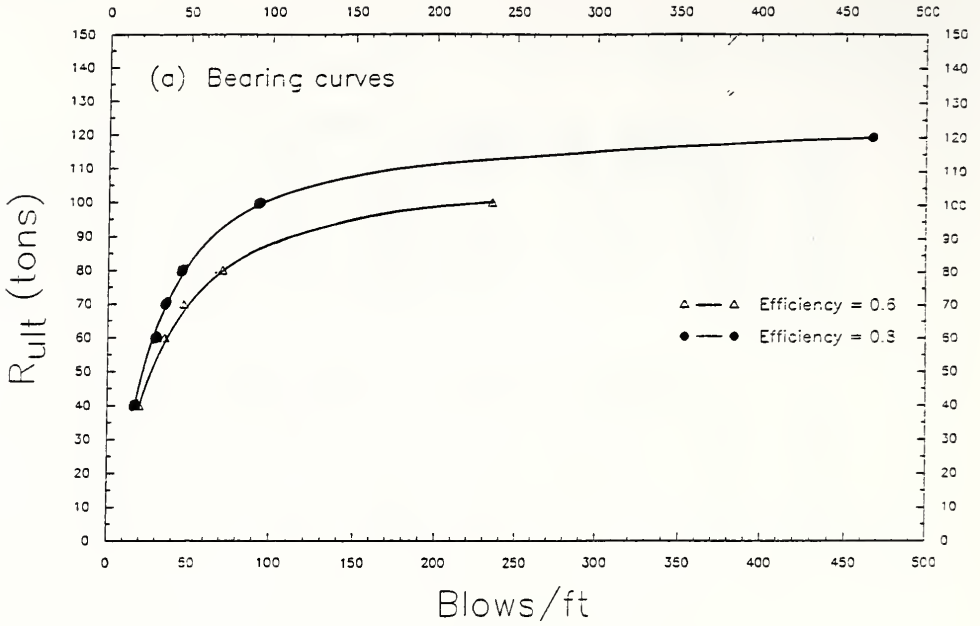


Figure 2.7 Variation in hammer efficiency

Section 2.3 Example - SR1 (TB-2) Case00										
KIPS	R ULT	BL CT	STROKE	(FT)	MINSTR	I,J	MAXSTR	I,J	ENTHRU	BL
	BPF	DOWN	UP	KSI					FT-KIP	BPM
	88.0	16.9	4.3	4.3	-0.74	( 4,380)	19.85	( 2,102)	8.1	5
	132.0	30.3	4.7	4.9	-1.43	( 4,337)	22.61	( 4,106)	7.5	5
	154.0	35.3	5.2	5.0	-1.69	( 4,294)	25.23	( 4,120)	8.2	5
	176.0	45.7	5.5	5.4	-1.61	( 4,275)	27.75	( 4,122)	8.4	5
	220.0	92.4	6.0	5.9	-2.69	( 4,253)	31.82	( 4,122)	8.8	4
	264.0	467.0	6.2	6.3	-3.33	( 4,246)	34.19	( 4,121)	8.9	4

Section 2.3 Example - SR1 (TB-2) Case20										
KIPS	R ULT	BL CT	STROKE	(FT)	MINSTR	I,J	MAXSTR	I,J	ENTHRU	BL RT
	BPF	DOWN	UP	KSI					FT-KIP	BPM
	88.0	19.8	4.5	4.5	-0.91	( 4,386)	18.88	( 2,111)	6.9	5
	132.0	35.2	5.1	5.0	-1.05	( 4,320)	22.01	( 3,112)	6.6	5
	154.0	46.7	5.4	5.3	-1.67	( 4,296)	24.28	( 4,128)	6.7	5
	176.0	70.8	5.6	5.5	-1.63	( 4,277)	26.17	( 4,130)	6.6	4
	220.0	234.3	6.0	6.0	-2.72	( 4,261)	29.26	( 4,129)	6.9	4
	264.0	9999.0	6.2	6.2	-3.09	( 4,255)	31.15	( 4,128)	6.9	4

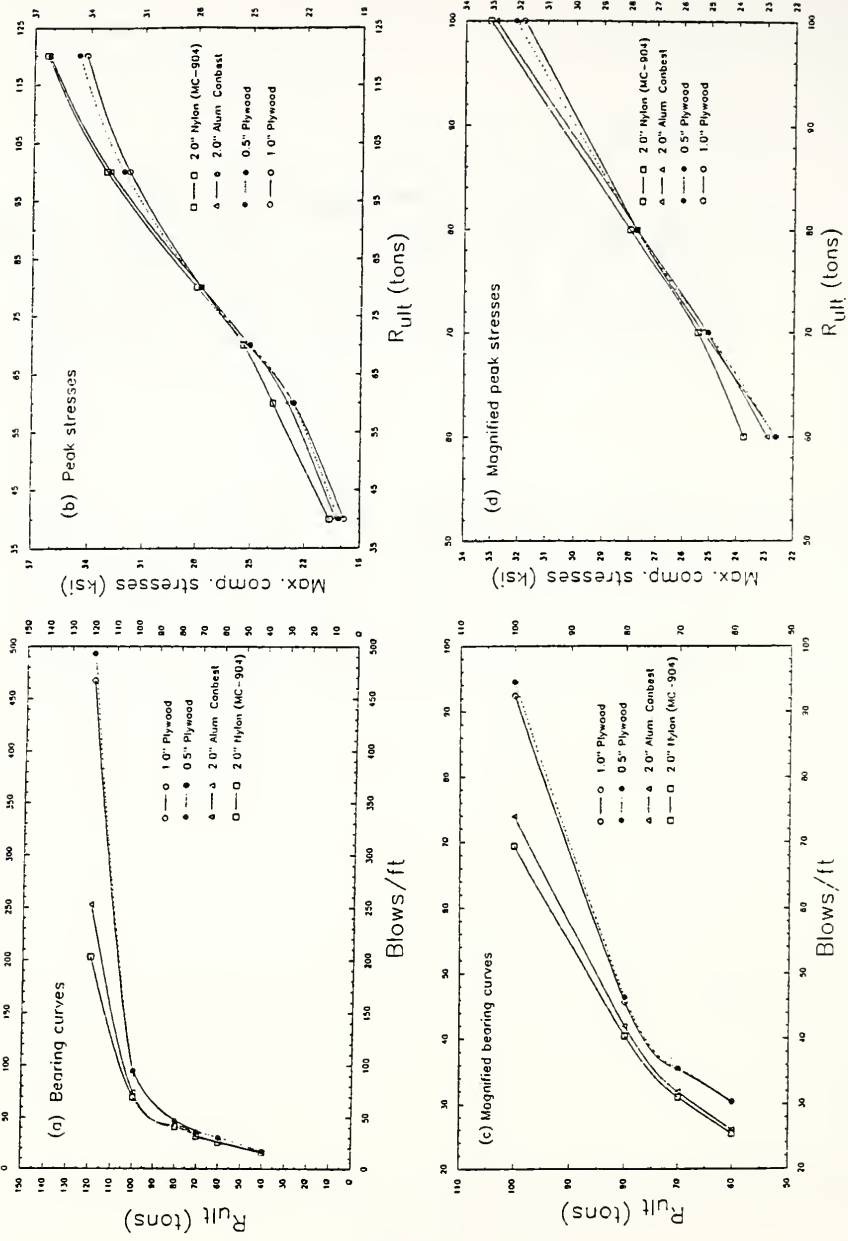


Figure 2.8 Comparison of different hammer cushions



Section 2.3 Example - SR1 (TB-2) Case00

R ULT	BL CT	STROKE (FT)	MINSTR	I,J	MAXSTR	I,J	ENTHRU	BL RT
KIPS	BPF	DOWN	UP	KSI	KSI		FT-KIP	BPM
88.0	16.9	4.3	4.3	-0.74	( 4,380)	19.85	( 2,102)	8.1 56.1
132.0	30.3	4.7	4.9	-1.43	( 4,337)	22.61	( 4,106)	7.5 53.5
154.0	35.3	5.2	5.0	-1.69	( 4,294)	25.23	( 4,120)	8.2 51.8
176.0	45.7	5.5	5.4	-1.61	( 4,275)	27.75	( 4,122)	8.4 50.3
220.0	92.4	6.0	5.9	-2.69	( 4,253)	31.82	( 4,122)	8.8 48.3
264.0	467.0	6.2	6.3	-3.33	( 4,246)	34.19	( 4,121)	8.9 47.0

Section 2.3 Example - SR1 (TB-2) Case03

R ULT	BL CT	STROKE (FT)	MINSTR	I,J	MAXSTR	I,J	ENTHRU	BL RT
KIPS	BPF	DOWN	UP	KSI	KSI		FT-KIP	BPM
88.0	16.9	4.3	4.3	-1.00	( 4,378)	20.15	( 4, 99)	8.1 56.4
132.0	30.4	4.7	4.8	-1.53	( 4,331)	22.65	( 4, 99)	7.5 53.7
154.0	35.5	5.2	5.0	-1.47	( 4,291)	25.05	( 4,122)	8.2 52.0
176.0	46.4	5.4	5.4	-1.74	( 4,271)	27.79	( 4,122)	8.3 50.5
220.0	94.5	5.9	5.9	-2.77	( 4,251)	32.14	( 4,122)	8.7 48.5
264.0	492.9	6.1	6.3	-3.38	( 4,245)	34.60	( 4,122)	8.8 47.2

Section 2.3 Example - SR1 (TB-2) Case04

R ULT	BL CT	STROKE (FT)	MINSTR	I,J	MAXSTR	I,J	ENTHRU	BL RT
KIPS	BPF	DOWN	UP	KSI	KSI		FT-KIP	BPM
88.0	15.8	4.2	4.2	-0.88	( 4,364)	20.28	( 4, 86)	8.8 57.1
132.0	26.0	4.7	4.7	-1.51	( 4,312)	22.93	( 2,102)	8.8 54.1
154.0	31.9	5.0	4.9	-1.51	( 4,287)	25.09	( 4,115)	9.1 52.9
176.0	42.0	5.1	5.1	-1.98	( 4,260)	27.74	( 4,115)	9.0 51.8
220.0	73.9	5.6	5.5	-3.14	( 4,241)	32.87	( 4,115)	9.7 49.8
264.0	252.8	5.9	6.0	-3.76	( 4,231)	36.20	( 4,115)	9.9 48.2

Section 2.3 Example - SR1 (TB-2) Case05

R ULT	BL CT	STROKE (FT)	MINSTR	I,J	MAXSTR	I,J	ENTHRU	BL RT
KIPS	BPF	DOWN	UP	KSI	KSI		FT-KIP	BPM
88.0	15.6	4.3	4.3	-0.90	( 4,372)	20.62	( 4, 98)	8.9 56.5
132.0	25.4	4.8	4.8	-1.57	( 4,329)	23.76	( 4, 99)	8.9 53.5
154.0	31.1	5.1	5.0	-1.59	( 4,288)	25.44	( 4,100)	9.1 52.2
176.0	40.5	5.2	5.3	-1.86	( 4,265)	28.01	( 4,118)	9.1 51.2
220.0	69.4	5.8	5.7	-3.05	( 4,246)	33.07	( 4,118)	9.8 49.1
264.0	202.9	6.1	6.2	-3.74	( 4,237)	36.30	( 4,119)	10.1 47.6

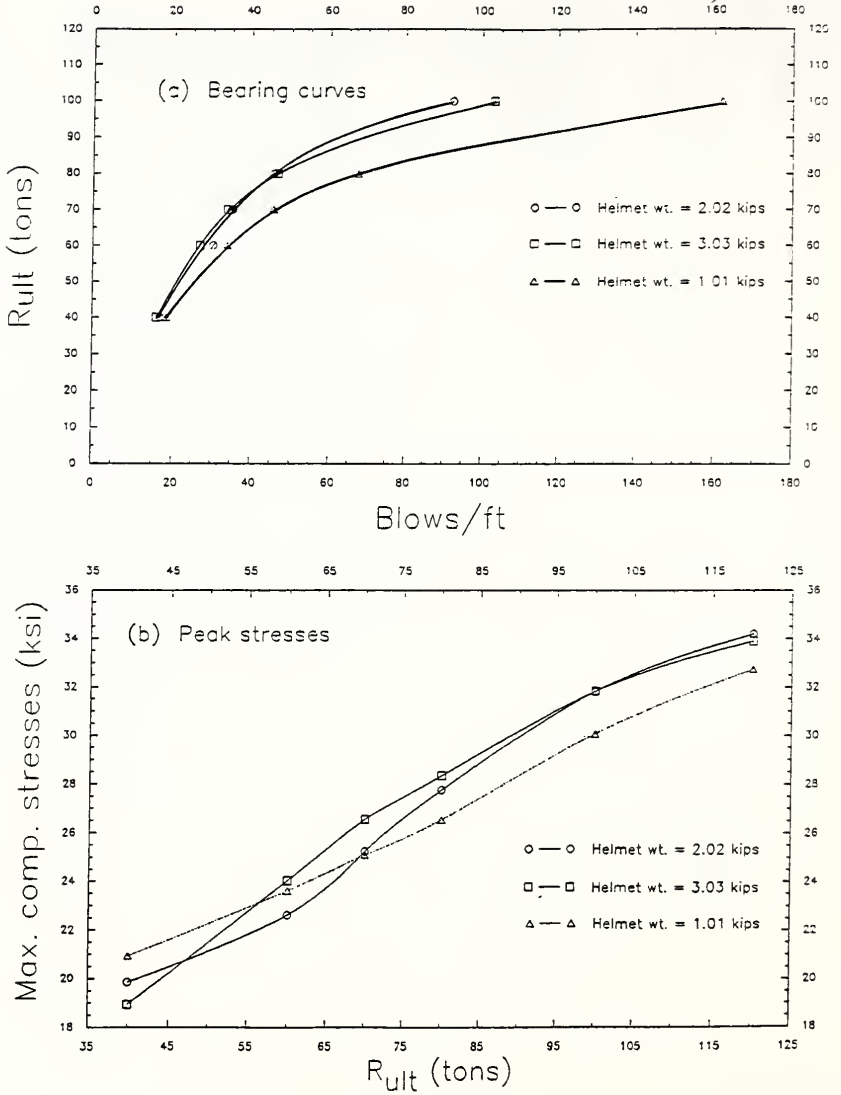


Figure 2.9 Variation in helmet weight

## Section 2.3 Example - SR1 (TB-2) Case00

R ULT	BL CT	STROKE (FT)		MINSTR	I,J	MAXSTR	I,J	ENTHRU	BL RT
KIPS	BPF	DOWN	UP	KSI		KSI		FT-KIP	BPM
88.0	16.9	4.3	4.3	-0.74	( 4,380)	19.85	( 2,102)	8.1	56.1
132.0	30.3	4.7	4.9	-1.43	( 4,337)	22.61	( 4,106)	7.5	53.5
154.0	35.3	5.2	5.0	-1.69	( 4,294)	25.23	( 4,120)	8.2	51.8
176.0	45.7	5.5	5.4	-1.61	( 4,275)	27.75	( 4,122)	8.4	50.3
220.0	92.4	6.0	5.9	-2.69	( 4,253)	31.82	( 4,122)	8.8	48.3
264.0	467.0	6.2	6.3	-3.33	( 4,246)	34.19	( 4,121)	8.9	47.0

## Section 2.3 Example - SR1 (TB-2) Case21

R ULT	BL CT	STROKE (FT)		MINSTR	I,J	MAXSTR	I,J	ENTHRU	BL RT
KIPS	BPF	DOWN	UP	KSI		KSI		FT-KIP	BPM
88.0	18.5	4.5	4.6	-0.32	( 4,342)	20.94	( 4, 63)	7.5	54.8
132.0	33.9	5.2	5.2	-0.86	( 4,319)	23.61	( 4, 62)	7.1	51.5
154.0	45.6	5.5	5.6	-0.20	( 4,276)	25.09	( 3, 99)	7.2	49.6
176.0	67.5	5.7	5.9	-0.71	( 4,278)	26.53	( 4,100)	7.2	48.9
220.0	162.0	6.4	6.5	-1.01	( 4,242)	30.07	( 4,100)	7.8	46.5
264.0	2093.3	6.7	6.8	-0.89	( 4,251)	32.73	( 4,100)	8.0	45.3

## Section 2.3 Example - SR1 (TB-2) Case22

R ULT	BL CT	STROKE (FT)		MINSTR	I,J	MAXSTR	I,J	ENTHRU	BL RT
KIPS	BPF	DOWN	UP	KSI		KSI		FT-KIP	BPM
88.0	16.0	4.2	4.2	-1.00	( 4,416)	18.94	( 2,110)	8.4	57.2
132.0	26.9	4.7	4.6	-1.58	( 4,342)	24.03	( 4,127)	8.2	54.3
154.0	34.0	5.0	4.8	-1.60	( 4,333)	26.56	( 4,128)	8.3	53.0
176.0	46.6	5.1	5.0	-1.99	( 4,295)	28.34	( 3,143)	8.2	52.1
220.0	103.2	5.4	5.4	-2.74	( 4,275)	31.83	( 4,145)	8.4	50.5
264.0	793.1	5.6	5.6	-3.54	( 4,268)	33.89	( 4,143)	8.4	49.5

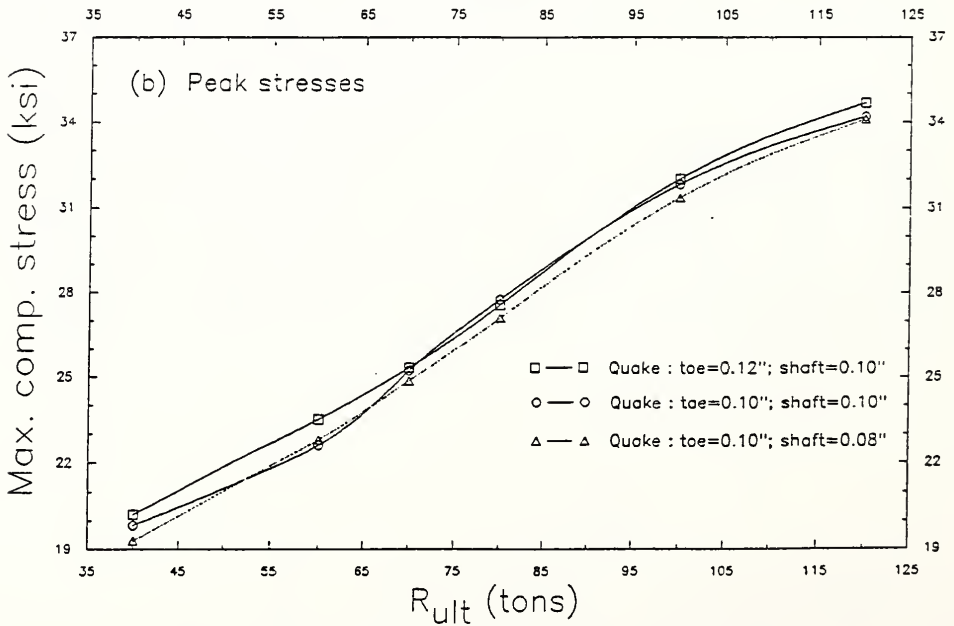
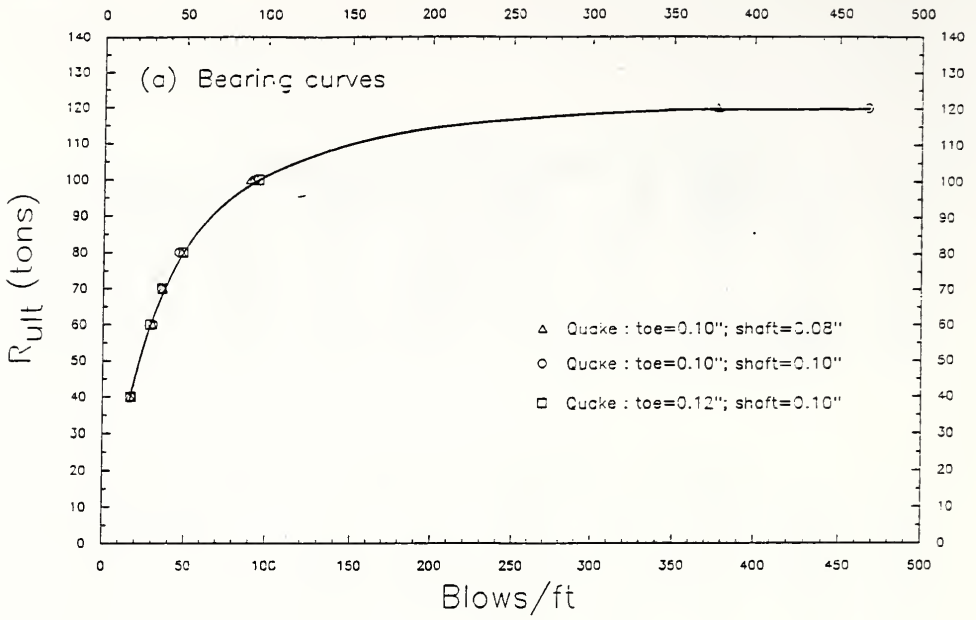


Figure 2.10 Variation in quake

Section 2.3 Example - SR1 (TB-2) Case00

R ULT	BL CT	STROKE (FT)		MINSTR	I,J	MAXSTR	I,J	ENTHRU	BL RT
KIPS	BPF	DOWN	UP	KSI		KSI		FT-KIP	BPM
88.0	16.9	4.3	4.3	-0.74	( 4,380)	19.85	( 2,102)	8.1	56.1
132.0	30.3	4.7	4.9	-1.43	( 4,337)	22.61	( 4,106)	7.5	53.5
154.0	35.3	5.2	5.0	-1.69	( 4,294)	25.23	( 4,120)	8.2	51.8
176.0	45.7	5.5	5.4	-1.61	( 4,275)	27.75	( 4,122)	8.4	50.3
220.0	92.4	6.0	5.9	-2.69	( 4,253)	31.82	( 4,122)	8.8	48.3
264.0	467.0	6.2	6.3	-3.33	( 4,246)	34.19	( 4,121)	8.9	47.0

Section 2.3 Example - SR1 (TB-2) Case13

R ULT	BL CT	STROKE (FT)		MINSTR	I,J	MAXSTR	I,J	ENTHRU	BL RT
KIPS	BPF	DOWN	UP	KSI		KSI		FT-KIP	BPM
88.0	16.7	4.4	4.4	-0.81	( 4,374)	19.30	( 3,103)	8.0	56.0
132.0	29.9	4.7	4.9	-1.31	( 4,330)	22.80	( 4,104)	7.5	53.5
154.0	35.9	5.1	5.1	-1.63	( 4,292)	24.87	( 4,104)	7.9	51.9
176.0	47.6	5.3	5.4	-1.70	( 4,288)	27.09	( 4,122)	8.0	50.7
220.0	89.8	5.9	5.9	-2.41	( 4,253)	31.35	( 4,122)	8.6	48.3
264.0	377.3	6.2	6.3	-3.18	( 4,247)	34.10	( 4,122)	8.8	47.0

Section 2.3 Example - SR1 (TB-2) Case14

R ULT	BL CT	STROKE (FT)		MINSTR	I,J	MAXSTR	I,J	ENTHRU	BL RT
KIPS	BPF	DOWN	UP	KSI		KSI		FT-KIP	BPM
88.0	17.0	4.3	4.3	-0.79	( 4,390)	20.23	( 3,105)	8.1	56.2
132.0	28.3	4.9	4.9	-1.02	( 4,322)	23.51	( 3,103)	8.1	52.9
154.0	35.4	5.2	5.1	-1.72	( 4,294)	25.34	( 4,121)	8.3	51.5
176.0	48.4	5.4	5.4	-1.73	( 4,276)	27.55	( 4,122)	8.2	50.4
220.0	94.8	6.0	5.9	-2.93	( 4,257)	32.01	( 4,124)	8.9	48.2
264.0	514.8	6.3	6.3	-3.57	( 4,248)	34.68	( 4,122)	9.1	46.8

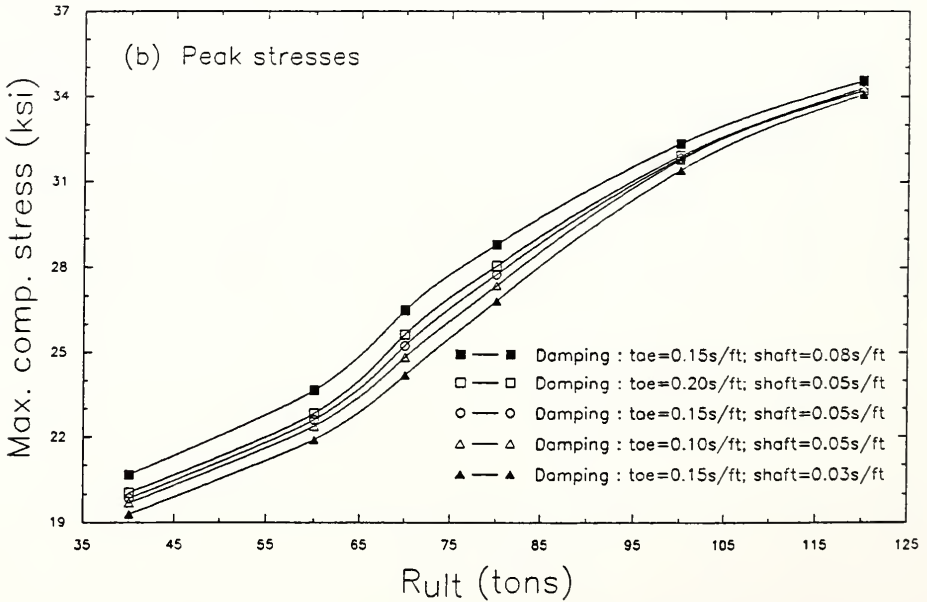
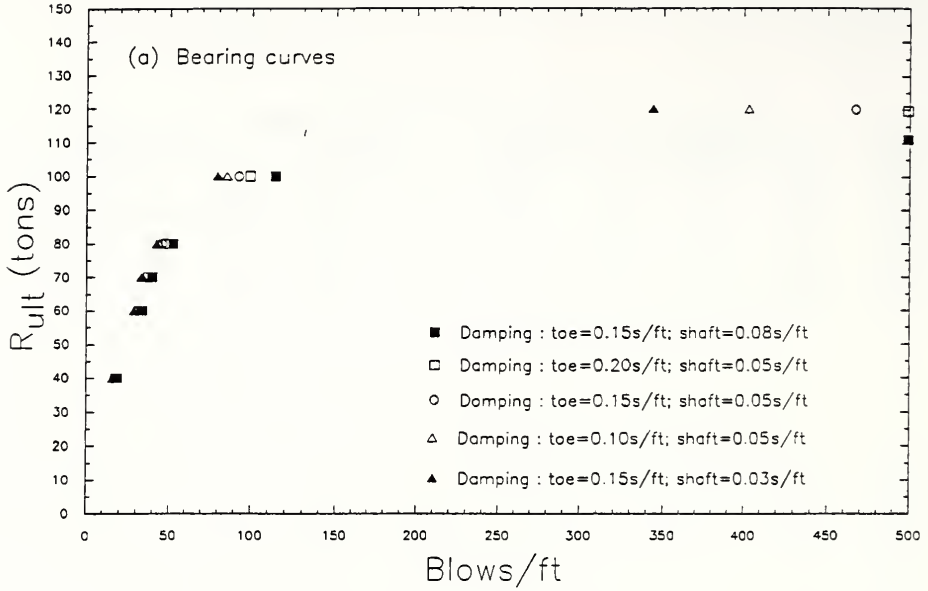


Figure 2.11 Effect of variation in damping

## Section 2.3 Example - SR1 (TB-2) Case00

R ULT	BL CT	STROKE (FT)		MINSTR	I,J	MAXSTR	I,J	ENTHRU	BL RT
KIPS	BPF	DOWN	UP	KSI		KSI		FT-KIP	BPM
88.0	16.9	4.3	4.3	-0.74	( 4,380)	19.85	( 2,102)	8.1	56.1
132.0	30.3	4.7	4.9	-1.43	( 4,337)	22.61	( 4,106)	7.5	53.5
154.0	35.3	5.2	5.0	-1.69	( 4,294)	25.23	( 4,120)	8.2	51.8
176.0	45.7	5.5	5.4	-1.61	( 4,275)	27.75	( 4,122)	8.4	50.3
220.0	92.4	6.0	5.9	-2.69	( 4,253)	31.82	( 4,122)	8.8	48.3
264.0	467.0	6.2	6.3	-3.33	( 4,246)	34.19	( 4,121)	8.9	47.0

## Section 2.3 Example - SR1 (TB-2) Case08

R ULT	BL CT	STROKE (FT)		MINSTR	I,J	MAXSTR	I,J	ENTHRU	BL RT
KIPS	BPF	DOWN	UP	KSI		KSI		FT-KIP	BPM
88.0	16.2	4.3	4.3	-0.59	( 4,380)	19.69	( 2,102)	8.1	56.3
132.0	29.2	4.7	4.8	-1.70	( 4,339)	22.38	( 4,105)	7.5	53.7
154.0	33.8	5.2	5.0	-1.67	( 4,297)	24.82	( 4,104)	8.2	52.0
176.0	43.7	5.4	5.4	-1.46	( 4,280)	27.35	( 4,122)	8.3	50.5
220.0	85.3	5.9	5.9	-2.47	( 4,253)	31.77	( 4,123)	8.7	48.4
264.0	403.1	6.2	6.3	-3.15	( 4,246)	34.28	( 4,122)	8.9	47.0

## Section 2.3 Example - SR1 (TB-2) Case09

R ULT	BL CT	STROKE (FT)		MINSTR	I,J	MAXSTR	I,J	ENTHRU	BL RT
KIPS	BPF	DOWN	UP	KSI		KSI		FT-KIP	BPM
88.0	17.6	4.4	4.4	-0.79	( 4,378)	20.05	( 3,104)	8.0	55.9
132.0	31.6	4.8	4.9	-1.18	( 4,335)	22.83	( 4,107)	7.5	53.3
154.0	37.0	5.3	5.2	-1.70	( 4,292)	25.63	( 4,121)	8.2	51.4
176.0	48.3	5.5	5.4	-1.84	( 4,273)	28.05	( 4,122)	8.4	50.1
220.0	99.2	6.0	5.9	-2.83	( 4,253)	31.90	( 4,122)	8.8	48.1
264.0	516.2	6.2	6.3	-3.44	( 4,247)	34.21	( 4,120)	8.9	46.9

## Section 2.3 Example - SR1 (TB-2) Case10

R ULT	BL CT	STROKE (FT)		MINSTR	I,J	MAXSTR	I,J	ENTHRU	BL RT
KIPS	BPF	DOWN	UP	KSI		KSI		FT-KIP	BPM
88.0	15.6	4.3	4.3	-0.56	( 4,386)	19.29	( 2,102)	8.2	56.5
132.0	28.3	4.7	4.8	-1.78	( 4,339)	21.90	( 4,105)	7.5	53.8
154.0	32.8	5.1	5.0	-1.62	( 4,300)	24.19	( 4,120)	8.2	52.2
176.0	42.1	5.4	5.3	-1.59	( 4,282)	26.81	( 4,122)	8.3	50.7
220.0	79.5	5.9	5.8	-2.39	( 4,254)	31.40	( 4,123)	8.8	48.5
264.0	343.4	6.2	6.3	-3.21	( 4,248)	34.06	( 4,123)	8.9	47.1

## Section 2.3 Example - SR1 (TB-2) Case11

R ULT	BL CT	STROKE (FT)		MINSTR	I,J	MAXSTR	I,J	ENTHRU	BL RT
KIPS	BPF	DOWN	UP	KSI		KSI		FT-KIP	BPM
88.0	18.7	4.4	4.4	-0.72	( 4,374)	20.68	( 3,104)	7.9	55.5
132.0	33.4	4.8	5.0	-1.11	( 4,309)	23.66	( 4,106)	7.5	53.0
154.0	39.5	5.3	5.2	-1.68	( 4,289)	26.48	( 4,121)	8.2	51.1
176.0	52.4	5.6	5.5	-1.96	( 4,270)	28.80	( 4,122)	8.4	49.9
220.0	113.8	6.0	6.0	-2.93	( 4,252)	32.33	( 4,122)	8.8	48.0
264.0	872.7	6.2	6.4	-3.38	( 4,245)	34.54	( 4,119)	8.8	46.8



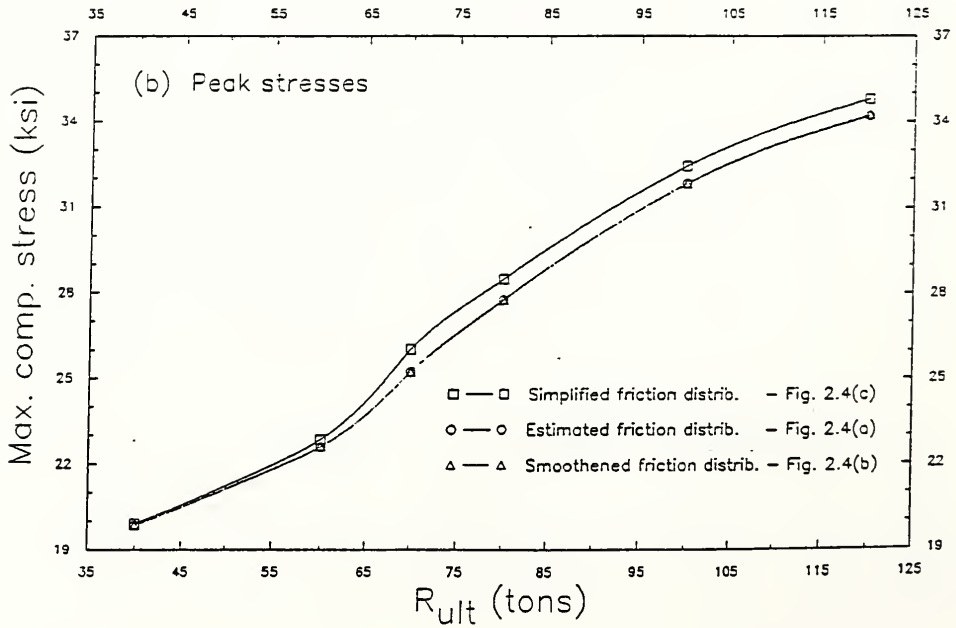
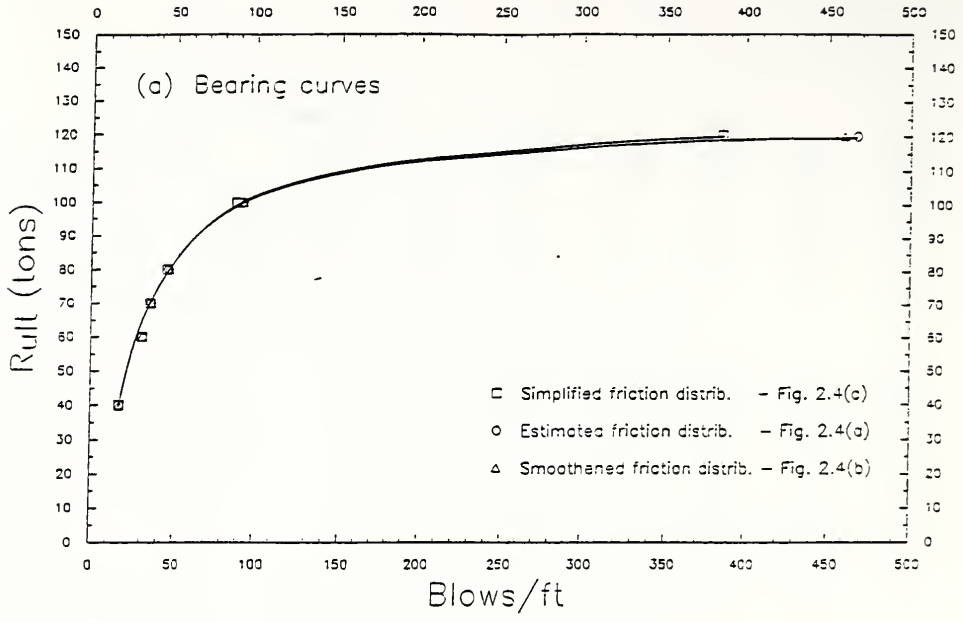


Figure 2.12 Variation in skin friction distribution

Section 2.3 Example - SR1 (TB-2) Case00

R ULT	BL CT	STROKE (FT)		MINSTR	I,J	MAXSTR	I,J	ENTHRU	BL RT
KIPS	BPF	DOWN	UP	KSI		KSI		FT-KIP	BPM
88.0	16.9	4.3	4.3	-0.74	( 4,380)	19.85	( 2,102)	8.1	56.1
132.0	30.3	4.7	4.9	-1.43	( 4,337)	22.61	( 4,106)	7.5	53.5
154.0	35.3	5.2	5.0	-1.69	( 4,294)	25.23	( 4,120)	8.2	51.8
176.0	45.7	5.5	5.4	-1.61	( 4,275)	27.75	( 4,122)	8.4	50.3
220.0	92.4	6.0	5.9	-2.69	( 4,253)	31.82	( 4,122)	8.8	48.3
264.0	467.0	6.2	6.3	-3.33	( 4,246)	34.19	( 4,121)	8.9	47.0

Section 2.3 Example - SR1 (TB-2) Case06

R ULT	BL CT	STROKE (FT)		MINSTR	I,J	MAXSTR	I,J	ENTHRU	BL RT
KIPS	BPF	DOWN	UP	KSI		KSI		FT-KIP	BPM
88.0	16.9	4.3	4.3	-0.73	( 4,380)	19.85	( 2,102)	8.1	56.1
132.0	30.3	4.7	4.9	-1.44	( 4,337)	22.63	( 4,105)	7.5	53.5
154.0	35.4	5.2	5.1	-1.70	( 4,294)	25.22	( 4,120)	8.2	51.8
176.0	46.1	5.5	5.4	-1.62	( 4,276)	27.73	( 4,123)	8.3	50.3
220.0	92.4	6.0	5.9	-2.69	( 4,254)	31.83	( 4,123)	8.8	48.2
264.0	459.3	6.2	6.3	-3.34	( 4,247)	34.24	( 4,121)	8.9	47.0

Section 2.3 Example - SR1 (TB-2) Case07

R ULT	BL CT	STROKE (FT)		MINSTR	I,J	MAXSTR	I,J	ENTHRU	BL RT
KIPS	BPF	DOWN	UP	KSI		KSI		FT-KIP	BPM
88.0	16.8	4.3	4.3	-0.70	( 4,384)	19.91	( 2,103)	8.1	56.1
132.0	30.1	4.7	4.9	-1.69	( 5,337)	22.87	( 5,115)	7.5	53.5
154.0	34.7	5.2	5.1	-1.80	( 5,300)	26.02	( 5,118)	8.3	51.6
176.0	44.8	5.5	5.4	-1.77	( 5,276)	28.48	( 5,119)	8.5	50.3
220.0	88.2	6.0	5.9	-3.11	( 5,258)	32.43	( 5,120)	8.9	48.2
264.0	384.9	6.2	6.3	-4.07	( 5,251)	34.78	( 5,119)	9.0	46.9

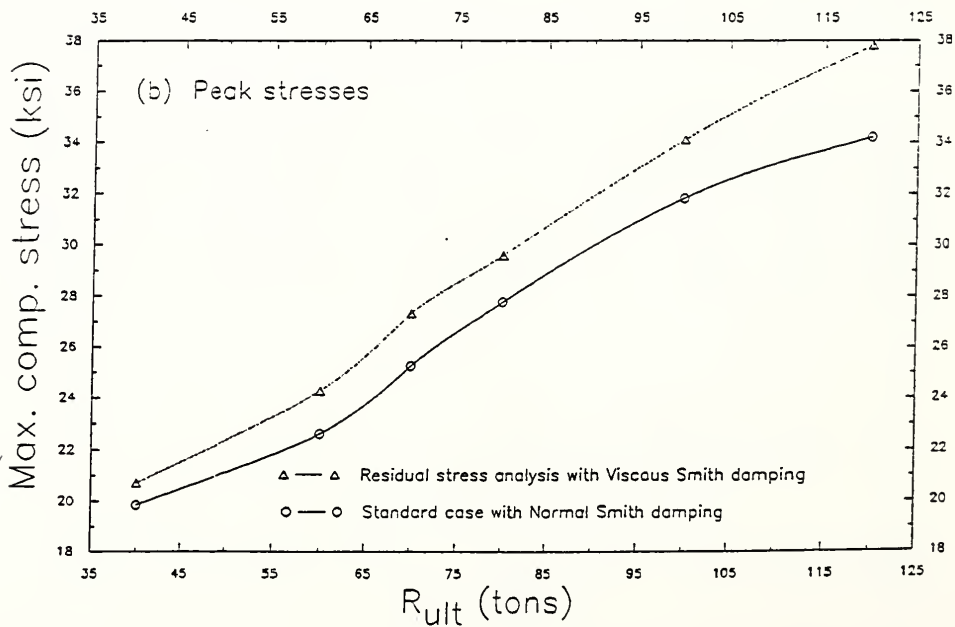
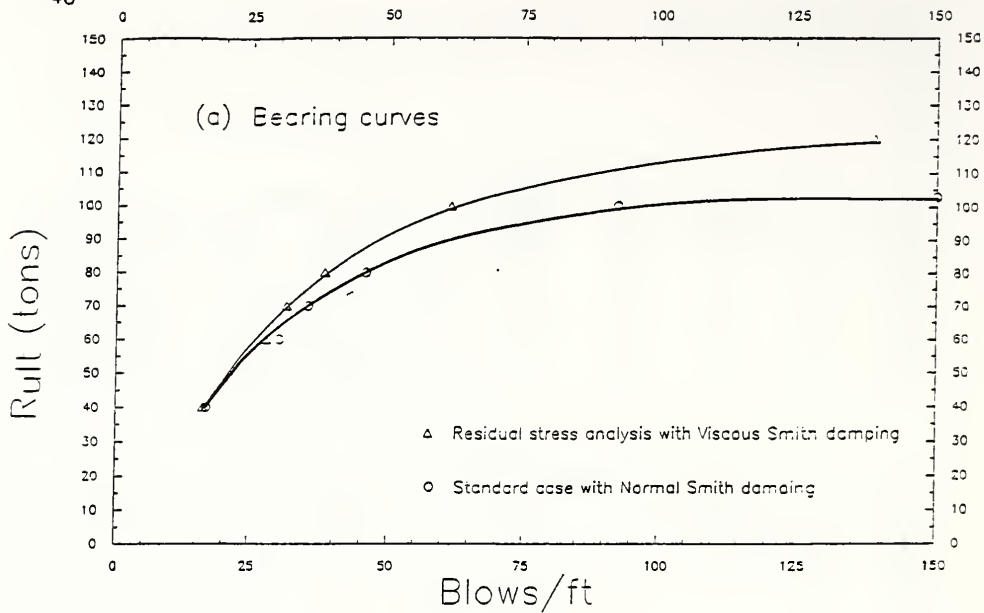


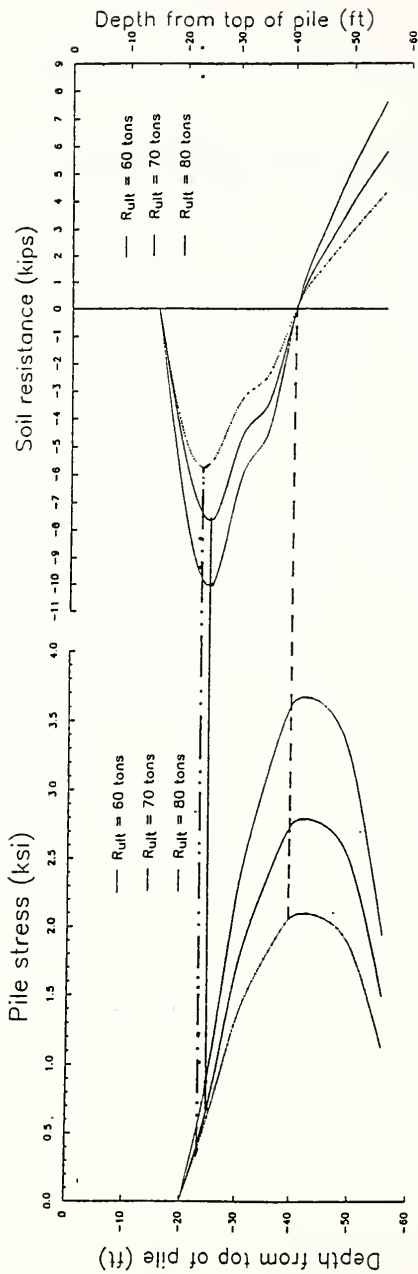
Figure 2.13 Residual stress analysis

## Section 2.3 Example - SR1 (TB-2) Case00

R ULT	BL CT	STROKE	(FT)	MINSTR	I,J	MAXSTR	I,J	ENTHRU	BL RT
KIPS	BPF	DOWN	UP	KSI		KSI		FT-KIP	BPM
88.0	16.9	4.3	4.3	-0.74	( 4,380)	19.85	( 2,102)	8.1	56.1
132.0	30.3	4.7	4.9	-1.43	( 4,337)	22.61	( 4,106)	7.5	53.5
154.0	35.3	5.2	5.0	-1.69	( 4,294)	25.23	( 4,120)	8.2	51.8
176.0	45.7	5.5	5.4	-1.61	( 4,275)	27.75	( 4,122)	8.4	50.3
220.0	92.4	6.0	5.9	-2.69	( 4,253)	31.82	( 4,122)	8.8	48.3
264.0	467.0	6.2	6.3	-3.33	( 4,246)	34.19	( 4,121)	8.9	47.0

## Sec. 2.3 RSA Example - SR1(TB-2) Case12

R ULT	BL CT	STROKE	(FT)	MINSTR	I,J	MAXSTR	I,J	ENTHRU	BL RT
KIPS	BPF	DOWN	UP	KSI		KSI		FT-KIP	BPM
88.0	16.2	4.3	4.4	-0.57	( 4,380)	20.72	( 3,104)	8.0	56.1
132.0	28.0	4.7	4.9	-1.38	( 4,336)	24.27	( 4,105)	7.4	53.4
154.0	31.5	5.2	5.1	-1.51	( 4,299)	27.31	( 4,106)	8.0	51.5
176.0	38.2	5.5	5.4	-1.26	( 4,270)	29.58	( 4,106)	8.2	50.2
220.0	61.4	6.0	6.0	-2.47	( 4,249)	34.09	( 4,119)	8.7	48.0
264.0	138.7	6.3	6.5	-3.37	( 4,240)	37.81	( 4,120)	8.7	46.5



(a) Residual pile stress distribution

(b) Residual shaft friction resistance distribution

Figure 2.14 Residual stress/force at end of analysis

Table 2.5  
Residual variables at end of analysis

From top of pile		R <sub>ult</sub> = 60t		R <sub>ult</sub> = 70t		R <sub>ult</sub> = 80t	
Element No.	Depth (ft)	Pile stress (ksf)	Soil Resistance (kips)	Pile stress (ksf)	Soil Resistance (kips)	Pile stress (ksf)	Soil Resistance (kips)
1	5.0	0.00	0.00	0.00	0.00	0.00	0.00
2	10.0	0.00	0.00	0.00	0.00	0.00	0.00
3	15.0	0.00	0.00	0.00	0.00	0.00	0.00
4	20.0	0.00	-4.80	0.00	-5.57	0.00	-7.51
5	25.0	0.62	-5.04	0.72	-6.90	0.97	-9.19
6	30.0	1.27	-3.79	1.60	-5.32	2.15	-6.92
7	35.0	1.75	-2.44	2.29	-3.47	3.04	-4.48
8	40.0	2.08	-0.27	2.74	-0.46	3.62	-0.53
9	45.0	2.10	1.77	2.80	2.35	3.69	3.08
10	50.0	1.88	3.28	2.49	4.38	3.28	5.82
11	55.5	1.11	4.39	1.47	5.85	1.93	7.63
At toe	55.5	-----	6.90	-----	9.16	-----	12.00

## 2.4 Drivability study

An example of a drivability study is presented in this section. The first step is the estimation of  $R_{ult}$  for various levels of pile toe penetration during driving. The calculations are performed at four depths ranging between 20 and 55 ft. Then the wave equation analysis is carried out to obtain bearing curves and expected maximum compressive stresses for each depth. The parameters from the standard case of Sec. 2.3.8 are used, and the skin friction along the shaft is estimated from Fig. 2.4(a). The resistance at the toe is determined from Figs. A.2(a), A.3 and A.4 using appropriate procedures similar to those used in Secs. 2.3.1 and 2.3.2. The values of IPERCS are listed in Table 2.6 along with the depth information and range in  $R_{ult}$ .

### 2.4.1 Discussion of Results

The results are plotted in a format similar to that followed in Sec. 2.3. The bearing curves are presented in Fig. 2.15 and the expected maximum compressive stresses in Fig. 2.16. As explained in Sec. 2.3.9, these results can be used to adjust the driving criteria to keep stresses within acceptable limits while achieving target penetration and bearing capacity.

Table 2.6  
 $R_{ult}$  for drivability study

Case##	Depth (ft)	$Q_{sd}$ (tons)	IPERCS (%)	Range of $R_{ult}$ (tons)				
Case16	20	4	-25	16	28	40	52	64
Case17	34	21	-100	21	28	35	42	49
Case18	42	36	-100	36	42	48	54	60
Case19	55	56	-100	56	63	70	77	84

Fig. 2.15(b) also shows best fit lines (a second order regression curve) for all of the drivability data and the standard case data (Case00). The two curves are very similar in



the range of interest and a single full penetration analysis would have sufficed to obtain an acceptable bearing curve in this case. Nevertheless, a closer look at Fig. 2.15(a) shows that there is a trend in the four sets of data. As the penetration depth increases, WEAP87 sees the shell as becoming slightly easier to drive for the same values of  $R_{ult}$ . This most likely happens because of the reduction in bearing capacity of the strata as the shell moves down. In this case the difference is not high but in cases where a much stronger strata overlies a weaker one the pile might face unexpectedly high resistance before it is driven into the weaker strata, and this could result in damaging stress levels. This is illustrated in Fig. 2.16(a) where the curve for penetration to 20 ft shows the highest stress levels because the pile toe is driven in a dense sandy gravel stratum at that stage.

#### 2.4.2 Three-dimensional representation of results

These results can be better visualized if they are presented as three-dimensional surface plots (Figs. 2.17(a) and 2.18(a)), or as contour plots (Figs. 2.17(b) and 2.18(b)). The blow count and the depth of penetration are the two primary variables which are tracked in the field during driving so these are used as the base parameters. Fig. 2.17(a) presents the same information as that in Fig. 2.15 but the variation of  $R_{ult}$  with depth and blow count can be seen clearly. Additionally, a contour plot of the ultimate capacity such as Fig. 2.17(b) - which contains the same information as Fig. 2.17(a) - can be used to obtain an estimate of  $R_{ult}$  for any observed pair of bpf and depth values. This is done by locating the two contours closest to the grid intersection point, defined by the pair of observed values, and then interpolating between the two contours. In a similar manner, Fig. 2.18 presents information about the estimated maximum compressive stresses occurring in the shell during driving.

Similar three-dimensional plots can be obtained using the adjustment factors developed in Section 2.3.9 to account for possible variations in any parameter, or set of parameters, whose values are not exactly known (estimated before driving). These plots can then be used to assess the actual stresses being generated and the  $R_{ult}$  being obtained. The plots given in Figs. 2.17 and 2.18 were generated by using standard graphics software for PC's.

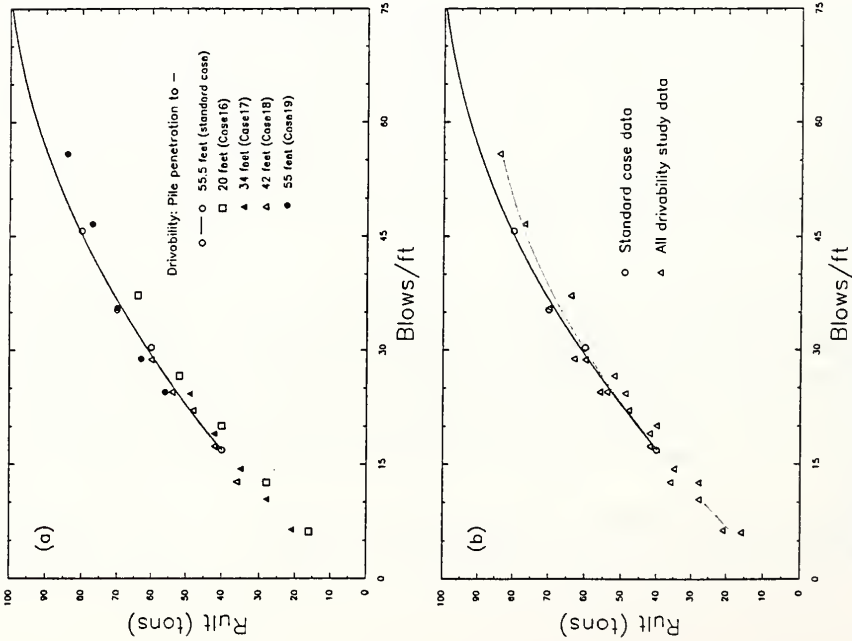


Figure 2.15 Bearing curves for drivability study (best fit lines)

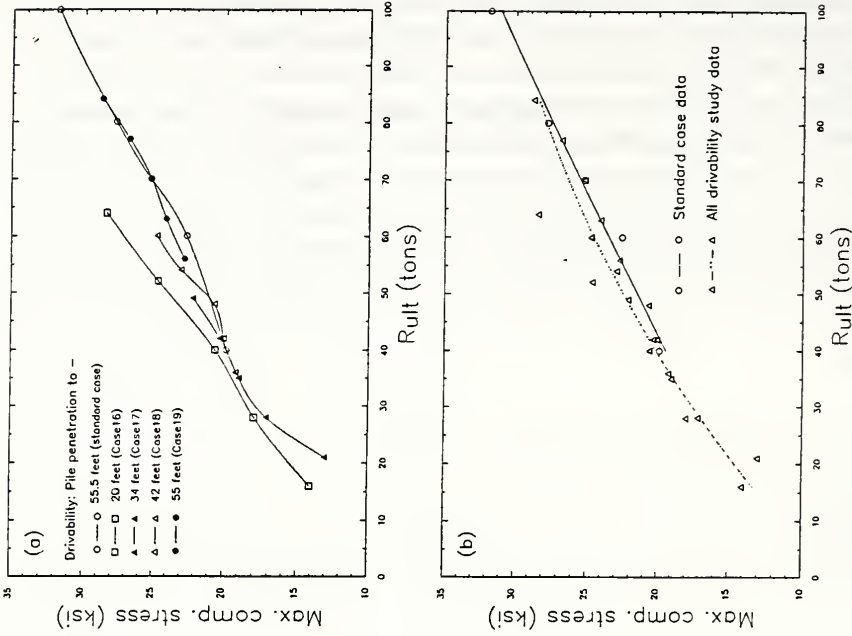


Figure 2.16 Maximum compressive stresses in drivability study

## Sec. 2.4 Drvblty:20' - SR1 (TB-2) Casel6

R ULT	BL CT	STROKE (FT)		MINSTR	I,J	MAXSTR	I,J	ENTHRU	BL RT
KIPS	BPF	DOWN	UP	KSI		KSI		FT-KIP	BPM
35.2	6.1	3.4	3.3	.00	( 1, 0)	14.06	( 1, 93)	9.9	63.6
61.6	12.6	4.0	3.9	-.64	( 6,460)	17.97	( 5,102)	8.8	58.8
88.0	20.1	4.3	4.4	-.88	( 6,377)	20.59	(10,116)	8.2	56.3
114.4	26.6	4.8	4.6	-1.66	( 6,329)	24.64	( 5,138)	8.8	53.9
140.8	37.2	5.0	5.0	-2.37	( 6,303)	28.38	( 5,139)	9.0	52.3

## Sec. 2.4 Drvblty:34' - SR1 (TB-2) Casel7

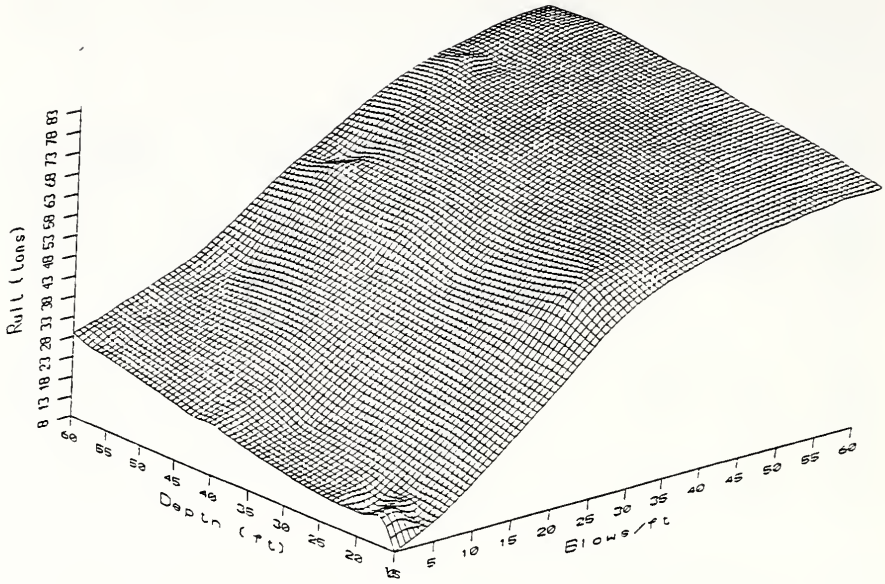
R ULT	BL CT	STROKE (FT)		MINSTR	I,J	MAXSTR	I,J	ENTHRU	BL RT
KIPS	BPF	DOWN	UP	KSI		KSI		FT-KIP	BPM
46.2	6.4	3.5	3.5	.00	( 1, 0)	13.02	( 1,106)	9.5	62.7
61.6	10.4	3.8	3.9	-1.22	( 8,488)	17.14	( 1,105)	8.7	59.4
77.0	14.4	4.2	4.1	-1.57	( 8,428)	19.01	( 3,110)	8.6	57.1
92.4	19.1	4.4	4.4	-1.91	( 8,388)	20.29	( 8,126)	8.3	55.6
107.8	24.3	4.5	4.7	-2.35	( 8,360)	22.13	( 8,124)	8.0	54.6

## Sec. 2.4 Drvblty:42' - SR1 (TB-2) Casel8

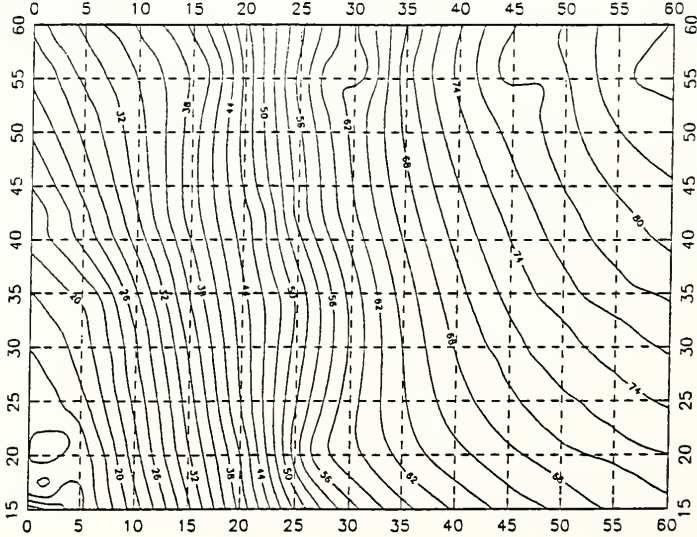
R ULT	BL CT	STROKE (FT)		MINSTR	I,J	MAXSTR	I,J	ENTHRU	BL RT
KIPS	BPF	DOWN	UP	KSI		KSI		FT-KIP	BPM
79.2	12.7	4.2	4.0	-.94	( 6,419)	19.22	( 2,105)	8.6	57.7
92.4	17.4	4.3	4.3	-1.53	( 6,390)	20.02	( 3,106)	8.2	56.1
105.6	22.1	4.4	4.6	-1.82	( 6,362)	20.66	( 3,107)	7.9	55.0
118.8	24.5	4.8	4.7	-2.59	( 6,355)	22.99	( 6,114)	8.4	53.8
132.0	28.7	5.0	4.8	-2.56	( 7,337)	24.74	( 6,115)	8.5	52.9

## Sec. 2.3 Drvblty:55' - SR1 (TB-2) Casel9

R ULT	BL CT	STROKE (FT)		MINSTR	I,J	MAXSTR	I,J	ENTHRU	BL RT
KIPS	BPF	DOWN	UP	KSI		KSI		FT-KIP	BPM
123.2	24.5	4.7	4.7	-2.08	( 4,343)	22.76	( 3,102)	7.7	53.9
138.6	28.8	5.0	4.8	-1.52	( 4,335)	24.09	( 3,103)	8.0	52.8
154.0	35.6	5.2	5.1	-1.71	( 4,295)	25.17	( 4,121)	8.1	51.6
169.4	46.6	5.3	5.4	-1.70	( 4,278)	26.79	( 4,122)	8.1	50.8
184.8	55.8	5.6	5.5	-2.12	( 4,271)	28.75	( 2,135)	8.6	49.7

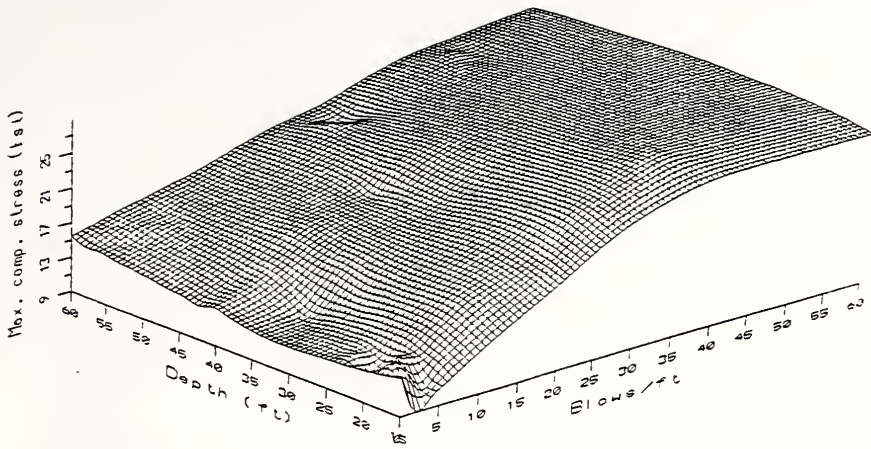


(a) Rult - Surface plot

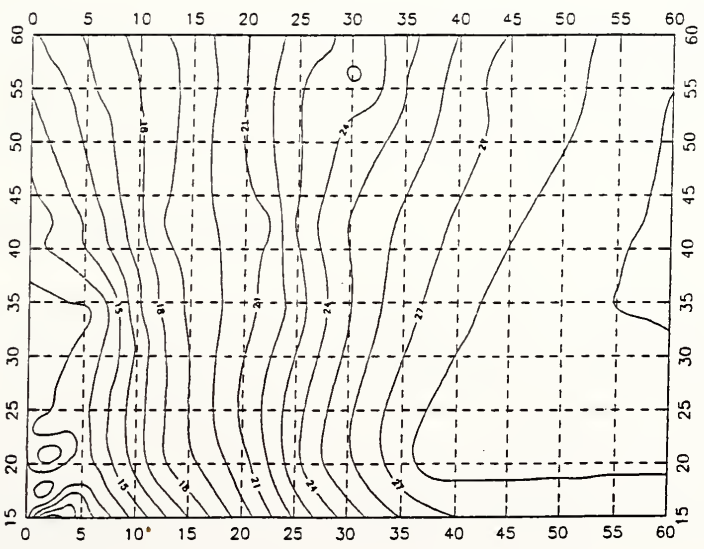


(b) Contours of Rult

Figure 2.17 Drivability study - three-dimensional representation of variation in ultimate capacity



(a) Max. comp. stress



(b) Contours of max. comp. stress

Figure 2.18 Drivability study - three-dimensional representation of variation in max. comp. stress



## EXAMPLES

### 3.1 SR26 over Coffee Run Creek

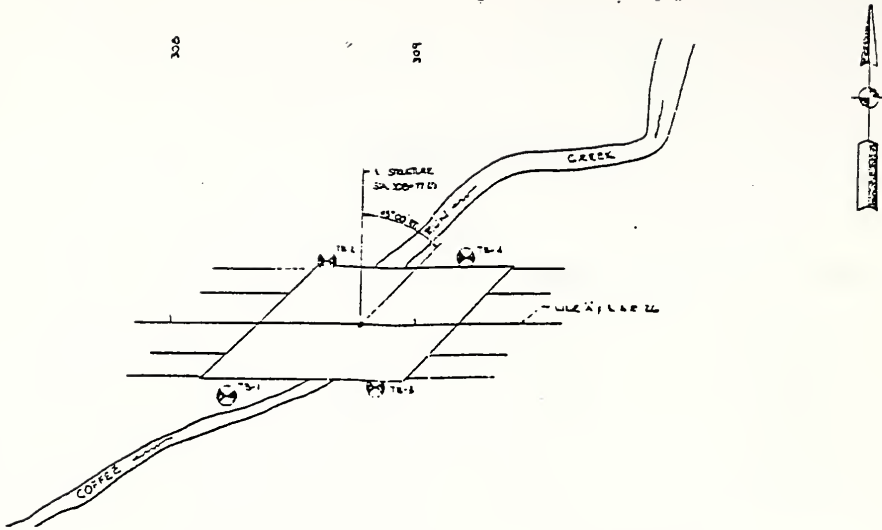
Project No:	ST-4479(A)
Contract No:	B-17432
Location:	Monitor, Tippecanoe County, Indiana
Structure:	3 span continuous reinforced concrete slab bridge
Piling done:	June, 1988

The plan layout of the four test borings (TB-1 to TB-4) used to obtain soil profiles is shown in Fig. 3.1(a). The chaining stations for these approximately match those for the piles along the roadway center line for each of the four bents (bent nos. 1 to 4 in Fig. 3.1(b)). Hence, it is assumed that the estimated soil profile from each test boring is representative of the conditions at the corresponding bent. Two examples are studied, one for piling at an end bent and one for piling at an interior bent.

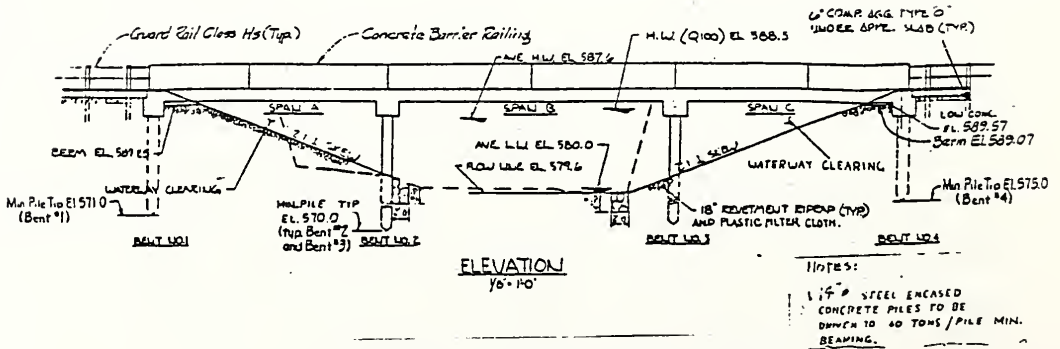
#### 3.1.1 Pile at bent number 4 (End bent)

Ground elevation at TB-4 was 582.7 ft which had been raised to 588 ft at the time of driving by placement of compacted fill. The specified minimum pile tip elevation is 575.0 ft, hence a shell length of 16 ft is used with the last 13 ft penetrating into the ground. The estimated values of  $Q_c$  and  $Q_s$  are 85 t and 20 t, respectively. These values are obtained based on the bore-hole data from TB-4. The value of  $Q_c$  is estimated assuming the pile is driven through the fill (approximate SPT value of 15), but if jetting is used to get past the fill, then  $Q_c = 13$  t. This difference is marginal and the maximum expected resistance at the toe, in the fill, is about 7 t, so no jetting needs to be done. The applicable friction distribution profile for input to WEAP87 is shown in Figure 3.2. The expected value of  $R_{ult}$  is 100 tons. Table 3.1 lists the range of  $R_{ult}$  values used for analysis.





(a) Plan layout of the four test borings (TB-1 to TB-4)



(b) Minimum pile toe elevations at each bent

Figure 3.1 Boring plan and bent location for the SR26 bridge over Coffee Run Creek



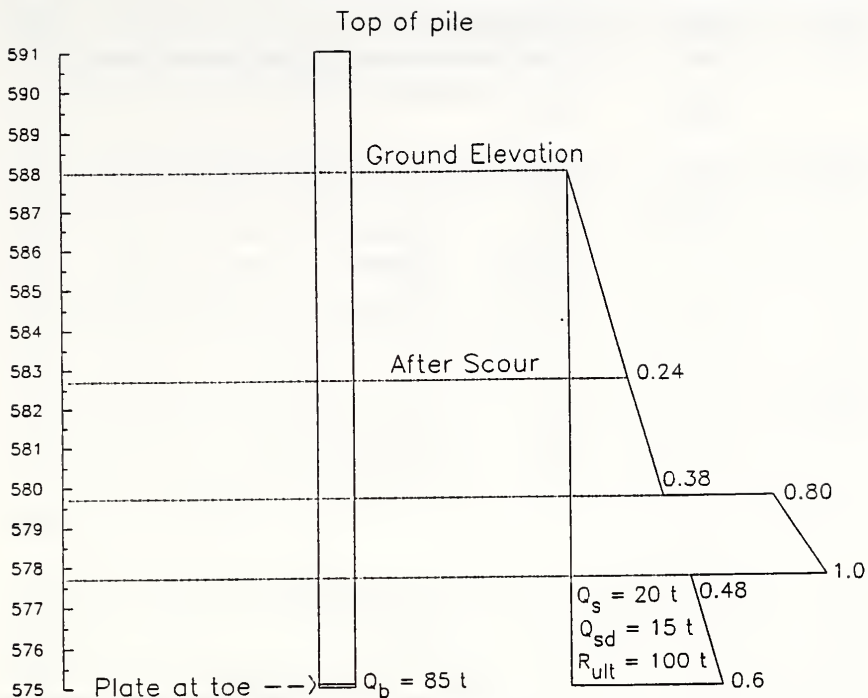


**Figure 3.2** Shaft friction distribution for bent no. 4 at State Road 26 over Coffee Run Creek

**Table 3.1**  
Range of  $R_{ult}$  : IPERCS = 20%

$R_{ult}$ (tons)	27.3	36.4	45.5	54.5	63.6	60	80	100	120	140
$R_{ult}$ (kips)	60	80	100	120	140	132	176	220	264	308
$Q_b$ (tons)	5.5	7.3	9.1	10.9	12.7	12	16	20	24	28
$Q_{sd}$ (tons)	21.8	29.1	36.4	43.6	50.9	48	64	80	96	112

The standard case (Case00) parameters are as follows:

Pile	Type	Thin steel shell		
	Gage	5 (wall thickness = 0.203"; c/s area = 8.8 in <sup>2</sup> )		
	$\phi$	14"		
	Length	16.0 ft		
Hammer	Type	Delmag D 12		
	Efficiency	0.8		
	Cushion	Area	283.5 in <sup>2</sup>	
		Material	Plywood	
		Thickness	0.75"	
Helmet	Weight	2.02 kips		
Soil Parameters	Quake	Shaft	0.1"	
		Toe	0.1"	
	Damping	Type	Smith (Normal)	
		Shaft	0.05 s/ft	
		Toe	0.15 s/ft	
$R_{ult}$	Table 3.1			
Shaft Friction	As a % of $R_{ult}$	20 (IPERCS = 20)		
	Distribution used	Fig. 3.2		

Parametric studies are conducted to assess the effects of different parameters. Only one parameter is varied at a time, with the remainder of the data identical to that of the standard case:

Pile	Gage	Case01	7 (wall thickness= 0.179"; c/s area=7.77 in <sup>2</sup> )
Hammer	Type	Case02	Delmag D 22
Damping	Toe	Case03	0.10 s/ft
		Case04	0.20 s/ft
Quake	Toe & Shaft	Case05	0.05"
	Toe & Shaft	Case06	0.15"

The results of these analyses are given as Figures 3.3 to 3.6. A tabular summary of WEAP87 results (for the five largest  $R_{ult}$  values) follows each figure.

Figure 3.3 shows the effect of using a different gage for the shell material. The thicker shell results in about 10% reduction (*i.e.*  $AF_s = 0.90$ ) in peak stresses with almost no

change (*i.e.*  $AF_B = 1.00$ ) in the number of blows required for driving in the range of interest. This implies that in cases where the expected stresses in the shell are close to the maximum allowable limit, the use of a shell with a greater wall thickness can mitigate the problem with limited increase in driving effort.

Fig. 3.4 shows that using a heavier hammer results in 50% reduction in the number of blows required to achieve comparable bearing capacity. The hammer with the higher rated energy, the Delmag D 22, required only 25 bpf to drive the shell to a capacity of 80 tons, whereas the standard Delmag D 12 required 49 bpf. However, using the heavier hammer results in an increase in stresses induced in the shell (Fig. 3.4). Using the D 22 causes a 7% to 12% increase in the maximum stress as compared to the stresses induced by the D 12 for the range of interest of  $R_{ult}$  values. However, the stresses are still within safe limits for  $R_{ult}$  values below 100 t, and overall *the results indicate that a D 22 would have been a better choice at this site*. Associated  $AF_B$  and  $AF_S$  values are 0.50 and 1.12, respectively (number of blows reduced by 50%, and maximum compressive stress increase of 12%).

The effect of variation in damping at toe follows a smooth pattern (Fig. 3.5). This observation combined with the trends observed in Chapter 2 leads to the conclusion that adjustment factors of 1.25 and 1.05 for  $AF_B$  and  $AF_S$ , respectively, would be appropriate when analyzing expected field driving conditions.

Changing the quake from the recommended values, 0.1" for both toe and shaft, has a small effect on the drivability (Fig. 3.6(a)) and negligible effect on the induced maximum compressive stresses (Fig. 3.6(b)). An adjustment factor of 7% would suffice to account for errors in the bearing curves, arising due to errors in estimating the soil quake. That is, an  $AF_B$  value of 1.07 and an  $AF_S$  value of 1.00 are adequate.

#### 3.1.1.1 *Drivability study and comparison with field observations*

A drivability study is presented in this section. The results are compared with field observations and conclusions are drawn. The first step is the estimation of  $R_{ult}$  for various levels of pile toe penetration during driving. The calculations are performed at the three depths of 8, 10 and 12 ft (below the final elevation of the top of the pile). Then the wave equation analysis is carried out for each depth to obtain bearing curves and expected maximum compressive stresses.

The parameters from the standard case (Case00) are used, and the skin friction along the shaft is estimated from Fig. 3.2. The resistance at the toe is determined from Figs. A.2(a), A.3 and A.4 using appropriate procedures similar to those used in Secs. 2.3.1 and 2.3.2. The values of IPERCS are listed in Table 3.2 along with the depth information and range in  $R_{ult}$ .

Table 3.2  
 $R_{ult}$  for drivability study

Case##	Depth* (ft)	IPERCS (%)	Range of $R_{ult}$ (tons)				
Case07	8	17	15	19	23	27	31
Case08	10	24	25	29	33	37	41
Case09	12	19	50	50	70	80	90
* Depth below original ground elevation. Labels on Figs. 3.7 and 3.8 show depth below final elevation of top of pile.							

The results are presented in Fig. 3.7 and Fig. 3.8. If obtained before driving in the field, these results could have been used in conjunction with the adjustment factors obtained from the parametric study to adjust the driving criteria to keep stresses within acceptable limits while achieving target penetration and bearing capacity.

To do a comparison with field observations, the first step is to obtain cumulative adjustment factors. For the first set of observations this is done using the adjustment factors for damping, quake, hammer efficiency (assumed 1.20 based on results from Chapter 2), and variation in shell gage (standard case is 5 gage, whereas shell used in the field was 7 gage). Using the preceding results, an  $AF_b$  value of 1.60 ( $= 1.25 \times 1.07 \times 1.20 \times 1.00$ ) is obtained. This implies that the blow count observed in the field would be at most 60% greater than the blow counts in Fig. 3.7. The blow count observed for driving from a depth of 12 ft to 13 ft (marked as elevation 16 ft in Figs. 3.7 and 3.8) was 160, which can now be taken as 100 ( $160 \div 1.6$ ) for comparison with the standard case results. It is seen from Fig. 3.7 that a blow count of 100 corresponds to a  $R_{ult}$  value of 120 tons. This is 50% higher than the value called for in the specifications. From Figs. 3.7 and 3.8, and by using an  $AF_s$  value of 0.7 ( $= 1.05 \times$

1.00  $\times$  0.60  $\div$  0.90), it is seen that the corresponding peak stress in the shell is more than 30 ksi.

The specifications called for the contractor to look for a final blow count of 20 blows per half-inch. This was achieved at a depth of 13.25 ft and subsequent driving damaged the shell. By extrapolating the bearing curve from the standard case and using the adjustment factors, the  $R_{ult}$  value is estimated to be at least 160 tons at this stage with a corresponding peak stress near 40 ksi - which is dangerously close to the safe limit of the shell material. *This unnecessary hard driving is the cause of damage to the shell.*

The second set of observations at the same bent was obtained for a 5 gage shell. This shell had a blow count of 240 bpf at a depth of 13 ft. Again, the adjustment factors are obtained assuming a worst case and are:  $AF_b = 1.60$ ; and  $AF_s = 0.63$ . The field results now correspond to a blow count of 150 bpf in the standard case (150 = 240  $\div$  1.6). From the bearing curve of Fig. 3.3 (or Fig. 3.7) it can be seen that 150 bpf corresponds to a  $R_{ult}$  value greater than 140 tons, which is much more than the required capacity. Using Fig. 3.3(b) with an  $AF_s$  value of 0.63 shows the corresponding peak stress to be greater than 30 ksi, which occurs near the top of the pile.

The specifications supplied to the contractor called for a final blow count of 40 bpi (blows per inch) as well as a minimum depth of embedment. Driving was concluded at a depth of 14 ft when the final blow count was 480 bpf. As is indicated by the preceding analysis, this resulted in a probable minimum  $R_{ult}$  of 160 tons being faced by the shell with corresponding peak stresses around 40 ksi.

The dynamic analysis indicates that a specification calling for a final set of 120 bpf (corresponding to an  $R_{ult}$  of 130 tons for the standard case) would have been more than adequate, for the shells driven at the bent under consideration, to achieve the required bearing of 80 tons in the worst case.

Since the bulk of the resistance to driving comes from the side friction, it would have been advisable to start driving after jetting or preboring through part, or all, of the fill material. This would have resulted in easier driving with less stress and it would still have been possible to achieve more than the desired bearing capacity. Additionally, if a heavier hammer such as the one used in Case02 had been used, the pile drivability would have been greatly improved as well as reducing the driving time to less than half.

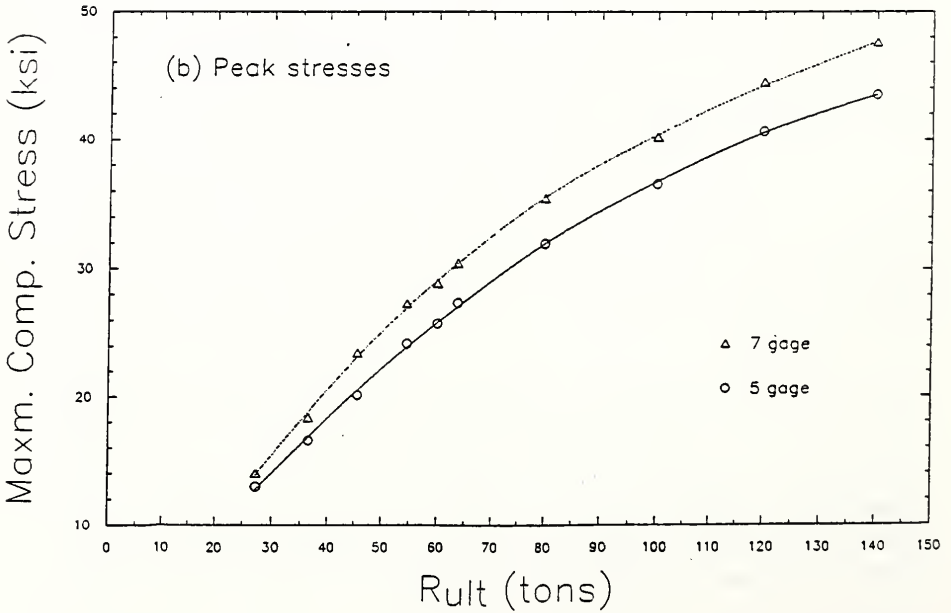
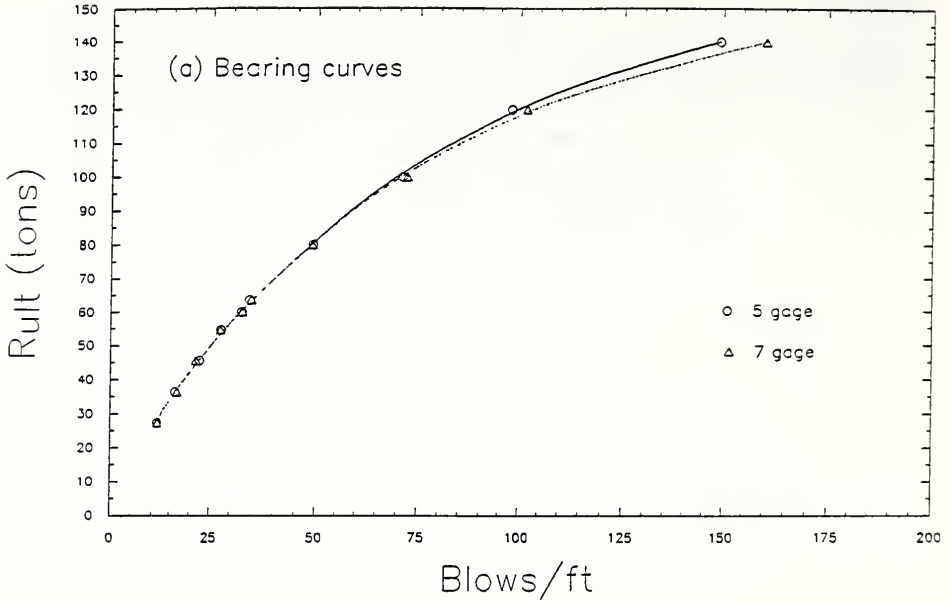


Figure 3.3 Variation in thin shell gage (SR26/TB-4)

## Section 3.1.1 Ex. - SR26 (TB-4) Case00

R <sub>ult</sub> kips	Bl bpf	Ct down	Stroke (ft) up	MinStr I,J ksi	MaxStr I,J ksi	Enthru ft-kip	Bl Rt bpm
132.0	32.6	4.9	5.0	.00( 1, 0)	25.78( 1, 87)	.0	53.1
176.0	49.1	5.4	5.4	.00( 1, 0)	31.92( 1, 88)	.0	50.8
220.0	71.1	5.6	5.7	.00( 1, 0)	36.53( 1, 89)	.0	49.7
264.0	97.9	6.0	6.0	.00( 1, 0)	40.64( 1, 89)	.0	48.2
308.0	149.2	6.2	6.3	.00( 1, 0)	43.50( 1, 91)	.0	47.1

## Section 3.1.1 Ex. - SR26 (TB-4) Case01

R <sub>ult</sub> kips	Bl bpf	Ct down	Stroke (ft) up	MinStr I,J ksi	MaxStr I,J ksi	Enthru ft-kip	Bl Rt bpm
132.0	32.7	4.8	4.9	.00( 1, 0)	28.87( 1, 89)	.0	53.2
176.0	49.0	5.3	5.4	.00( 1, 0)	35.41( 1, 89)	.0	50.9
220.0	72.2	5.6	5.7	.00( 1, 0)	40.18( 1, 92)	.0	49.7
264.0	101.8	6.0	6.0	.00( 1, 0)	44.48( 1, 93)	.0	48.1
308.0	160.5	6.3	6.4	.00( 1, 0)	47.58( 1, 94)	.0	47.0

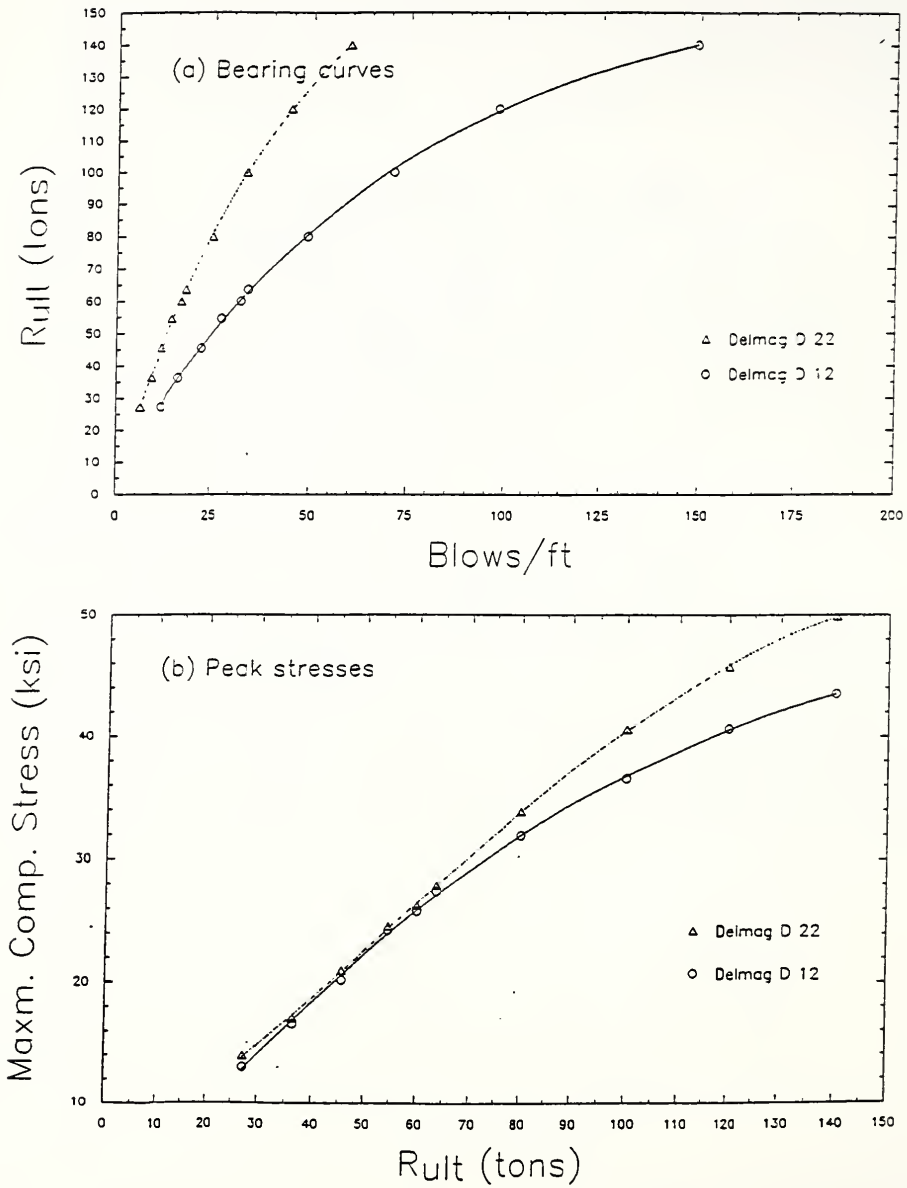


Figure 3.4 Effect of heavier hammer (SR26/TB-4)



## Section 3.1.1 Ex. - SR26 (TB-4) Case00

R <sub>ult</sub> kips	Bl bpf	Ct down	Stroke (ft) up	MinStr I,J ksi	MaxStr I,J ksi	Enthru ft-kip	Bl Rt bpm
132.0	32.6	4.9	5.0	.00( 1, 0)	25.78( 1, 87)	.0	53.1
176.0	49.1	5.4	5.4	.00( 1, 0)	31.92( 1, 88)	.0	50.8
220.0	71.1	5.6	5.7	.00( 1, 0)	36.53( 1, 89)	.0	49.7
264.0	97.9	6.0	6.0	.00( 1, 0)	40.64( 1, 89)	.0	48.2
308.0	149.2	6.2	6.3	.00( 1, 0)	43.50( 1, 91)	.0	47.1

## Section 3.1.1 Ex. - SR26 (TB-4) Case02

R <sub>ult</sub> kips	Bl bpf	Ct down	Stroke (ft) up	MinStr I,J ksi	MaxStr I,J ksi	Enthru ft-kip	Bl Rt bpm
132.0	17.0	3.8	3.9	.00( 1, 0)	26.21( 1,101)	.0	59.4
176.0	25.1	4.2	4.3	.00( 1, 0)	33.86( 1, 99)	.0	56.6
220.0	33.7	4.6	4.6	.00( 1, 0)	40.54( 1, 99)	.0	54.5
264.0	44.6	4.8	4.9	.00( 1, 0)	45.75( 1, 99)	.0	53.1
308.0	59.4	4.9	5.1	.00( 1, 0)	49.86( 1,101)	.0	52.3

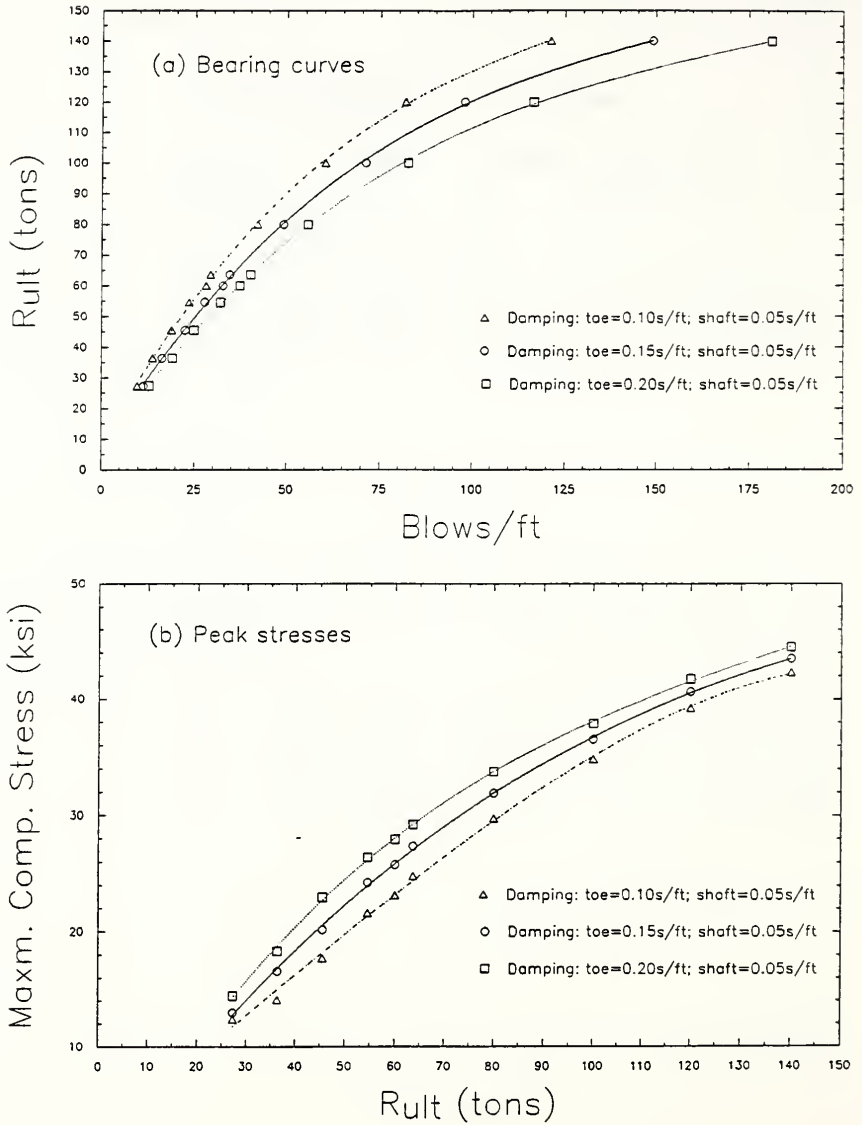


Figure 3.5 Variation in damping at toe(SR26/TB-4

## Section 3.1.1 Ex. - SR26 (TB-4) Case00

R <sub>ult</sub> kips	Bl bpf	Ct	Stroke (ft) down up	MinStr I,J ksi	MaxStr I,J ksi	Enthru ft-kip	Bl Rt bpm
132.0	32.6	4.9	5.0	.00( 1, 0)	25.78( 1, 87)	.0	53.1
176.0	49.1	5.4	5.4	.00( 1, 0)	31.92( 1, 88)	.0	50.8
220.0	71.1	5.6	5.7	.00( 1, 0)	36.53( 1, 89)	.0	49.7
264.0	97.9	6.0	6.0	.00( 1, 0)	40.64( 1, 89)	.0	48.2
308.0	149.2	6.2	6.3	.00( 1, 0)	43.50( 1, 91)	.0	47.1

## Section 3.1.1 Ex. - SR26 (TB-4) Case03

R <sub>ult</sub> kips	Bl bpf	Ct	Stroke (ft) down up	MinStr I,J ksi	MaxStr I,J ksi	Enthru ft-kip	Bl Rt bpm
132.0	28.0	4.7	4.8	.00( 1, 0)	23.15( 1, 86)	.0	54.0
176.0	42.1	5.2	5.3	.00( 1, 0)	29.75( 1, 86)	.0	51.3
220.0	60.3	5.5	5.6	.00( 1, 0)	34.85( 1, 86)	.0	50.0
264.0	81.8	5.9	5.9	.00( 1, 0)	39.24( 1, 88)	.0	48.6
308.0	121.1	6.1	6.2	.00( 1, 0)	42.30( 1, 90)	.0	47.5

## Section 3.1.1 Ex. - SR26 (TB-4) Case04

R <sub>ult</sub> kips	Bl bpf	Ct	Stroke (ft) down up	MinStr I,J ksi	MaxStr I,J ksi	Enthru ft-kip	Bl Rt bpm
132.0	37.2	5.0	5.1	.00( 1, 0)	27.94( 1, 87)	.0	52.4
176.0	55.7	5.4	5.5	.00( 1, 0)	33.75( 1, 89)	.0	50.5
220.0	82.5	5.6	5.8	.00( 1, 0)	37.91( 1, 90)	.0	49.4
264.0	116.6	6.1	6.1	.00( 1, 0)	41.74( 1, 90)	.0	47.9
308.0	181.0	6.3	6.4	.00( 1, 0)	44.50( 1, 92)	.0	46.9

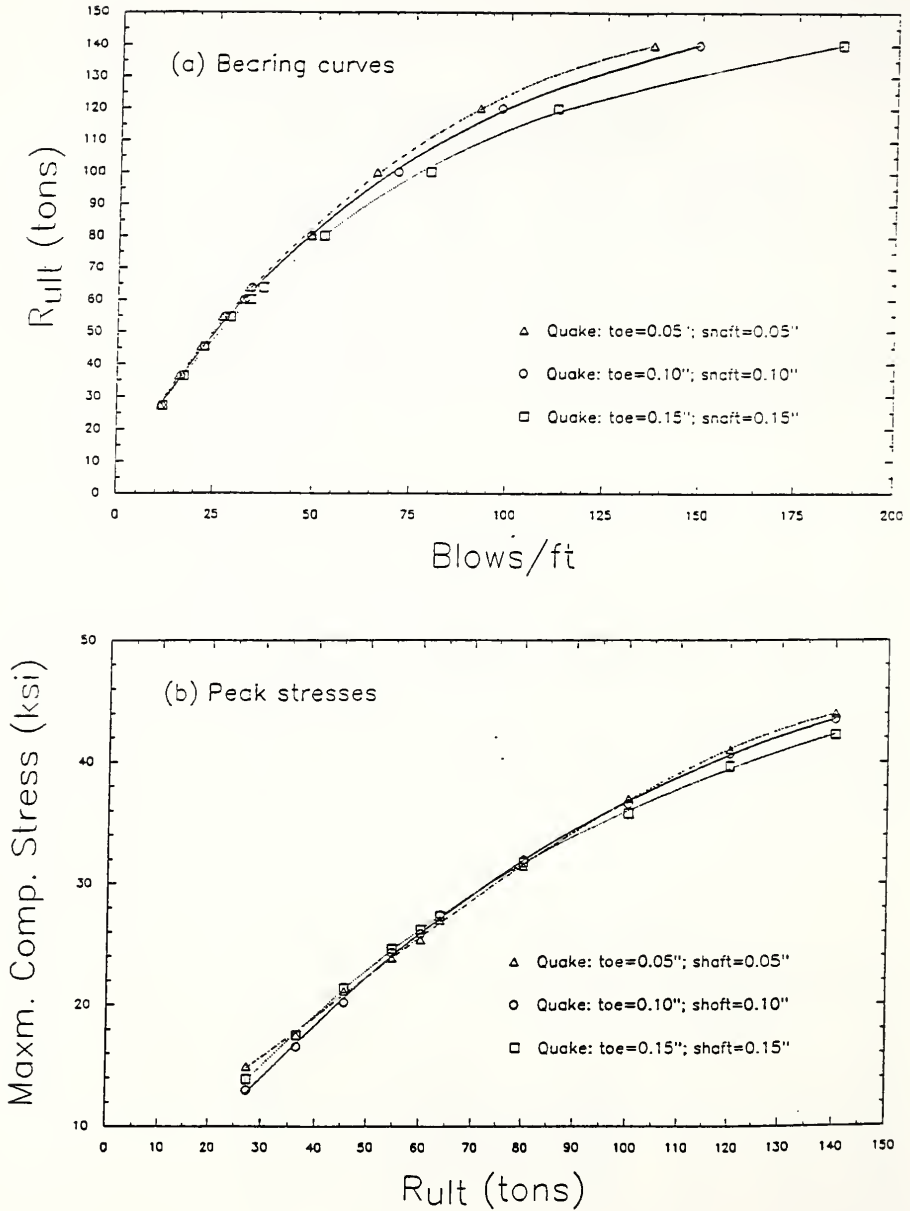


Figure 3.6 Variation in quake (SR26/TB-4)

## Section 3.1.1 Ex. - SR26 (TB-4) Case00

R <sub>ult</sub> kips	Bl bpf	Ct	Stroke (ft) down up	MinStr I,J ksi	MaxStr I,J ksi	Enthru ft-kip	Bl Rt bpm
132.0	32.6	4.9	5.0	.00( 1, 0)	25.78( 1, 87)	.0	53.1
176.0	49.1	5.4	5.4	.00( 1, 0)	31.92( 1, 88)	.0	50.8
220.0	71.1	5.6	5.7	.00( 1, 0)	36.53( 1, 89)	.0	49.7
264.0	97.9	6.0	6.0	.00( 1, 0)	40.64( 1, 89)	.0	48.2
308.0	149.2	6.2	6.3	.00( 1, 0)	43.50( 1, 91)	.0	47.1

## Section 3.1.1 Ex. - SR26 (TB-4) Case05

R <sub>ult</sub> kips	Bl bpf	Ct	Stroke (ft) down up	MinStr I,J ksi	MaxStr I,J ksi	Enthru ft-kip	Bl Rt bpm
132.0	31.9	4.9	5.0	.00( 1, 0)	25.29( 1, 80)	.0	53.1
176.0	49.1	5.2	5.3	.00( 1, 0)	31.40( 1, 82)	.0	51.4
220.0	65.7	5.7	5.6	.00( 1, 0)	36.94( 1, 84)	.0	49.6
264.0	92.0	5.9	5.9	.00( 1, 0)	40.99( 1, 86)	.0	48.5
308.0	137.0	6.0	6.3	.00( 1, 0)	43.94( 1, 87)	.0	47.6

## Section 3.1.1 Ex. - SR26 (TB-4) Case06

R <sub>ult</sub> kips	Bl bpf	Ct	Stroke (ft) down up	MinStr I,J ksi	MaxStr I,J ksi	Enthru ft-kip	Bl Rt bpm
132.0	34.1	4.8	4.9	.00( 1, 0)	26.13( 1, 91)	.0	53.3
176.0	52.4	5.3	5.3	.00( 1, 0)	31.72( 1, 92)	.0	51.1
220.0	79.3	5.5	5.7	.00( 1, 0)	35.74( 1, 93)	.0	49.7
264.0	112.6	6.0	6.0	.00( 1, 0)	39.62( 1, 93)	.0	48.2
308.0	186.0	6.3	6.3	.00( 1, 0)	42.20( 1, 95)	.0	47.1

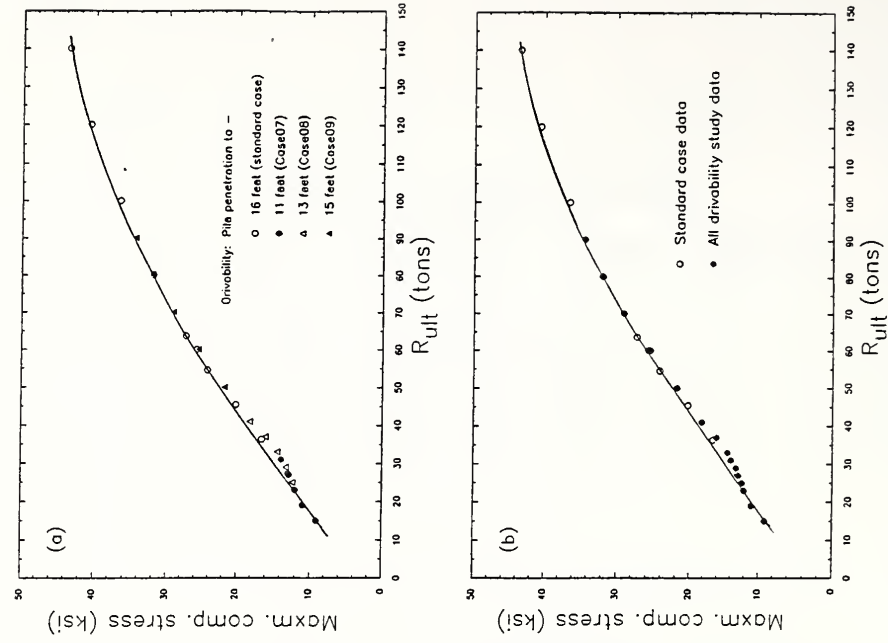


Figure 3.7 Bearing curves for drivability study at SR26/TB-4

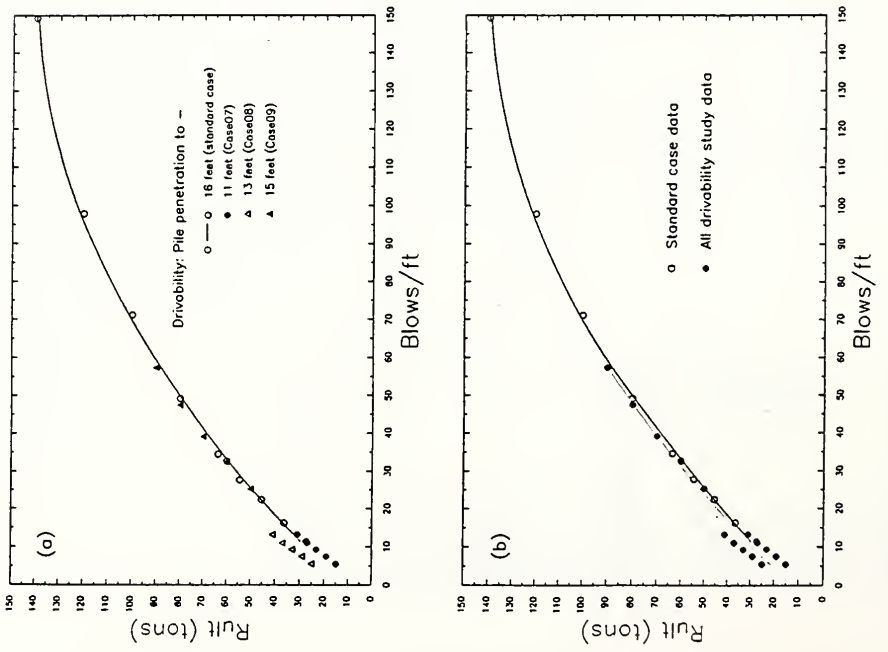


Figure 3.8 Maximum compressive stresses in drivability study at SR26/TB-4

## Section 3.1.1 Ex. - SR26 (TB-4) Case00

R <sub>ult</sub> kips	Bl Ct bpf	Stroke down	(ft) up	MinStr I,J ksi	MaxStr I,J ksi	Enthru ft-kip	Bl Rt bpm
132.0	32.6	4.9	5.0	.00( 1, 0)	25.78( 1, 87)	.0	53.1
176.0	49.1	5.4	5.4	.00( 1, 0)	31.92( 1, 88)	.0	50.8
220.0	71.1	5.6	5.7	.00( 1, 0)	36.53( 1, 89)	.0	49.7
264.0	97.9	6.0	6.0	.00( 1, 0)	40.64( 1, 89)	.0	48.2
308.0	149.2	6.2	6.3	.00( 1, 0)	43.50( 1, 91)	.0	47.1

## Section 3.1.1 Ex. - SR26 (TB-4) Case07

33.0	5.5	3.2	3.2	.00( 1, 0)	9.11( 1, 65)	.0	65.7
41.8	7.5	3.3	3.5	.00( 1, 0)	11.01( 1, 63)	.0	63.7
50.6	9.3	3.5	3.6	.00( 1, 0)	12.05( 1, 64)	.0	61.9
59.4	11.0	3.9	3.8	.00( 1, 0)	12.87( 1, 67)	.0	60.1
68.2	13.2	4.0	4.0	.00( 1, 0)	13.94( 1, 91)	.0	58.9

## Section 3.1.1 Ex. - SR26 (TB-4) Case08

55.0	9.9	3.7	3.7	.00( 1, 0)	12.37( 1, 66)	.0	61.1
63.8	11.7	3.9	3.8	.00( 1, 0)	13.25( 1, 68)	.0	59.6
72.6	13.9	4.1	4.0	.00( 1, 0)	14.45( 1, 90)	.0	58.5
81.4	16.4	4.1	4.2	.00( 1, 0)	16.03( 1, 89)	.0	57.6
90.2	18.3	4.4	4.3	.00( 1, 0)	18.21( 1, 87)	.0	56.3

## Section 3.1.1 Ex. - SR26 (TB-4) Case09

110.0	25.2	4.5	4.7	.00( 1, 0)	21.77( 1, 88)	.0	54.8
132.0	32.4	4.8	5.0	.00( 1, 0)	25.48( 1, 87)	.0	53.2
154.0	39.0	5.2	5.2	.00( 1, 0)	29.12( 1, 87)	.0	51.6
176.0	47.3	5.4	5.4	.00( 1, 0)	32.00( 1, 87)	.0	50.7
198.0	57.3	5.5	5.5	.00( 1, 0)	34.39( 1, 88)	.0	50.1

### 3.1.2 Pile at bent number 3 (interior bent)

This is an interior bent with a ground elevation, at time of piling, equal to 581 ft. Scour is estimated to be 6 ft, the recommended minimum pile tip elevation is 570 ft. This leaves an embedded length of 5 ft under the worst conditions which is still enough to provide an ultimate capacity greater than 100 tons from embedment in the hard dense silty loam. the estimated values of  $Q_b$  and  $Q_s$  are 160 t and 25 t, respectively. These values are obtained based on the bore-hole data from TB-3. If jetting is used to get past scour depth, then  $Q_s$  is reduced to 20 t. However, the resistance to driving of the material likely to be lost to scour is marginal, and no jetting is considered necessary. The  $R_{ult}$  value used is 180 tons with WEAP87 input side resistance distribution as shown in Fig. 3.9(a). Table 3.3 lists the range of  $R_{ult}$  values used for analysis.

**Table 3.3**  
Range of  $R_{ult}$  : IPERCS = 12%

$R_{ult}$ (tons)	54.5	68.2	81.8	95.5	109	120	150	180	210	240
$R_{ult}$ (kips)	120	150	180	210	240	264	330	396	462	528
$Q_b$ (tons)	6.5	8	9.8	11.5	13	14	18	21	25	29
$Q_{sd}$ (tons)	48	60.2	72	84	96	106	132	159	185	211

The standard case (Case00) parameters are as follows:

Pile	Type	Thin steel shell		
	Gage	5 (wall thickness = 0.203"; c/s area = 8.8 in <sup>2</sup> )		
	$\phi$	14"		
	Length	20.0 ft		
Hammer	Type	Delmag D 12		
	Efficiency	0.8		
	Cushion	Area	283.5 in <sup>2</sup>	
		Material	Plywood	
		Thickness	0.75"	
Helmet	Weight	2.02 kips		



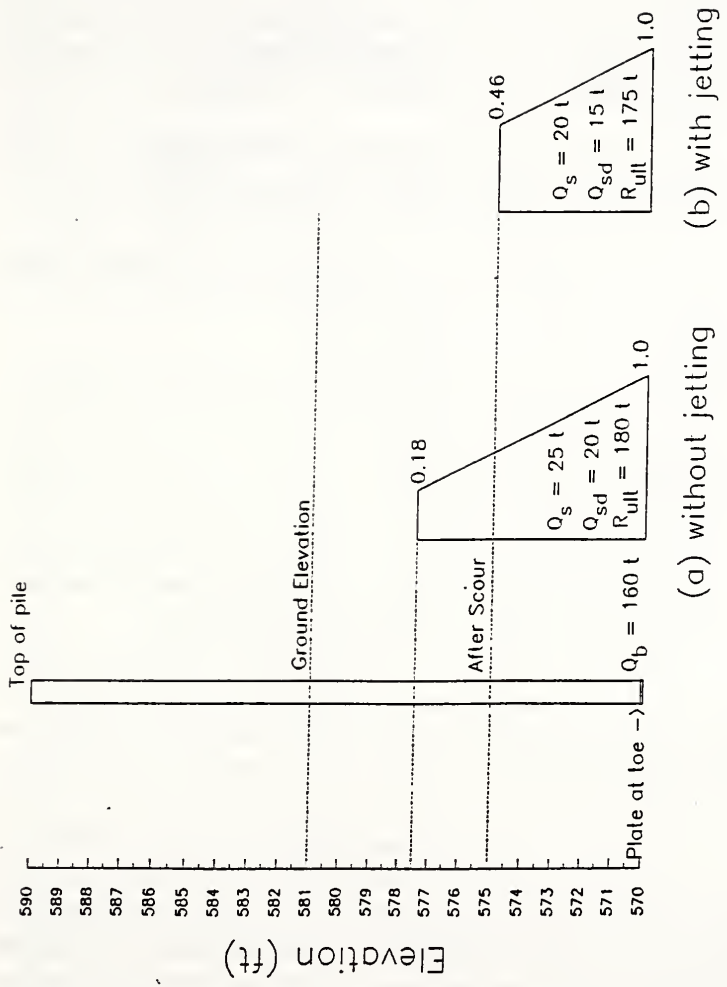


Figure 3.9 Shaft friction distribution for bent no. 3 State Road 26 over Coffee Run Creek

Soil Parameters	Quake	Shaft	0.1"
		Toe	0.1"
	Damping	Type	Smith (Normal)
		Shaft	0.05 s/ft
		Toe	0.15 s/ft

$R_{ult}$  Table 3.3

Shaft Friction	As a % of $R_{ult}$ Distribution used	12 (IPERCS = 12) Fig. 3.9
----------------	---------------------------------------	------------------------------

Parametric studies are conducted to assess the effects of different parameters. Only one parameter is varied at a time, with the remainder of the data identical to that of the standard case:

Pile	Gage	Case01	7 (wall thickness = 0.179"; c/s area = 7.77 in <sup>2</sup> )
Hammer	Type	Case02	Delmag D 22
Damping	Toe	Case03	0.10 s/ft
		Case04	0.20 s/ft
Quake	Toe & Shaft	Case05	0.05"
	Toe & Shaft	Case06	0.15"

The results of these analyses are given as Figures 3.10 to 3.13. A tabular summary of WEAP87 results (for the five largest  $R_{ult}$  values) follows each figure.

The results show that the standard hammer is inadequate to drive the pile to the required depth for high values of  $R_{ult}$ . Hence, only  $R_{ult}$  values less than 180 t are included in the following discussions.

Figure 3.10 shows the effect of using a different gage for the shell material. The thinner shell results in a 9% increase in peak stresses over the entire range of  $R_{ult}$  values studied. The blow count does not change appreciably for capacities below 100 t, but then increases at a very fast rate as  $R_{ult}$  increases. Although this makes it difficult to estimate an adjustment factor,  $AF_B$  and  $AF_S$  values of 1.10 and 1.09, respectively, are adequate for all practical purposes. These results also indicate that for the present driving train, it is preferable to use 5 gage shells for all piles at this bent.

Fig. 3.11 shows that using the hammer with the higher rated energy (the Delmag D 22) results in 50% reduction in the number of blows required to achieve comparable bearing at low values of  $R_{ult}$ . The heavier hammer is capable of driving the shell to capacities much greater than the lighter hammer used at the site. However, using the heavier hammer results in an increase in stresses induced in the shell (Fig. 3.11(b)). Using the D 22 causes a 15% to 20% increase, as compared to the D 12, in the maximum stress for  $R_{ult}$  values in the range of interest. *The preceding analysis indicates that a D 12 hammer was not a judicious choice at this site and a D 22 hammer would have performed the job much more efficiently.* The associated adjustment factors are 0.50 ( $AF_B$ ) and 1.20 ( $AF_S$ ).

The effect of variation in damping at the toe follows a smooth pattern (Fig. 3.12). This observation combined with the trends observed in Chapter 2 leads to the conclusion that adjustment factors of 1.25 and 1.05 for  $AF_B$  and  $AF_S$ , respectively, would be appropriate when analyzing expected field driving conditions.

Changing the quake from the recommended values, 0.1" for both toe and shaft, has a small effect on the drivability and negligible effect on the induced maximum compressive stresses at low  $R_{ult}$  values (Fig. 3.13). For ultimate capacities greater than 100 tons, the blow count increases by 20% to 40% when damping is 50% higher than the standard case. The corresponding decrease in peak stress is about 4%. Adjustment factors of 1.3 and 0.96 for  $AF_B$  and  $AF_S$ , respectively, would suffice to account for errors in the bearing curves, arising due to errors in estimating the soil quake.

### 3.1.2.1 Drivability study and comparison with field observations

$R_{ult}$  values were estimated for various levels of pile toe penetration during driving. The calculations are performed at the three depths of 4, 6 and 8 ft (below original ground elevation). Then the wave equation analysis was carried out to obtain bearing curves and expected maximum compressive stresses for each depth.

The parameters from the standard case (Case00) are used, and the skin friction along the shaft is estimated from Fig. 3.9. The resistance at the toe is determined from Figs. A.2(a), A.3 and A.4 using appropriate procedures similar to those used in Secs. 2.3.1 and 2.3.2. The values of IPERCS are listed in Table 3.4 along with the depth information and range in  $R_{ult}$ .

The results are presented in Fig. 3.14 and Fig. 3.15. If obtained before driving in the field, these results could have been used in conjunction with the adjustment factors obtained from the parametric study to adjust the driving criteria to keep stresses within acceptable limits while achieving target penetration and bearing capacity.

Table 3.4  
 $R_{ult}$  for drivability study

Case##	Depth* (ft)	IPERCs (%)	Range of $R_{ult}$ (tons)		
Case07	4	0	15	20	25
Case08	6	3	130	160	190
Case09	8	7	140	170	200
* Depth below original ground elevation. Labels on Figs. 3.14 and 3.15 also show depth below original ground elevation.					

To do a comparison with field observations, the first step is to obtain cumulative adjustment factors. For the first set of observations this is done using the adjustment factors for damping, quake and hammer efficiency (assumed 1.20 based on results from Chapter 2). Using the preceding results an  $AF_b$  value of 1.95 ( $= 1.25 \times 1.30 \times 1.20$ ) is obtained. This implies that the blow count observed in the field could at most be twice that of the blow counts in the bearing curves of Fig. 3.14. There are two approaches to assess the stress occurring in the piles. The first is to use the *adjusted*  $R_{ult}$  value and obtain the corresponding stress from Fig. 3.15 (peak stress *versus*  $R_{ult}$  plots). The second approach is to use the observed blow count to obtain a value of  $R_{ult}$  from Fig. 3.14 and then use that  $R_{ult}$  to obtain a peak stress from Fig. 3.15 and *adjust* it using the stress adjustment factor,  $AF_s$ , which is estimated to be 0.60 ( $= 1.05 \times 0.96 \times 0.60$ ).

The specifications called for the contractor achieve a minimum embedment of 11 ft and a final blow count of 20 bpi (480 bpf). For the first set of observations (8th shell - counting from South to North) the specifications were successfully met.

For the second set of observations (9th shell - counting from South to North) the shell was driven to a depth from 5 ft to 6 ft with 20 blows. This corresponds to Case08 of the drivability study and to an ultimate capacity of 45 t (Fig. 3.14) without any adjustment, and 25 t if the adjustment factor  $AF_b$  is used. The number of blows required to drive from 7 ft to 8 ft embedment was 57 and this corresponds to an  $R_{ult}$  of 90 t and 60 t, without and with adjustment, respectively. Difficulties began after a depth of 9 ft, when the blow count rose sharply from 70 bpf (at 9 ft embedment) to 480 bpf (at 10 ft embedment); then to 960 bpf (at 10 ft 4 inch embedment) and finally to 1920 bpf (at 10 ft 8 inch embedment) when driving was stopped. The bearing curve shows that the hammer had probably reached the limit of its driving capacity much before this, and that state corresponds to a peak  $R_{ult}$  of 180 t and 400 bpf. Even under the assumed worst conditions, this peak would be reached at 800 bpf, however these high values do not translate to dangerous peak stresses. After adjustment, the peak stresses are estimated to be about 30 to 35 ksi which, although high, are not close to the yield stress.<sup>14</sup> These conclusions are borne out by the observations in the field, where no damage occurred to the shells even at very high blow counts. The problem in this case was in terms of time lost and inability to reach the required minimum depth of embedment (based on scour considerations).

Jetting the pile through the scour depth would not have been of help in this case since the bulk of the resistance to driving builds up once the hard till is reached at a depth of around 9 ft. A possible solution would have been to pre-bore through part of the till (as well as the scour depth) before driving the pile through the remaining material. But this may not be considered desirable due to the relatively shallow final depth. *A judicious approach at this site would have been to use a heavier hammer, such as that used in the parametric study (a Delmag D 22).* The results of the parametric study indicate that a D 22 would have been capable of driving the shell to the required depth with a manageable blow count of 120 bpf under assumed conditions and 240 bpf (the specified blow count) in the assumed worst case (that is,  $AF_b = 2.00$ ). Although the corresponding stresses would have been higher, they would not have been close to the yield limit (Fig. 3.11).

---

<sup>14</sup> ASTM A-572 Grade 50 steel has a yield point of 345 Mpa (50 ksi). The tolerable driving stress for steel shells is usually taken to be between 45 ksi and 55 ksi.

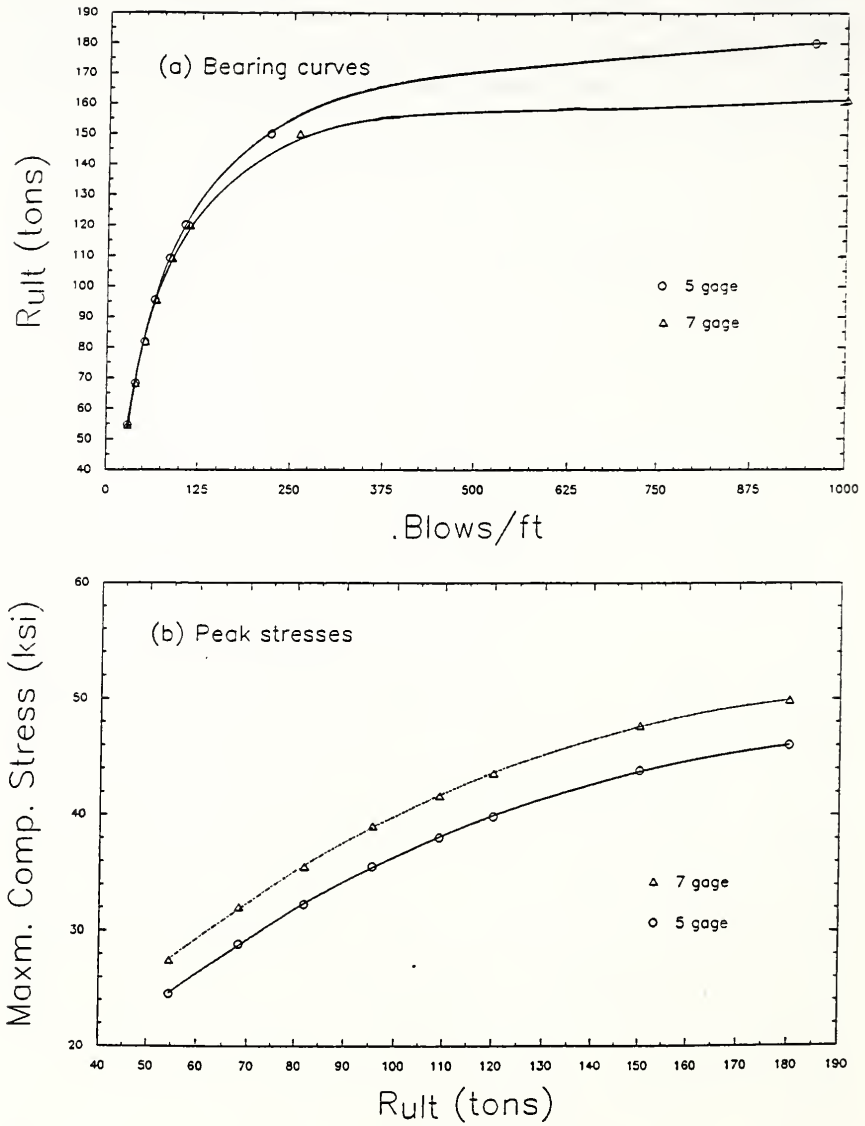


Figure 3.10 Variation in thin shell gage (SR26/TB-3)

## Section 3.1.2 Ex. - SR26 (TB-3) Case00

R <sub>ult</sub> kips	Bl bpf	Ct bpf	Stroke (ft) down up	MinStr I,J ksi	MaxStr I,J ksi	Enthru ft-kip	Bl Rt bpm
264.0	105.9	6.0	6.0	.00( 1, 0)	39.83( 1, 96)	.0	48.1
330.0	218.8	6.5	6.5	.00( 1, 0)	43.81( 1, 97)	.0	46.3
396.0	958.4	6.8	6.9	.00( 1, 0)	46.00( 1,100)	.0	45.3
462.0	9999.0	6.9	7.0	.00( 1, 0)	47.02( 1, 99)	.0	44.8
528.0	9999.0	6.9	7.1	.00( 1, 0)	47.67( 1, 99)	.0	44.6

## Section 3.1.2 Ex. - SR26 (TB-3) Case01

R <sub>ult</sub> kips	Bl bpf	Ct bpf	Stroke (ft) down up	MinStr I,J ksi	MaxStr I,J ksi	Enthru ft-kip	Bl Rt bpm
264.0	112.0	6.0	6.0	.00( 1, 0)	43.55( 1, 98)	.0	48.2
330.0	260.6	6.5	6.5	.00( 1, 0)	47.68( 1,101)	.0	46.4
396.0	2176.7	6.7	6.8	.00( 1, 0)	49.87( 1,103)	.0	45.4
462.0	9999.0	6.8	7.0	.00( 1, 0)	50.75( 1,103)	.0	44.9
528.0	9999.0	6.9	7.0	.00( 1, 0)	51.47( 1,102)	.0	44.8

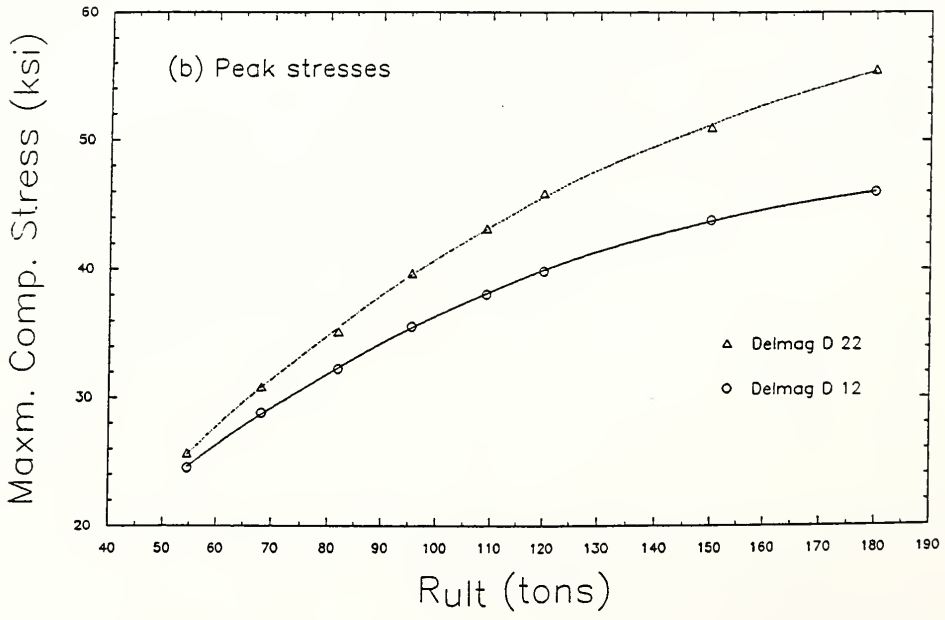
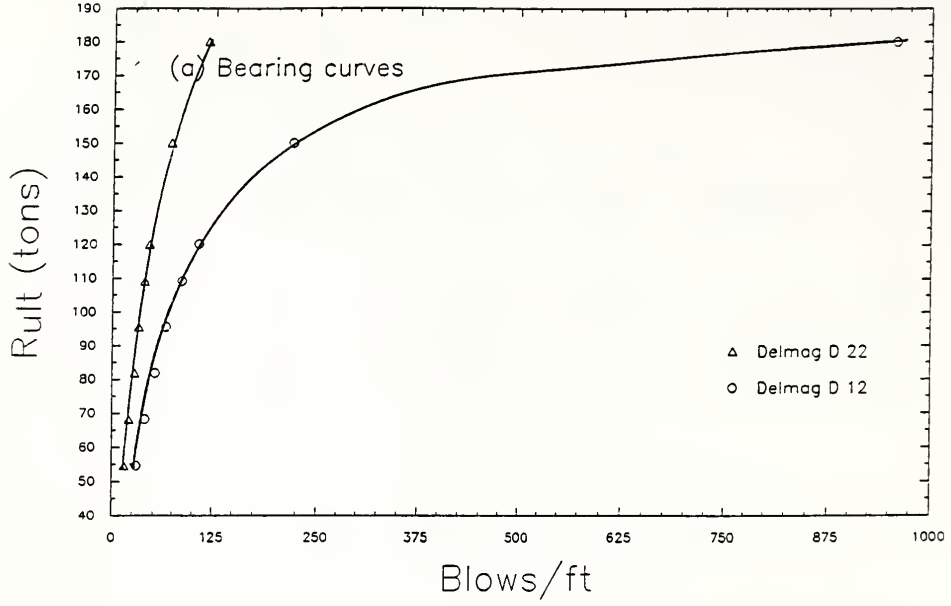


Figure 3.11 Effect of heavier hammer (SR26/TB-3)



## Section 3.1.2 Ex. - SR26 (TB-3) Case00

R <sub>ult</sub> kips	Bl bpf	Ct	Stroke (ft) down up	MinStr I,J ksi	MaxStr I,J ksi	Enthru ft-kip	Bl Rt bpm
264.0	105.9	6.0	6.0	.00( 1, 0)	39.83( 1, 96)	.0	48.1
330.0	218.8	6.5	6.5	.00( 1, 0)	43.81( 1, 97)	.0	46.3
396.0	958.4	6.8	6.9	.00( 1, 0)	46.00( 1,100)	.0	45.3
462.0	9999.0	6.9	7.0	.00( 1, 0)	47.02( 1, 99)	.0	44.8
528.0	9999.0	6.9	7.1	.00( 1, 0)	47.67( 1, 99)	.0	44.6

## Section 3.1.2 Ex. - SR26 (TB-3) Case02

R <sub>ult</sub> kips	Bl bpf	Ct	Stroke (ft) down up	MinStr I,J ksi	MaxStr I,J ksi	Enthru ft-kip	Bl Rt bpm
264.0	44.1	5.0	4.8	.00( 1, 0)	45.87( 1,104)	.0	53.0
330.0	70.5	5.1	5.2	.00( 1, 0)	50.99( 1,108)	.0	51.7
396.0	116.0	5.4	5.4	.00( 1, 0)	55.46( 1,109)	.0	50.5
462.0	240.9	5.6	5.6	.00( 1, 0)	58.51( 1,112)	.0	49.6
528.0	1018.1	5.7	5.8	.00( 1, 0)	60.36( 1,115)	.0	49.1

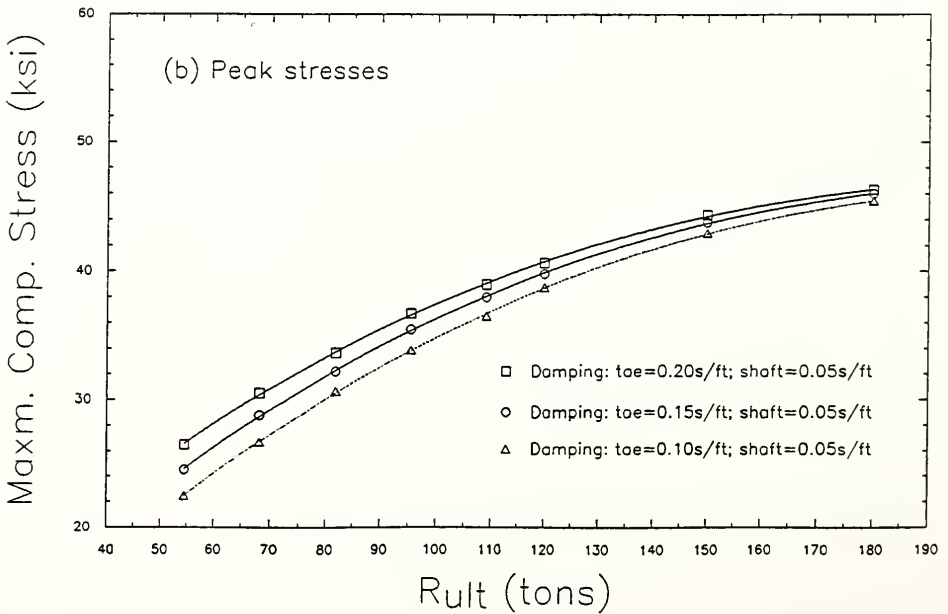
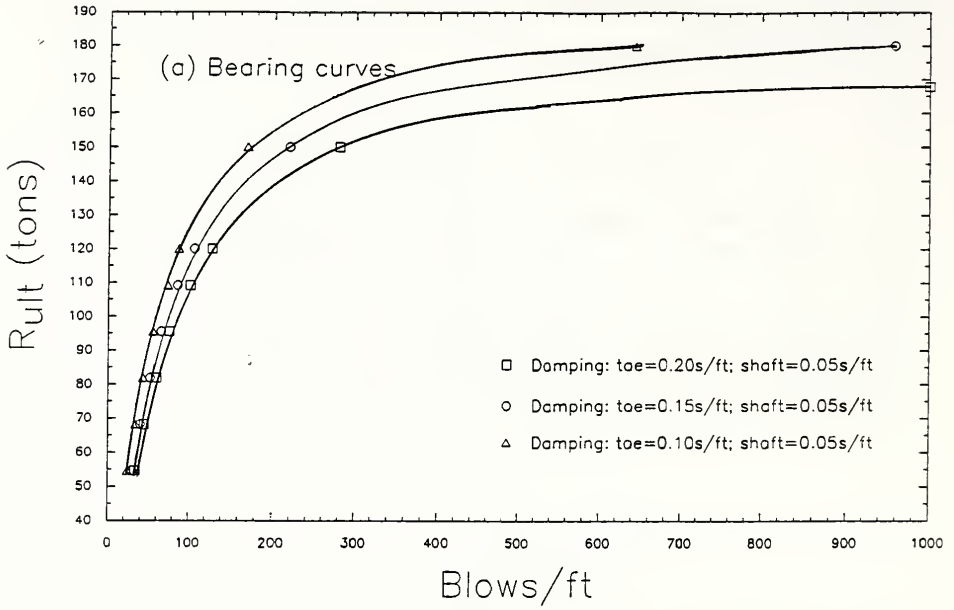


Figure 3.12 Variation in damping at toe (SR26/TB-3)

## Section 3.1.2 Ex. - SR26 (TB-3) Case00

R <sub>ult</sub> kips	Bl Ct bpf	Stroke (ft) down up	MinStr I,J ksi	MaxStr I,J ksi	Enthru ft-kip	Bl Rt bpm
264.0	105.9	6.0 6.0	.00( 1, 0)	39.83( 1, 96)	.0	48.1
330.0	218.8	6.5 6.5	.00( 1, 0)	43.81( 1, 97)	.0	46.3
396.0	958.4	6.8 6.9	.00( 1, 0)	46.00( 1,100)	.0	45.3
462.0	9999.0	6.9 7.0	.00( 1, 0)	47.02( 1, 99)	.0	44.8
528.0	9999.0	6.9 7.1	.00( 1, 0)	47.67( 1, 99)	.0	44.6

## Section 3.1.2 Ex. - SR26 (TB-3) Case03

R <sub>ult</sub> kips	Bl Ct bpf	Stroke (ft) down up	MinStr I,J ksi	MaxStr I,J ksi	Enthru ft-kip	Bl Rt bpm
264.0	86.6	5.9 5.9	.00( 1, 0)	38.79( 1, 94)	.0	48.6
330.0	169.8	6.4 6.4	.00( 1, 0)	42.97( 1, 97)	.0	46.7
396.0	642.8	6.6 6.8	.00( 1, 0)	45.44( 1,100)	.0	45.5
462.0	9999.0	7.1 7.2	.00( 1, 0)	47.59( 1, 99)	.0	44.3

## Section 3.1.2 Ex. - SR26 (TB-3) Case04

R <sub>ult</sub> kips	Bl Ct bpf	Stroke (ft) down up	MinStr I,J ksi	MaxStr I,J ksi	Enthru ft-kip	Bl Rt bpm
264.0	127.9	6.1 6.1	.00( 1, 0)	40.68( 1, 96)	.0	47.8
330.0	280.5	6.6 6.6	.00( 1, 0)	44.38( 1, 98)	.0	46.1
396.0	1489.1	6.8 6.9	.00( 1, 0)	46.31( 1,100)	.0	45.2
462.0	9999.0	7.0 7.0	.00( 1, 0)	47.25( 1, 99)	.0	44.8

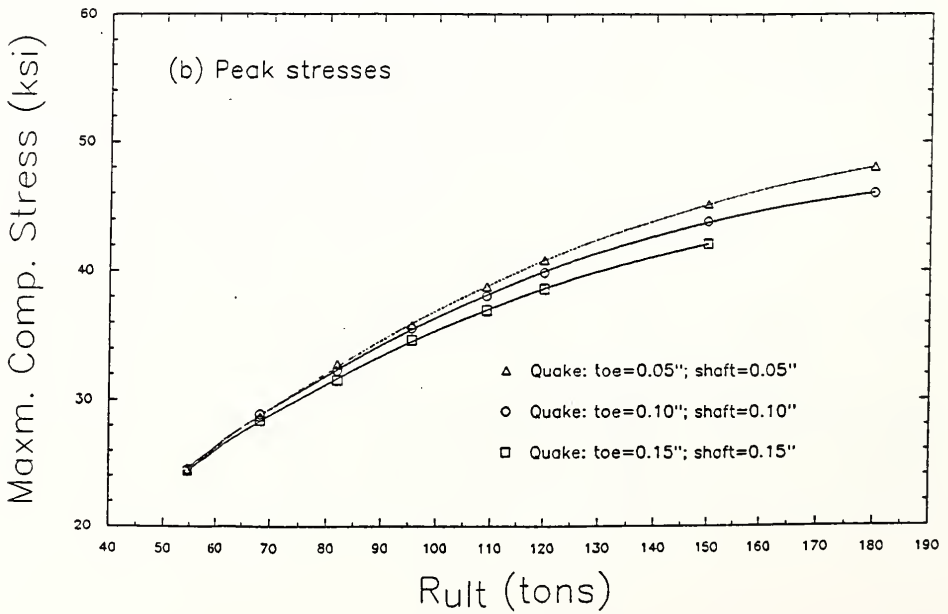
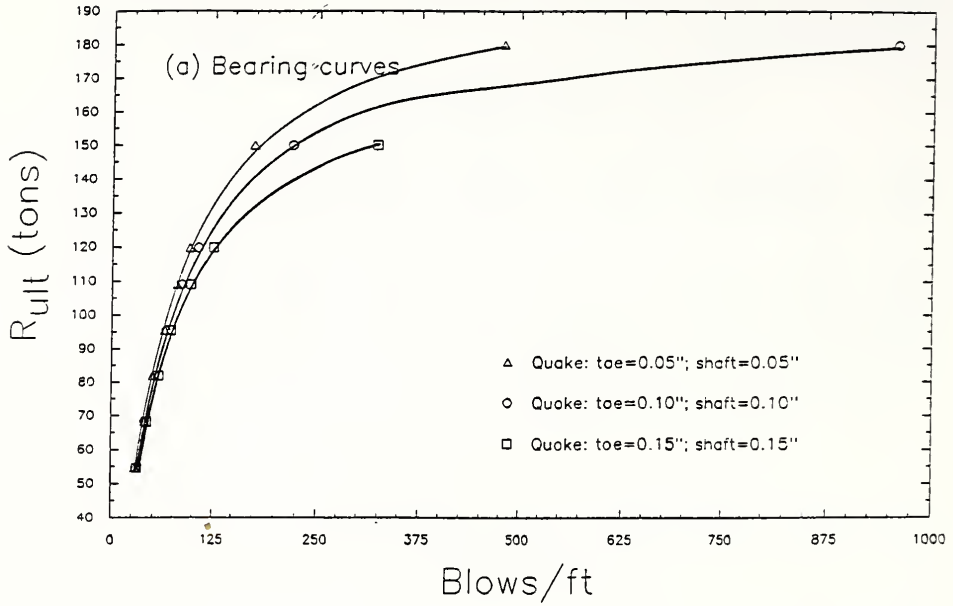


Figure 3.13 Variation in quake (SR26/TB-3)

## Section 3.1.2 Ex. - SR26 (TB-3) Case00

R <sub>ult</sub> kips	Bl bpf	Ct down	Stroke (ft) up	MinStr I,J ksi	MaxStr I,J ksi	Enthru ft-kip	Bl Rt bpm
264.0	105.9	6.0	6.0	.00( 1, 0)	39.83( 1, 96)	.0	48.1
330.0	218.8	6.5	6.5	.00( 1, 0)	43.81( 1, 97)	.0	46.3
396.0	958.4	6.8	6.9	.00( 1, 0)	46.00( 1,100)	.0	45.3
462.0	9999.0	6.9	7.0	.00( 1, 0)	47.02( 1, 99)	.0	44.8
528.0	9999.0	6.9	7.1	.00( 1, 0)	47.67( 1, 99)	.0	44.6

## Section 3.1.2 Ex. - SR26 (TB-3) Case05

R <sub>ult</sub> kips	Bl bpf	Ct down	Stroke (ft) up	MinStr I,J ksi	MaxStr I,J ksi	Enthru ft-kip	Bl Rt bpm
264.0	95.4	6.0	6.0	.00( 1, 0)	40.78( 1, 92)	.0	48.1
330.0	174.3	6.6	6.5	.00( 1, 0)	45.14( 1, 94)	.0	46.2
396.0	478.2	6.8	6.9	.00( 1, 0)	48.01( 1, 95)	.0	45.1
462.0	9999.0	6.9	7.2	.00( 1, 0)	49.32( 1, 97)	.0	44.5
528.0	9999.0	7.0	7.3	.00( 1, 0)	49.73( 1, 97)	.0	44.3

## Section 3.1.2 Ex. - SR26 (TB-3) Case06

R <sub>ult</sub> kips	Bl bpf	Ct down	Stroke (ft) up	MinStr I,J ksi	MaxStr I,J ksi	Enthru ft-kip	Bl Rt bpm
264.0	124.9	6.0	6.0	.00( 1, 0)	38.57( 1, 99)	.0	48.3
330.0	321.9	6.4	6.4	.00( 1, 0)	42.06( 1,102)	.0	46.6
396.0	9999.0	6.7	6.8	.00( 1, 0)	43.87( 1,102)	.0	45.6

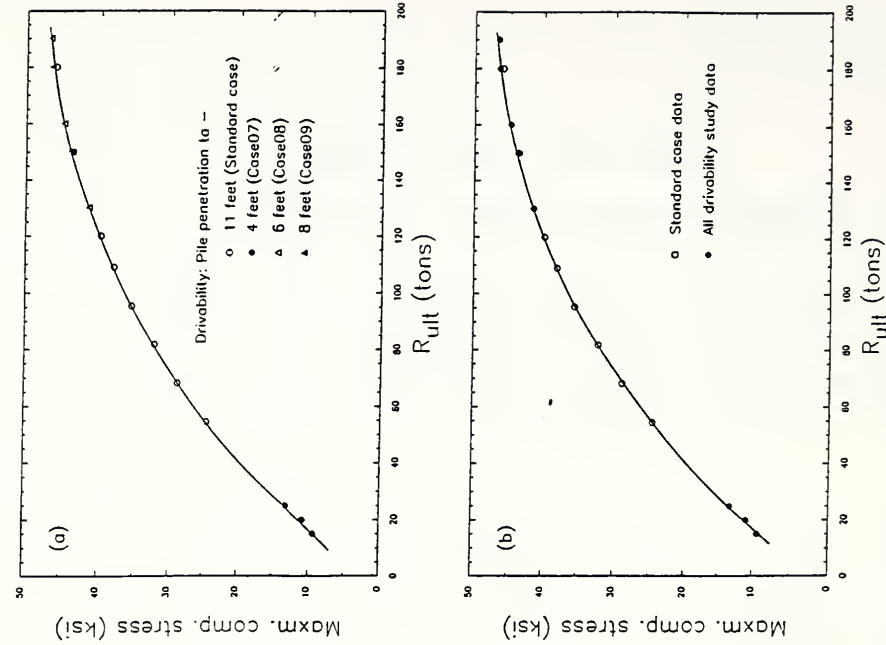


Figure 3.14 Bearing curves for drivability study at SR26/TB-3

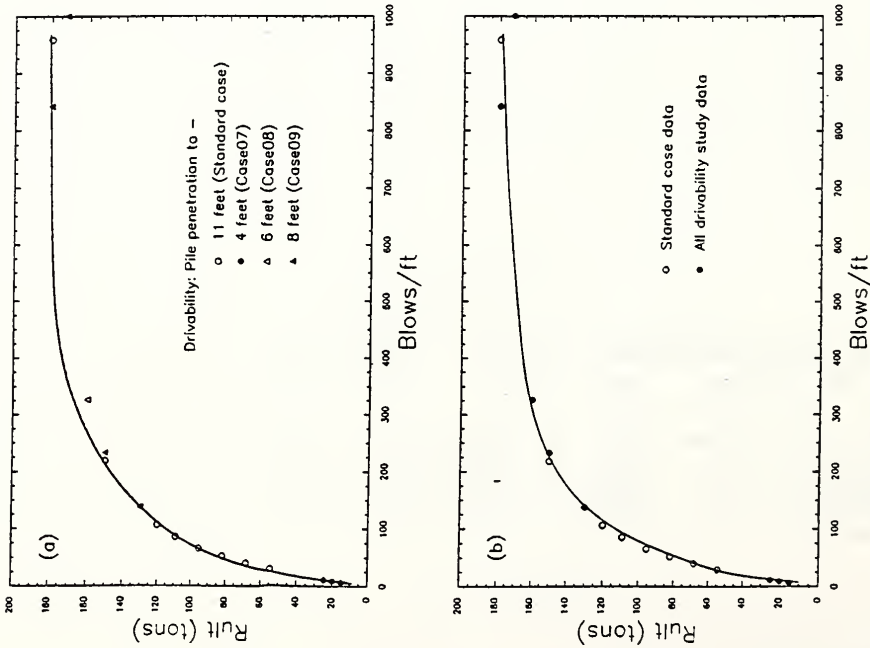


Figure 3.15 Maximum compressive stresses in drivability study at SR26/TB-3

## Section 3.1.2 Ex. - SR26 (TB-3) Case00

R <sub>ult</sub> kips	Bl bpf	Ct down	Stroke (ft) up	MinStr I,J ksi	MaxStr I,J ksi	Enthru ft-kip	Bl Rt bpm
264.0	105.9	6.0	6.0	.00( 1, 0)	39.83( 1, 96)	.0	48.1
330.0	218.8	6.5	6.5	.00( 1, 0)	43.81( 1, 97)	.0	46.3
396.0	958.4	6.8	6.9	.00( 1, 0)	46.00( 1,100)	.0	45.3
462.0	9999.0	6.9	7.0	.00( 1, 0)	47.02( 1, 99)	.0	44.8
528.0	9999.0	6.9	7.1	.00( 1, 0)	47.67( 1, 99)	.0	44.6

## Section 3.1.2 Ex. - SR26 (TB-3) Case07

33.0	5.9	3.2	3.2	.00( 1, 0)	9.30( 1, 68)	.0	65.2
44.0	8.4	3.4	3.5	.00( 1, 0)	10.84( 1, 70)	.0	62.9
55.0	10.6	3.9	3.7	.00( 1, 0)	13.23( 1, 94)	.0	60.4

## Section 3.1.2 Ex. - SR26 (TB-3) Case08

286.0	137.1	6.2	6.2	.00( 1, 0)	41.48( 1, 97)	.0	47.4
352.0	325.8	6.7	6.7	.00( 1, 0)	44.88( 1, 98)	.0	45.8
418.0	3115.4	6.9	7.0	.00( 1, 0)	46.73( 1, 99)	.0	44.9

## Section 3.1.2 Ex. - SR26 (TB-3) Case09

330.0	232.8	6.5	6.5	.00( 1, 0)	43.69( 1, 98)	.0	46.4
396.0	842.3	6.9	6.9	.00( 1, 0)	46.50( 1, 99)	.0	45.0
462.0	9999.0	7.2	7.1	.00( 1, 0)	47.82( 1, 98)	.0	44.3

### 3.2 East 206th Street over White River

Project No: RS-8229(1)  
 Location: Hamilton County, Indiana  
 Piling done: July, 1988

The plan layout of the six test borings (TB-1 to TB-6) used to obtain the soil profiles is as shown in Fig. 3.16. Fig. 3.17 is a sketch of the generalized subsurface conditions at the site. The estimated shaft friction distribution from TB-1 (Fig. 3.18) is used for piles along bent no. 1 (end bent - studied in Sec. 3.2.1) and the profile from TB-2 (Fig. 3.23) is used for piles along bent no. 2 (interior bent studied in Sec. 3.2.2).

#### 3.2.1 Pile at bent number 1 (end bent)

Ground elevation at TB-1 was 762.3 ft at time of driving. The specified minimum pile tip elevation is 735 ft. A shell length of 30 ft is used. The estimated values of  $Q_b$  and  $Q_s$  are 65 t and 36 t, respectively. These values are obtained based on the bore-hole data from TB-1. The value of  $Q_{sd}$  is estimated assuming that the side resistance faced by the shell is 75% of the calculated static side friction resistance. The applicable friction distribution profile for input to WEAP87 is shown in Figure 3.18. The expected value of  $R_{ult}$  is 92 t. Table 3.5 lists the range of  $R_{ult}$  values used for analysis.

Table 3.5  
 Range of  $R_{ult}$  : IPERCS = 29%

	(tons)	27.3	34.1	40.9	47.7	54.5	60	75	90	105	120
$R_{ult}$	(kips)	60	75	90	105	120	132	165	198	231	264
$Q_b$	(tons)	7.9	9.9	11.9	13.8	15.8	17.4	21.8	26.1	30.5	34.8
$Q_{sd}$	(tons)	19.4	24.2	29	33.9	38.7	42.6	53.2	63.9	74.5	85.2



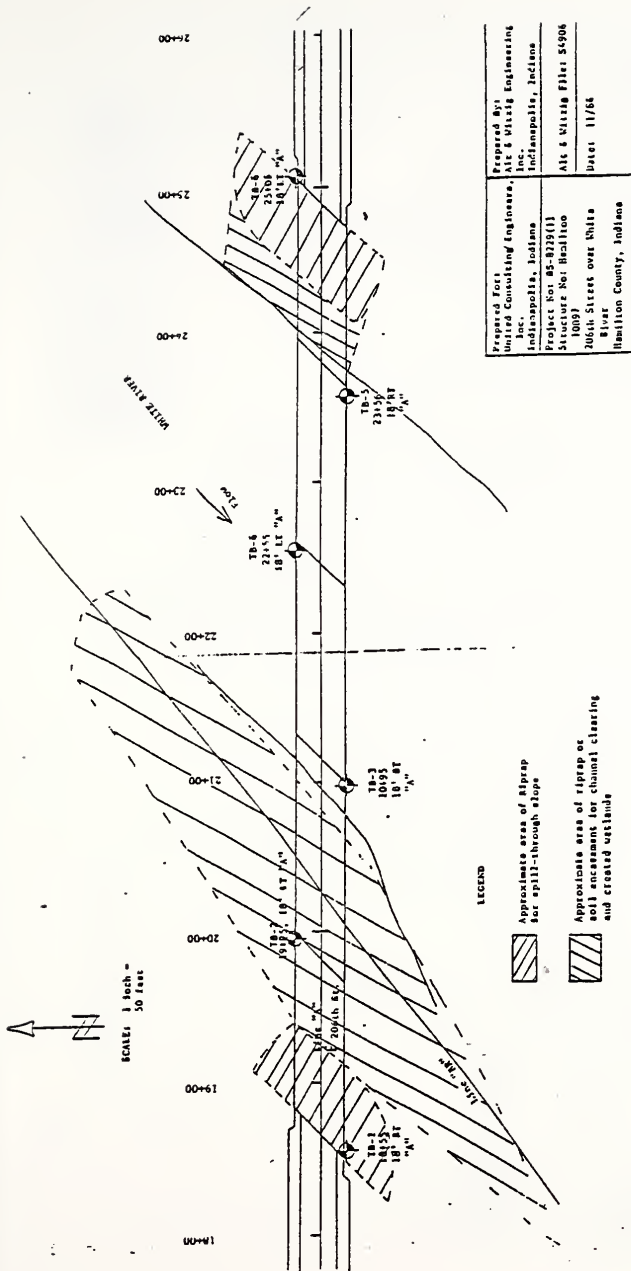


Figure 3.16 Plan layout of the six test borings (TB-1 to TB-6) used to obtain the soil profiles for the East 206th street bridge over White river

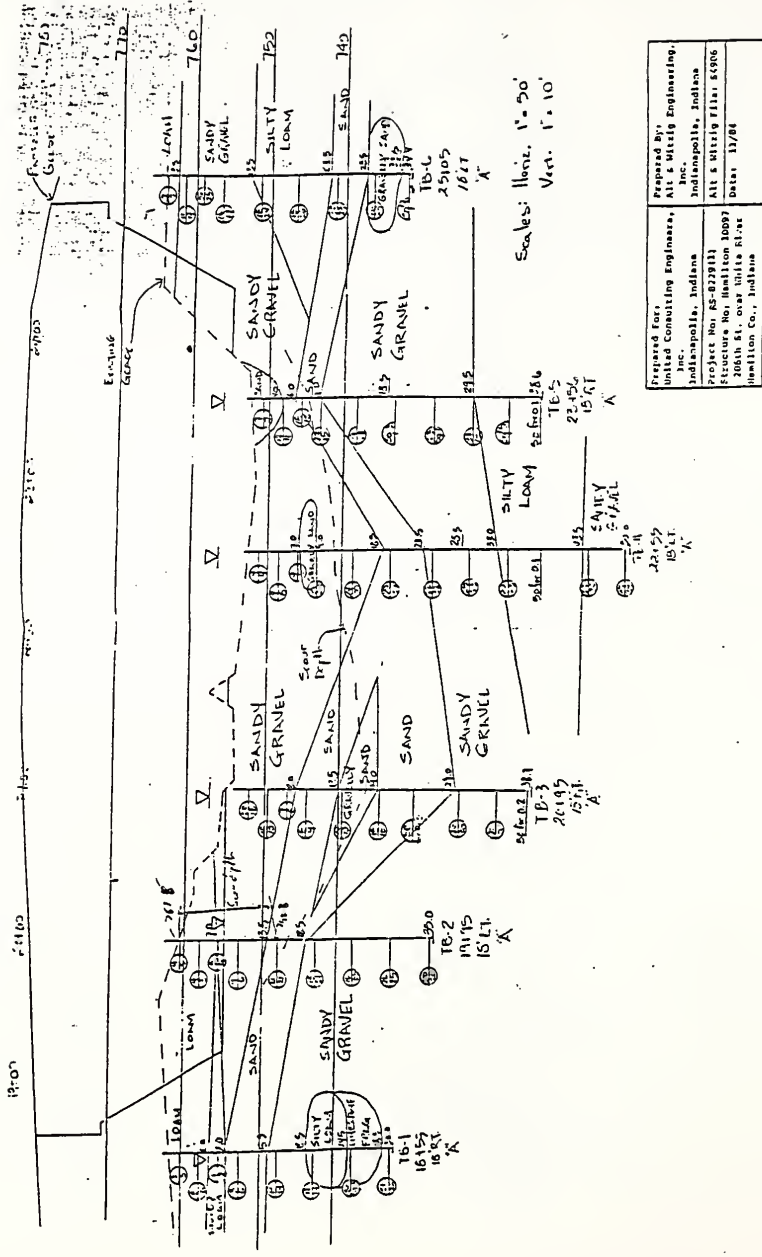


Figure 3.17 Generalized subsurface conditions at site of bridge structure (East 206th street bridge over White river)

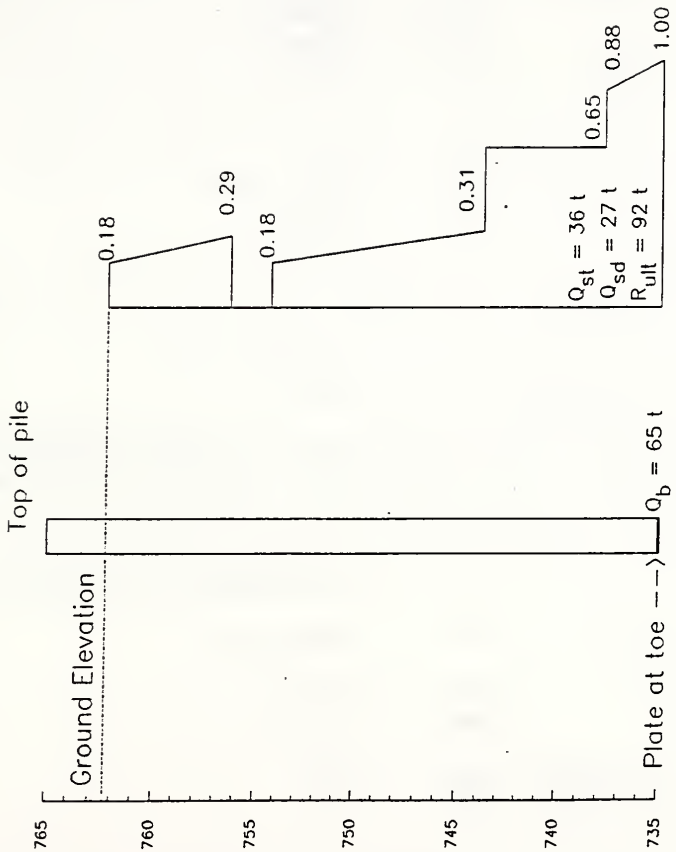


Figure 3.18 Shaft friction distribution for bent no. 1  
East 206th Street over White River

The standard case (Case00) parameters are as follows:

Pile	Type	Thin steel shell		
	Gage	5 (wall thickness = 0.203"; c/s area = 8.8 in <sup>2</sup> )		
	$\phi$	14"		
	Length	30 ft		
Hammer	Type	Delmag D 12		
	Efficiency	0.8		
	Cushion	Area	283.5 in <sup>2</sup>	
		Material	Plywood	
		Thickness	0.75"	
Helmet	Weight	2.02 kips		
Soil Parameters	Quake	Shaft	0.1"	
		Toe	0.1"	
	Damping	Type	Smith (Normal)	
		Shaft	0.05 s/ft	
		Toe	0.15 s/ft	
$R_{ult}$	Table 3.5			
Shaft Friction	As a % of $R_{ult}$	29 (IPERCS = 29)		
	Distribution used	Fig. 3.18		

Parametric studies are conducted to assess the effects of different parameters. Only one parameter is varied at a time, with the remainder of the data identical to that of the standard case:

Pile	Gage	Case01	7 (wall thickness= 0.179"; c/s area=7.77 in <sup>2</sup> )
Hammer	Type	Case02	Delmag D 22
Damping	Toe	Case03	0.10 s/ft
		Case04	0.20 s/ft
Quake	Toe & Shaft	Case05	0.05"
	Toe & Shaft	Case06	0.15"

The results of these analyses are given as Figures 3.19 to 3.22. A tabular summary of WEAP87 results (for the five largest  $R_{ult}$  values) follows each figure.

Figure 3.19 shows the effect of using a different gage for the shell material. The 7 gage shell is harder to drive than the 5 gage shell for values of  $R_{ult}$  higher than 80 t. The increase in the blow count is small and an  $AF_B$  of 1.05 (*i.e.*, a 5% increase in blow count) will be adequate. The thinner shell also results in an increase in stress (*i.e.*,  $AF_S = 1.11$ ), which is smooth over the entire range of  $R_{ult}$  studied.

Using a heavier hammer results in considerable reduction in the blow count (Fig. 3.20). The Delmag D 22 hammer is capable of driving the shell with a blow count which is less than half (*i.e.*,  $AF_B = 0.50$ ) that needed by the lighter D 12 hammer, to achieve comparable bearing capacity. However, using the heavier hammer results in an increase in stresses induced in the shell (Fig. 3.20(b)). This increase can be accounted for by using an adjustment factor of 12% (*i.e.*,  $AF_S = 1.12$ ) for  $R_{ult}$  values in the range of interest. However, the stresses are still within safe limits, and overall *the results indicate that the heavier hammer (D 22) would have been a better choice at this site also.*

The effect of variation in damping at toe follows the smooth trends (Fig. 3.21) detected in the previous cases studied. Adjustment factors of 1.15 and 1.05 for  $AF_B$  and  $AF_S$ , respectively, would suffice to account for the variations in damping.

Changing the quake from the recommended values, 0.1" for both toe and shaft, has a small effect on the drivability for low values of  $R_{ult}$  (Fig. 3.22(a)). For capacities greater than 70 t, the blow count increases by 6% to 15% when damping is 50% higher than the standard case. The corresponding decrease in peak stress is 3-4%. Adjustment factors of 1.15 ( $AF_B$ ) and 0.96 ( $AF_S$ ) would suffice to account for errors in the bearing curves, arising due to errors in estimating the soil quake.

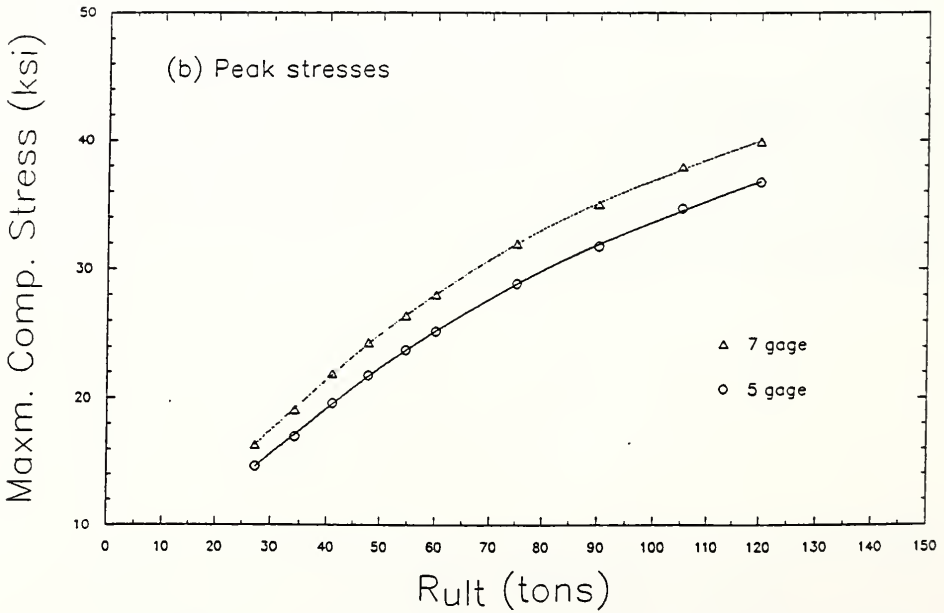
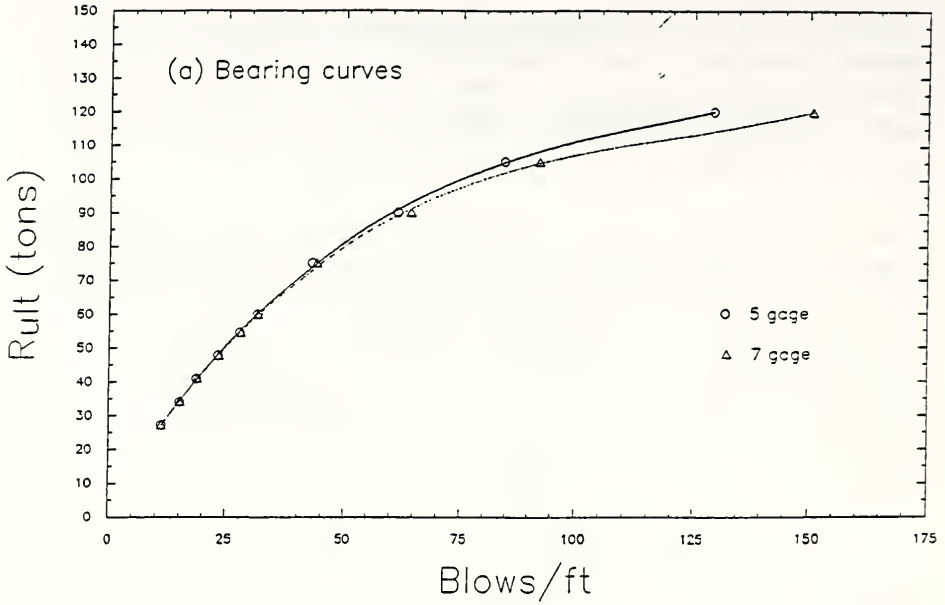


Figure 3.19 Variation in thin shell gage (E206/TB-1)

## Section 3.2.1 - E206 St. (TB-1) Case00

R <sub>ult</sub> kips	Bl Ct bpf	Stroke (ft) down up	MinStr I,J ksi	MaxStr I,J ksi	Enthru ft-kip	Bl Rt bpm
132.0	31.7	4.6 4.7	.00( 1, 0)	25.15( 1,104)	.0	54.4
165.0	42.9	5.0 5.0	.00( 1, 0)	28.85( 1,106)	.0	52.6
198.0	61.4	5.2 5.4	.00( 1, 0)	31.75( 1,107)	.0	51.4
231.0	84.4	5.6 5.6	.00( 1, 0)	34.69( 1,108)	.0	49.7
264.0	129.6	5.9 5.9	.00( 1, 0)	36.75( 1,109)	.0	48.7

## Section 3.2.1 - E206 St. (TB-1) Case01

R <sub>ult</sub> kips	Bl Ct bpf	Stroke (ft) down up	MinStr I,J ksi	MaxStr I,J ksi	Enthru ft-kip	Bl Rt bpm
132.0	31.8	4.6 4.7	.00( 1, 0)	27.98( 1,106)	.0	54.6
165.0	43.9	5.0 5.0	.00( 1, 0)	31.95( 1,109)	.0	52.7
198.0	64.2	5.2 5.3	.00( 1, 0)	35.02( 1,110)	.0	51.4
231.0	92.2	5.6 5.6	.00( 1, 0)	37.95( 1,112)	.0	49.8
264.0	150.7	5.8 5.8	.00( 1, 0)	39.91( 1,114)	.0	48.9

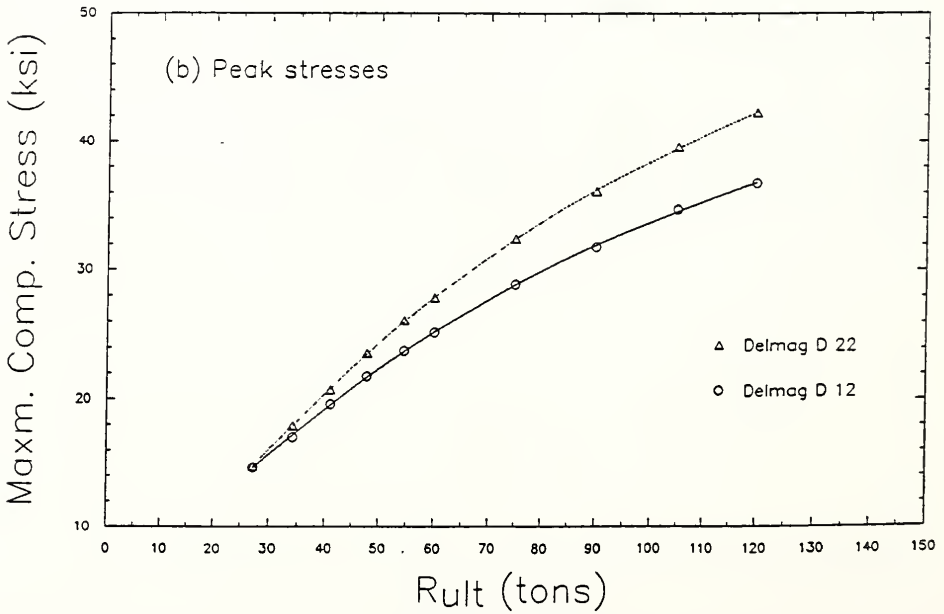
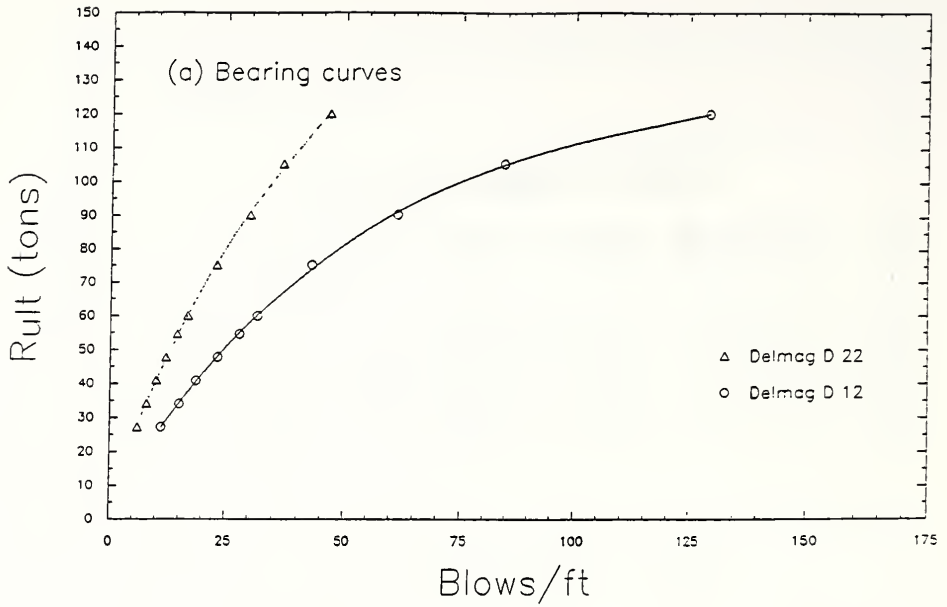


Figure 3.20 Effect of heavier hammer (E206/TB-1)



## Section 3.2.1 - E206 St. (TB-1) Case00

R <sub>ult</sub> kips	Bl bpf	Ct down	Stroke (ft) up	MinStr I,J ksi	MaxStr I,J ksi	Enthru ft-kip	Bl Rt bpm
132.0	31.7	4.6	4.7	.00( 1, 0)	25.15( 1,104)	.0	54.4
165.0	42.9	5.0	5.0	.00( 1, 0)	28.85( 1,106)	.0	52.6
198.0	61.4	5.2	5.4	.00( 1, 0)	31.75( 1,107)	.0	51.4
231.0	84.4	5.6	5.6	.00( 1, 0)	34.69( 1,108)	.0	49.7
264.0	129.6	5.9	5.9	.00( 1, 0)	36.75( 1,109)	.0	48.7

## Section 3.2.1 - E206 St. (TB-1) Case02

R <sub>ult</sub> kips	Bl bpf	Ct down	Stroke (ft) up	MinStr I,J ksi	MaxStr I,J ksi	Enthru ft-kip	Bl Rt bpm
132.0	16.8	3.7	3.7	.00( 1, 0)	27.81( 1,114)	.0	60.5
165.0	23.0	4.0	4.1	.00( 1, 0)	32.40( 1,114)	.0	58.2
198.0	30.0	4.1	4.3	.00( 1, 0)	36.07( 1,117)	.0	56.9
231.0	36.7	4.5	4.5	.00( 1, 0)	39.57( 1,117)	.0	55.2
264.0	46.6	4.7	4.7	.00( 1, 0)	42.23( 1,119)	.0	54.2

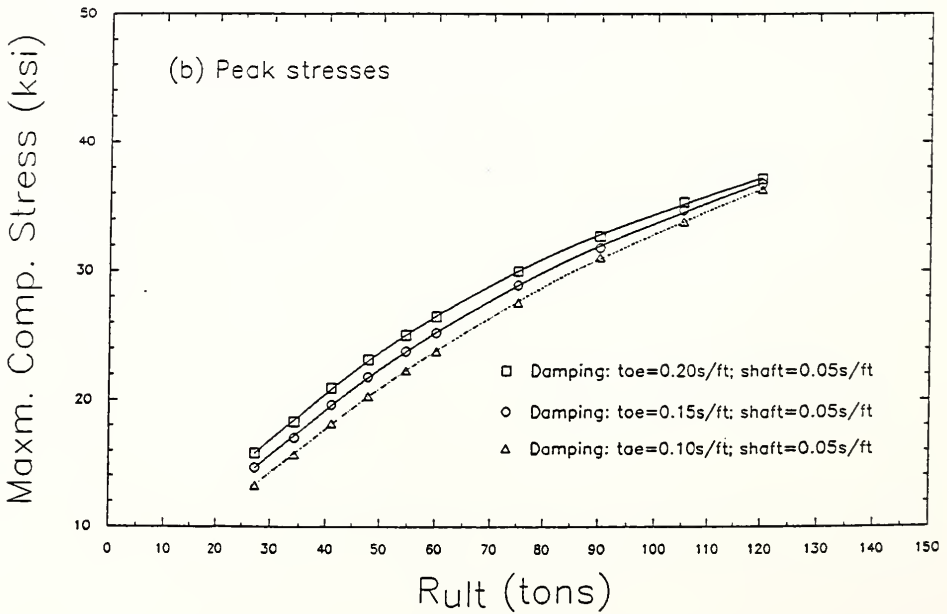
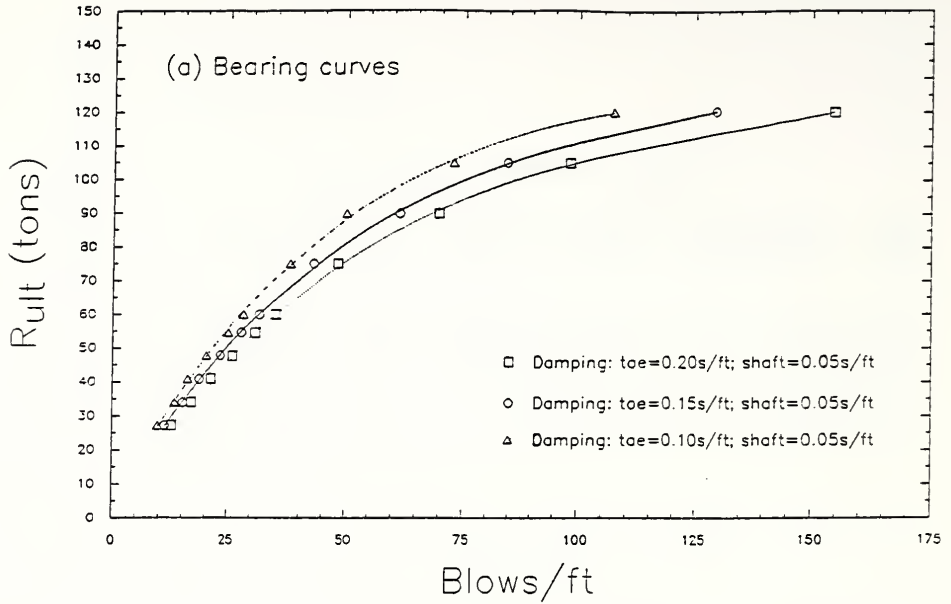


Figure 3.21 Variation in damping at toe (E206/TB-1)

## Section 3.2.1 - E206 St. (TB-1) Case00

R <sub>ult</sub> kips	Bl bpf	Ct down	Stroke (ft) up	MinStr I,J ksi	MaxStr I,J ksi	Enthru ft-kip	Bl Rt bpm
132.0	31.7	4.6	4.7	.00( 1, 0)	25.15( 1,104)	.0	54.4
165.0	42.9	5.0	5.0	.00( 1, 0)	28.85( 1,106)	.0	52.6
198.0	61.4	5.2	5.4	.00( 1, 0)	31.75( 1,107)	.0	51.4
231.0	84.4	5.6	5.6	.00( 1, 0)	34.69( 1,108)	.0	49.7
264.0	129.6	5.9	5.9	.00( 1, 0)	36.75( 1,109)	.0	48.7

## Section 3.2.1 - E206 St. (TB-1) Case03

R <sub>ult</sub> kips	Bl bpf	Ct down	Stroke (ft) up	MinStr I,J ksi	MaxStr I,J ksi	Enthru ft-kip	Bl Rt bpm
132.0	28.4	4.5	4.6	.00( 1, 0)	23.72( 1,103)	.0	55.1
165.0	37.9	4.8	4.9	.00( 1, 0)	27.51( 1,105)	.0	53.3
198.0	50.0	5.2	5.2	.00( 1, 0)	31.00( 1,106)	.0	51.5
231.0	72.6	5.4	5.5	.00( 1, 0)	33.79( 1,107)	.0	50.4
264.0	107.2	5.8	5.8	.00( 1, 0)	36.30( 1,108)	.0	49.0

## Section 3.2.1 - E206 St. (TB-1) Case04

R <sub>ult</sub> kips	Bl bpf	Ct down	Stroke (ft) up	MinStr I,J ksi	MaxStr I,J ksi	Enthru ft-kip	Bl Rt bpm
132.0	35.0	4.7	4.8	.00( 1, 0)	26.40( 1,104)	.0	53.9
165.0	48.2	5.1	5.1	.00( 1, 0)	29.95( 1,105)	.0	52.1
198.0	69.7	5.3	5.4	.00( 1, 0)	32.64( 1,108)	.0	50.9
231.0	98.2	5.7	5.7	.00( 1, 0)	35.32( 1,108)	.0	49.4
264.0	154.6	5.9	5.9	.00( 1, 0)	37.13( 1,110)	.0	48.5

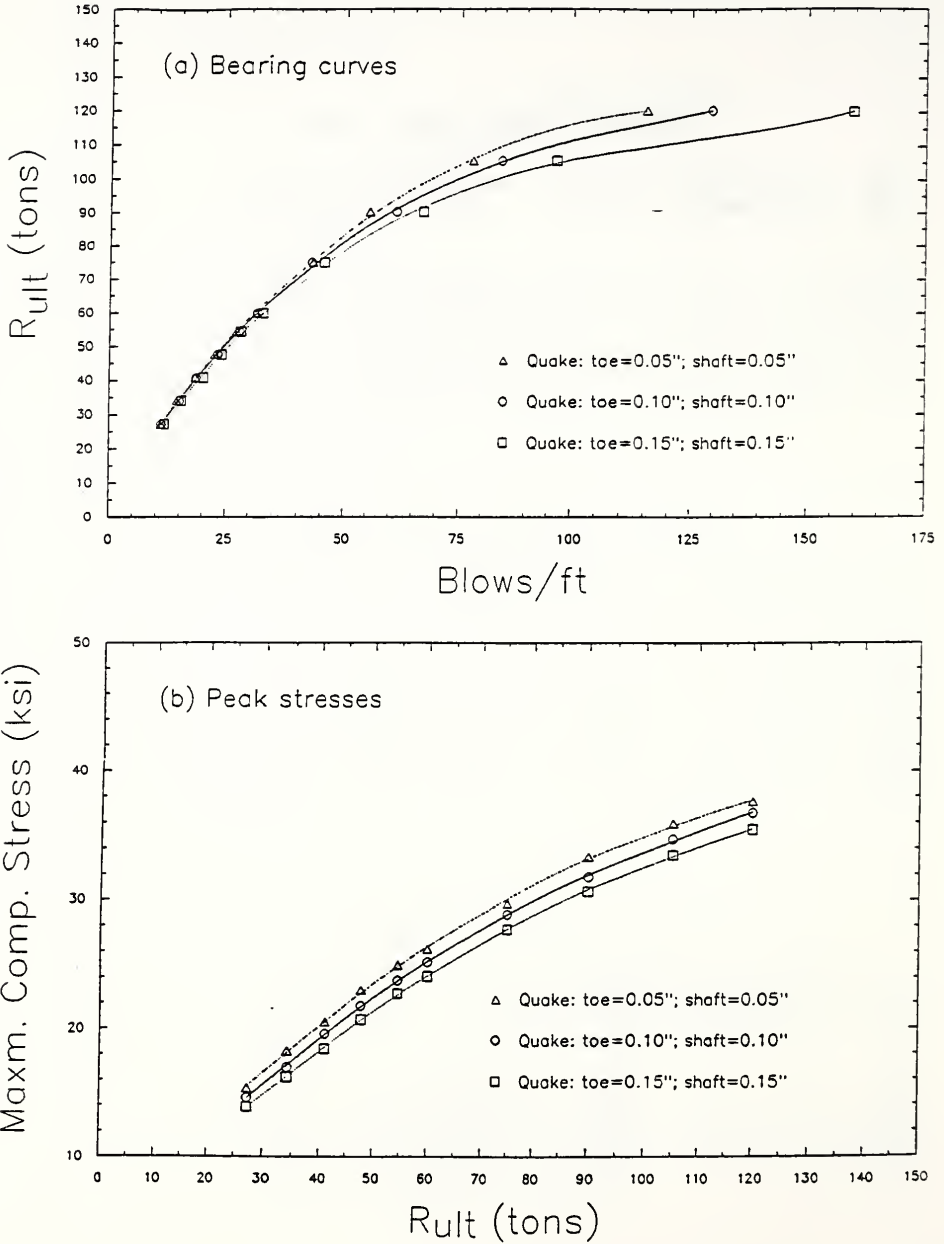


Figure 3.22 Variation in quake (E206/TB-1)

## Section 3.2.1 - E206 St. (TB-1) Case00

R <sub>ult</sub> kips	Bl bpf	Ct	Stroke (ft) down up	MinStr I,J ksi	MaxStr I,J ksi	Enthru ft-kip	Bl Rt bpm
132.0	31.7	4.6	4.7	.00( 1, 0)	25.15( 1,104)	.0	54.4
165.0	42.9	5.0	5.0	.00( 1, 0)	28.85( 1,106)	.0	52.6
198.0	61.4	5.2	5.4	.00( 1, 0)	31.75( 1,107)	.0	51.4
231.0	84.4	5.6	5.6	.00( 1, 0)	34.69( 1,108)	.0	49.7
264.0	129.6	5.9	5.9	.00( 1, 0)	36.75( 1,109)	.0	48.7

## Section 3.2.1 - E206 St. (TB-1) Case05

R <sub>ult</sub> kips	Bl bpf	Ct	Stroke (ft) down up	MinStr I,J ksi	MaxStr I,J ksi	Enthru ft-kip	Bl Rt bpm
132.0	31.5	4.6	4.7	.00( 1, 0)	26.16( 1, 98)	.0	54.4
165.0	43.1	4.9	4.9	.00( 1, 0)	29.71( 1,100)	.0	53.2
198.0	55.5	5.4	5.4	.00( 1, 0)	33.31( 1,101)	.0	50.7
231.0	77.7	5.7	5.7	.00( 1, 0)	35.89( 1,103)	.0	49.5
264.0	115.2	5.8	5.9	.00( 1, 0)	37.64( 1,105)	.0	48.7

## Section 3.2.1 - E206 St. (TB-1) Case06

R <sub>ult</sub> kips	Bl bpf	Ct	Stroke (ft) down up	MinStr I,J ksi	MaxStr I,J ksi	Enthru ft-kip	Bl Rt bpm
132.0	32.8	4.6	4.7	.00( 1, 0)	24.05( 1,108)	.0	54.6
165.0	45.6	4.9	5.0	.00( 1, 0)	27.71( 1,111)	.0	52.9
198.0	67.1	5.1	5.3	.00( 1, 0)	30.63( 1,112)	.0	51.7
231.0	96.7	5.6	5.5	.00( 1, 0)	33.46( 1,112)	.0	50.0
264.0	159.6	5.8	5.8	.00( 1, 0)	35.45( 1,114)	.0	49.0

### 3.2.2 Pile at bent number 2 (interior bent)

This is an interior bent with a ground elevation, at time of piling, equal to 762.8 ft. Scour is estimated to be 14 ft, the recommended minimum pile tip elevation is 740.8 ft. A shell length of 25.2 ft is used. The estimated values of  $Q_b$  and  $Q_s$  are 70 t and 32 t, respectively. These values are obtained based on the bore-hole data from TB-2. Under the worst estimated scouring conditions, the embedded length of the pile is 8 ft which is still sufficient to provide an ultimate capacity of 90 t ( $Q_b = 70$  t, and  $Q_s = 20$  t). The estimated values for  $R_{ult}$  are 94 t and 84 t for corresponding to driving without jetting and driving after jetting past the scour depth, respectively. The standard case is considered without jetting and the case with jetting is treated as a variation (Case07). Since the subgrade at this bent is almost entirely composed of sand and sandy gravel, a simple side friction distribution profile (Fig. 3.23) is used for input to WEAP87. The  $R_{ult}$  value used is 94 t and Table 3.6 lists the range of  $R_{ult}$  values used for analysis.

**Table 3.6**  
Range of  $R_{ult}$  : IPERCS = 26%

$R_{ult}$ (tons)	29.5	36.4	43.2	50	56.8	65	80	95	110	125
$R_{ult}$ (kips)	65	80	95	110	125	143	176	209	242	275
$Q_b$ (tons)	7.7	9.5	11.2	13	14.8	16.9	20.8	24.7	28.6	32.5
$Q_{sd}$ (tons)	21.8	26.9	32	37	42	48.1	59.2	70.3	81.4	92.5

The standard case (Case00) parameters are as follows:

Pile	Type	Thin steel shell	
	Gage	5 (wall thickness = 0.203"; c/s area = 8.8 in <sup>2</sup> )	
	$\phi$	14"	
	Length	25.2 ft	
Hammer	Type	Delmag D 12	
	Efficiency	0.8	
	Cushion	Area	283.5 in <sup>2</sup>
		Material	Plywood
Thickness		0.75"	

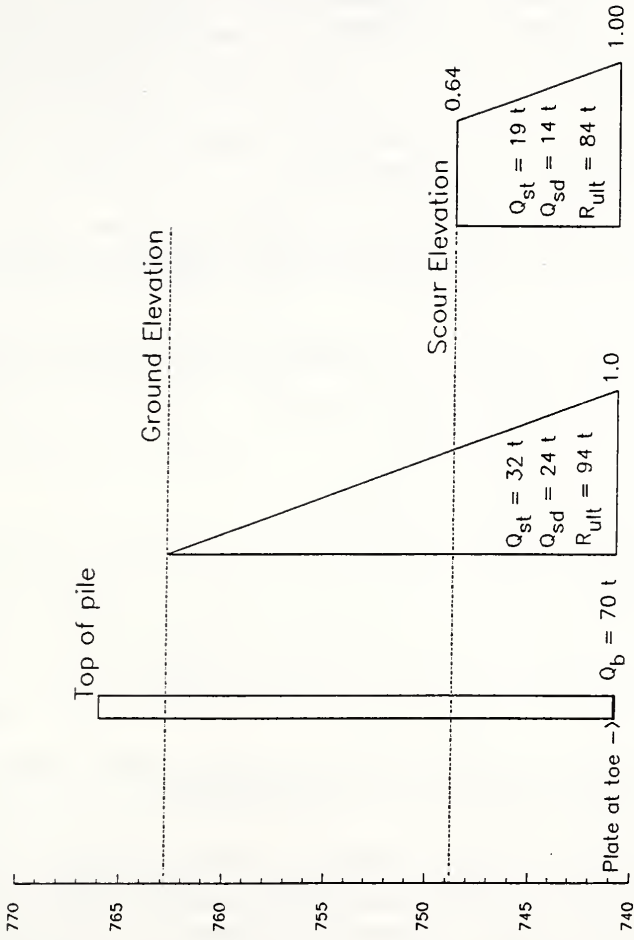


Figure 3.23 Shaft friction distribution for bent no. 2 East 206th Street over White River

Hammer	Helmet	Weight	2.02 kips
Soil Parameters	Quake	Shaft	0.1"
		Toe	0.1"
	Damping	Type	Smith (Normal)
		Shaft	0.05 s/ft
		Toe	0.15 s/ft
$R_{ult}$	Table 3.6		
Shaft Friction	As a % of $R_{ult}$ Distribution used		26 (IPERCS = 26) Fig. 3.23

Parametric studies are conducted to assess the effects of different parameters. Only one parameter is varied at a time, with the remainder of the data identical to that of the standard case:

Pile	Gage	Case01	7 (wall thickness = 0.179"; c/s area = 7.77 in <sup>2</sup> )
Hammer	Type	Case02	Delmag D 22
Damping	Toe	Case03	0.10 s/ft
		Case04	0.20 s/ft
Quake	Toe & Shaft	Case05	0.05"
	Toe & Shaft	Case06	0.15"
Driving after jetting past scour depth		Case07	$R_{ult} = 84 \text{ t}$ ( $Q_b = 70 \text{ t}$ ; $Q_{sd} = 24 \text{ t}$ )

The results of these analyses are given as Figures 3.24 to 3.28. A tabular summary of WEAP87 results (for the five largest  $R_{ult}$  values) follows each figure.

Figure 3.24 shows the effect of using a different gage for the shell material. The thinner shell (7 gage) results in about 11% increase in peak stresses (*i.e.*,  $AF_s = 1.11$ ) with almost no change in the number of blows required for driving (*i.e.*,  $AF_b = 1.00$ ) in the range of interest. This implies that at this bent, the use of 7 gage shells would not have caused any problems. However, the 5 gage shells used were probably a better choice in case unexpected hard layers were encountered.



Fig. 3.25 shows that using a heavier hammer results in 50% reduction in the number of blows required (*i.e.*,  $AF_b = 0.5$ ) to achieve comparable bearing capacity. The hammer with the higher rated energy, the Delmag D 22, required only 32 bpf to drive the shell to a capacity of 95 t, whereas the standard Delmag D 12 required 66 bpf. However, using the heavier hammer results in an increase in stresses induced in the shell (Fig. 3.25(b)). Using the D 22 causes a 7% to 12% increase in the maximum stress as compared to the D 12 hammer at  $R_{ult}$  values from 60 to 110 t. An  $AF_s$  value of 1.10 would suffice for the range of interest of  $R_{ult}$  values. Although the stress increase is not large it could possibly lead to peak stresses close to the yield limit of the shell material. *These results indicate that a D 22 hammer would have enabled faster driving but would have required careful control during driving to avoid damage to the shells.*

The effect of variation in damping is again the same as the trends observed in earlier cases (Fig. 3.26). The adjustment factors, for an increase in damping at the toe from 0.15 s/ft to 0.20 s/ft, are estimated to be 1.15 and 1.04 (*i.e.*, a 15% increase in the blow count, and a 5% increase in the expected maximum peak stress). Based on results in Chapter 2, it is concluded that the effect of a change in the damping along the shaft would have similar results, hence the final adjustment factors to be used are 1.3 and 1.1 for  $AF_b$  and  $AF_s$ , respectively.

Changing the quake to 0.15 inch (from the recommended values, 0.1" for both toe and shaft) has a small effect on the drivability (Fig. 3.27(a)) and marginal effect on the induced maximum compressive stresses (Fig. 3.27(b)). An adjustment factor of 7% (*i.e.*,  $AF_b = 1.07$ ) would suffice to account for errors in the bearing curves, arising due to errors in estimating the soil quake. The corresponding decrease (compared to the standard case) in stresses can be accounted for by using an  $AF_s$  value of 0.96.

Finally, the effect of jetting past the scour depth is also evaluated. Fig. 3.28 seems to indicate that the use of jetting to get past the scour depth does not have any effect on the results (the bearing curves and the curves for peak stresses are almost overlapping for the two cases compared). However, the results in this case need to be evaluated differently from the other comparisons done so far. Since the shape of the side friction distribution is similar in both cases, the dynamic analysis results in comparable results for comparable values of  $R_{ult}$ . The advantage of using jetting comes in the form of lowered  $R_{ult}$  values (as compared to the standard case) being seen by the shell and this translates to lower peak stresses occurring in the shell, and reduced blow counts required to drive the shell to the same depth.

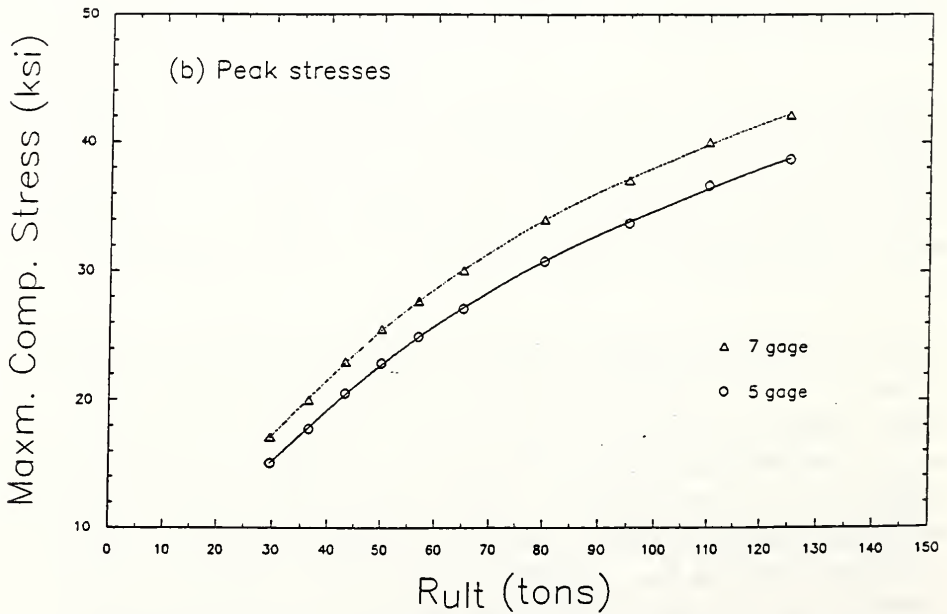
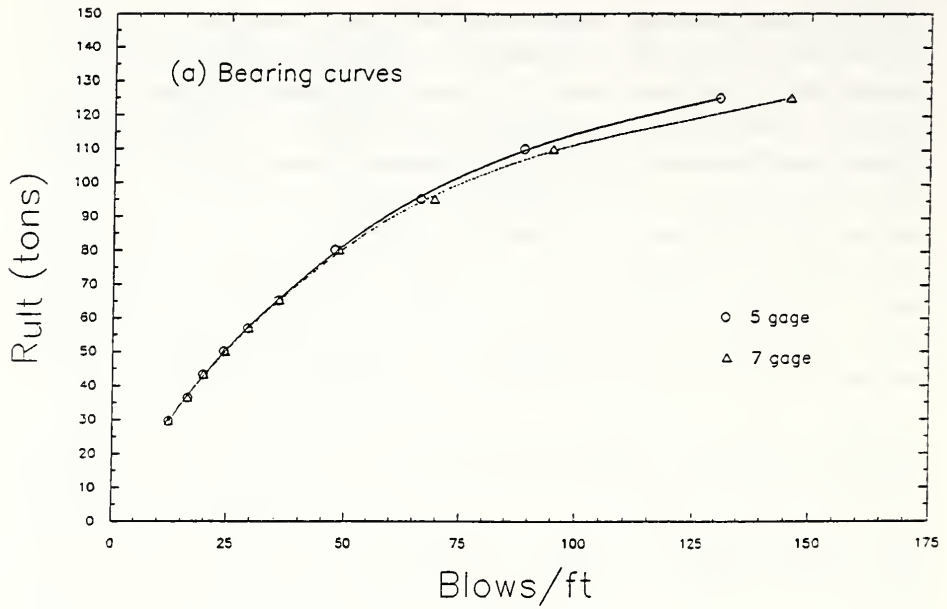


Figure 3.24 Variation in thin shell gage (E206/TB-2)

## Section 3.2.2 - E206 St. (TB-2) Case00

R <sub>ult</sub> kips	Bl bpf	Ct down	Stroke (ft) up	MinStr I,J ksi	MaxStr I,J ksi	Enthru ft-kip	Bl Rt bpm
143.0	35.5	4.8	4.9	.00( 1, 0)	27.07( 1, 99)	.0	53.4
176.0	47.5	5.2	5.2	.00( 1, 0)	30.77( 1,100)	.0	51.7
209.0	66.3	5.3	5.5	.00( 1, 0)	33.73( 1,101)	.0	50.7
242.0	88.6	5.8	5.7	.00( 1, 0)	36.65( 1,102)	.0	49.2
275.0	130.8	6.0	6.0	.00( 1, 0)	38.66( 1,103)	.0	48.2

## Section 3.2.2 - E206 St. (TB-2) Case01

R <sub>ult</sub> kips	Bl bpf	Ct down	Stroke (ft) up	MinStr I,J ksi	MaxStr I,J ksi	Enthru ft-kip	Bl Rt bpm
143.0	35.6	4.8	4.9	.00( 1, 0)	30.04( 1,101)	.0	53.5
176.0	48.4	5.1	5.2	.00( 1, 0)	34.03( 1,102)	.0	51.8
209.0	69.1	5.3	5.5	.00( 1, 0)	37.04( 1,104)	.0	50.7
242.0	94.8	5.7	5.7	.00( 1, 0)	40.03( 1,105)	.0	49.3
275.0	145.9	5.9	6.0	.00( 1, 0)	42.12( 1,107)	.0	48.3

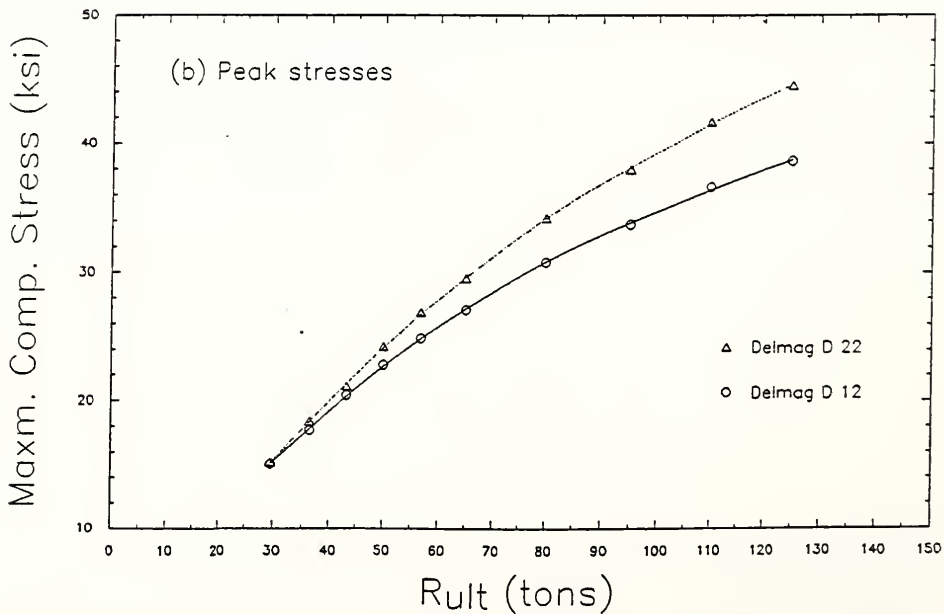
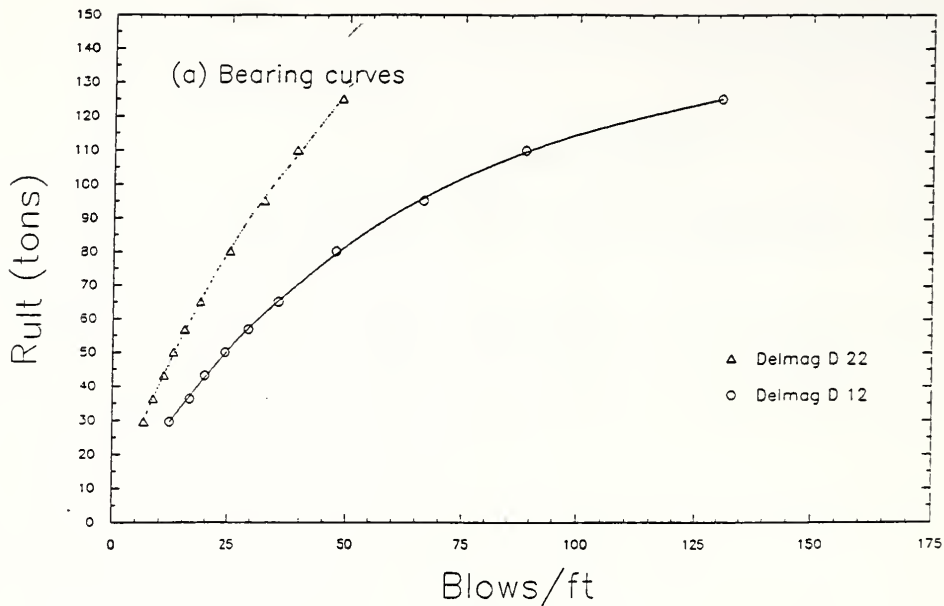


Figure 3.25 Effect of heavier hammer (E206/TB-2)

## Section 3.2.2 - E206 St. (TB-2) Case00

R <sub>ult</sub> kips	Bl bpf	Ct down	Stroke (ft) up	MinStr I,J ksi	MaxStr I,J ksi	Enthru ft-kip	Bl Rt bpm
143.0	35.5	4.8	4.9	.00( 1, 0)	27.07( 1, 99)	.0	53.4
176.0	47.5	5.2	5.2	.00( 1, 0)	30.77( 1,100)	.0	51.7
209.0	66.3	5.3	5.5	.00( 1, 0)	33.73( 1,101)	.0	50.7
242.0	88.6	5.8	5.7	.00( 1, 0)	36.65( 1,102)	.0	49.2
275.0	130.8	6.0	6.0	.00( 1, 0)	38.66( 1,103)	.0	48.2

## Section 3.2.2 - E206 St. (TB-2) Case02

R <sub>ult</sub> kips	Bl bpf	Ct down	Stroke (ft) up	MinStr I,J ksi	MaxStr I,J ksi	Enthru ft-kip	Bl Rt bpm
143.0	18.7	3.8	3.9	.00( 1, 0)	29.54( 1,110)	.0	59.4
176.0	25.0	4.1	4.2	.00( 1, 0)	34.23( 1,109)	.0	57.3
209.0	32.4	4.3	4.4	.00( 1, 0)	37.97( 1,111)	.0	56.1
242.0	38.9	4.6	4.6	.00( 1, 0)	41.68( 1,111)	.0	54.5
275.0	48.5	4.8	4.8	.00( 1, 0)	44.51( 1,113)	.0	53.5

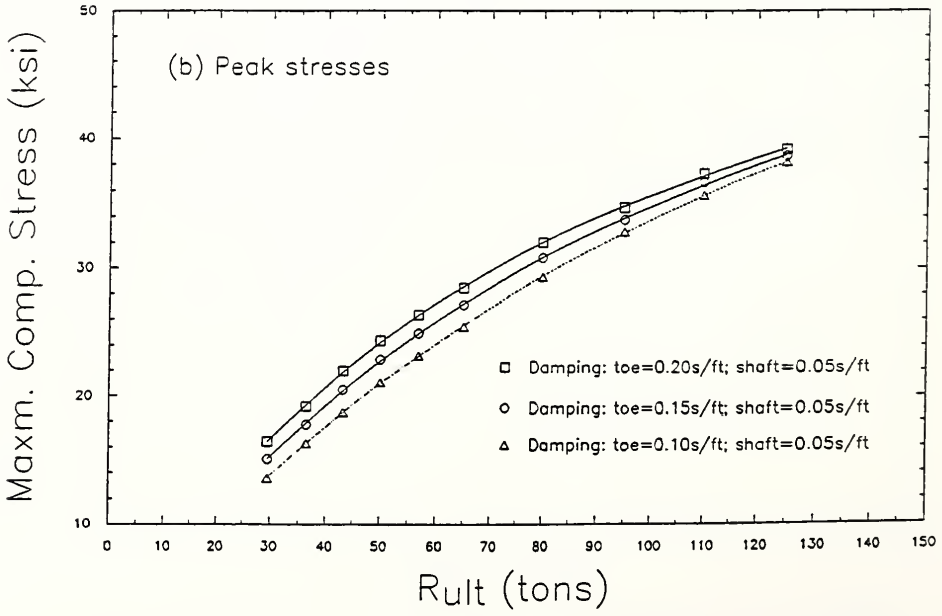
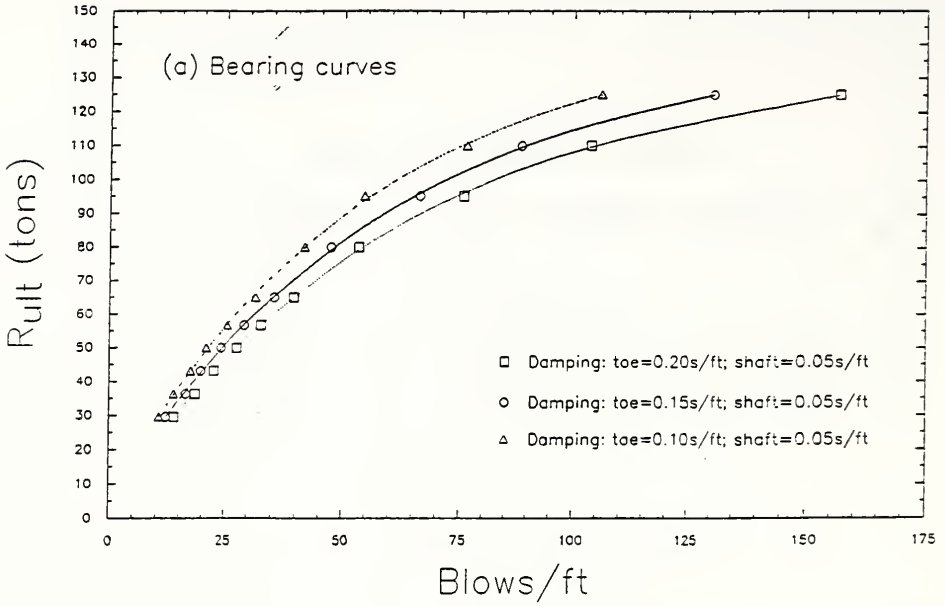


Figure 3.26 Variation in damping at toe (E206/TB-2)

## Section 3.2.2 - E206 St. (TB-2) Case00

R <sub>ult</sub> kips	Bl bpf	Ct down	Stroke (ft) up	MinStr I,J ksi	MaxStr I,J ksi	Enthru ft-kip	Bl Rt bpm
143.0	35.5	4.8	4.9	.00( 1, 0)	27.07( 1, 99)	.0	53.4
176.0	47.5	5.2	5.2	.00( 1, 0)	30.77( 1,100)	.0	51.7
209.0	66.3	5.3	5.5	.00( 1, 0)	33.73( 1,101)	.0	50.7
242.0	88.6	5.8	5.7	.00( 1, 0)	36.65( 1,102)	.0	49.2
275.0	130.8	6.0	6.0	.00( 1, 0)	38.66( 1,103)	.0	48.2

## Section 3.2.2 - E206 St. (TB-2) Case03

R <sub>ult</sub> kips	Bl bpf	Ct down	Stroke (ft) up	MinStr I,J ksi	MaxStr I,J ksi	Enthru ft-kip	Bl Rt bpm
143.0	31.6	4.7	4.8	.00( 1, 0)	25.38( 1, 97)	.0	54.0
176.0	41.7	5.0	5.1	.00( 1, 0)	29.29( 1, 99)	.0	52.4
209.0	54.6	5.4	5.4	.00( 1, 0)	32.81( 1,100)	.0	50.8
242.0	76.2	5.6	5.6	.00( 1, 0)	35.66( 1,101)	.0	49.8
275.0	105.9	5.9	5.9	.00( 1, 0)	38.19( 1,102)	.0	48.5

## Section 3.2.2 - E206 St. (TB-2) Case04

R <sub>ult</sub> kips	Bl bpf	Ct down	Stroke (ft) up	MinStr I,J ksi	MaxStr I,J ksi	Enthru ft-kip	Bl Rt bpm
143.0	39.5	4.9	5.0	.00( 1, 0)	28.41( 1, 99)	.0	52.8
176.0	53.4	5.3	5.3	.00( 1, 0)	31.99( 1,100)	.0	51.2
209.0	75.6	5.4	5.6	.00( 1, 0)	34.68( 1,101)	.0	50.2
242.0	103.8	5.8	5.8	.00( 1, 0)	37.33( 1,103)	.0	48.8
275.0	156.9	6.0	6.1	.00( 1, 0)	39.16( 1,104)	.0	47.9

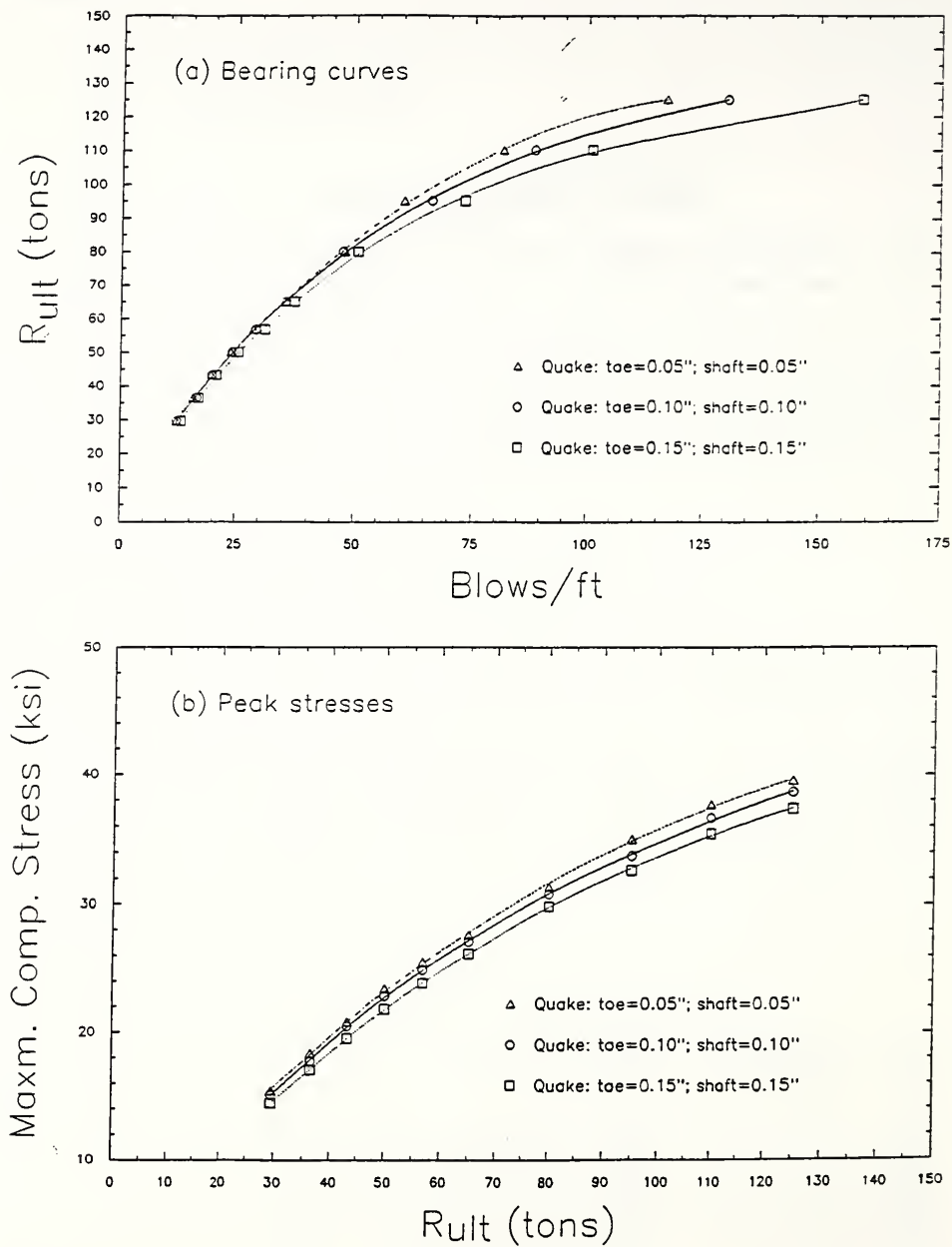


Figure 3.27 Variation in quake (E206/TB-2)



## Section 3.2.2 - E206 St. (TB-2) Case00

R <sub>ult</sub> kips	Bl bpf	Ct down	Stroke (ft) up	MinStr I,J ksi	MaxStr I,J ksi	Enthru ft-kip	Bl Rt bpm
143.0	35.5	4.8	4.9	.00( 1, 0)	27.07( 1, 99)	.0	53.4
176.0	47.5	5.2	5.2	.00( 1, 0)	30.77( 1,100)	.0	51.7
209.0	66.3	5.3	5.5	.00( 1, 0)	33.73( 1,101)	.0	50.7
242.0	88.6	5.8	5.7	.00( 1, 0)	36.65( 1,102)	.0	49.2
275.0	130.8	6.0	6.0	.00( 1, 0)	38.66( 1,103)	.0	48.2

## Section 3.2.2 - E206 St. (TB-2) Case05

R <sub>ult</sub> kips	Bl bpf	Ct down	Stroke (ft) up	MinStr I,J ksi	MaxStr I,J ksi	Enthru ft-kip	Bl Rt bpm
143.0	35.5	4.8	4.9	.00( 1, 0)	27.60( 1, 94)	.0	53.6
176.0	47.8	5.0	5.1	.00( 1, 0)	31.32( 1, 95)	.0	52.5
209.0	60.4	5.5	5.5	.00( 1, 0)	34.99( 1, 96)	.0	50.2
242.0	81.5	5.8	5.8	.00( 1, 0)	37.70( 1, 97)	.0	49.0
275.0	116.9	5.9	6.1	.00( 1, 0)	39.55( 1,100)	.0	48.2

## Section 3.2.2 - E206 St. (TB-2) Case06

R <sub>ult</sub> kips	Bl bpf	Ct down	Stroke (ft) up	MinStr I,J ksi	MaxStr I,J ksi	Enthru ft-kip	Bl Rt bpm
143.0	37.1	4.8	4.8	.00( 1, 0)	26.14( 1,103)	.0	53.6
176.0	50.7	5.1	5.1	.00( 1, 0)	29.82( 1,104)	.0	52.0
209.0	73.2	5.3	5.4	.00( 1, 0)	32.62( 1,105)	.0	50.9
242.0	101.0	5.7	5.7	.00( 1, 0)	35.45( 1,106)	.0	49.3
275.0	158.8	6.0	6.0	.00( 1, 0)	37.38( 1,107)	.0	48.3

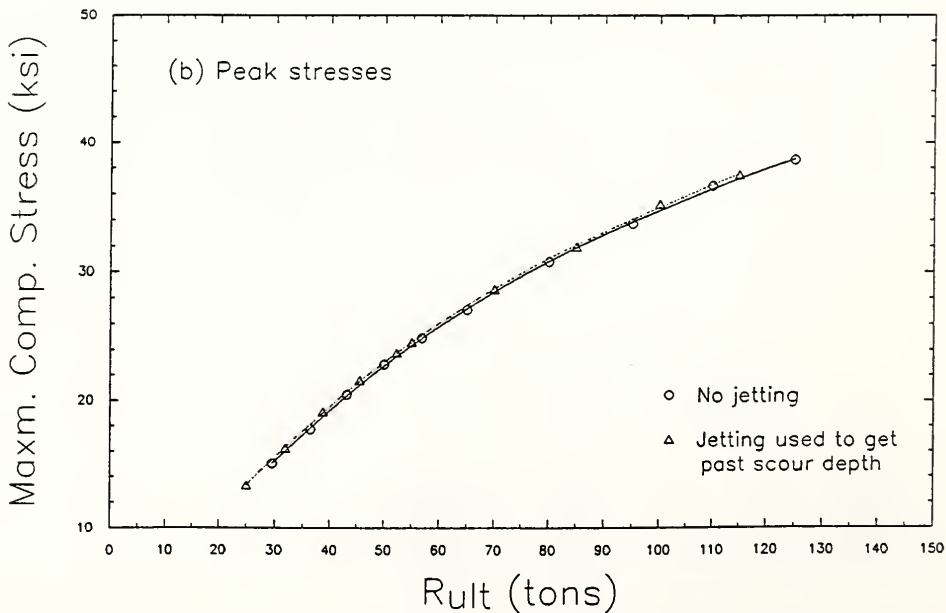
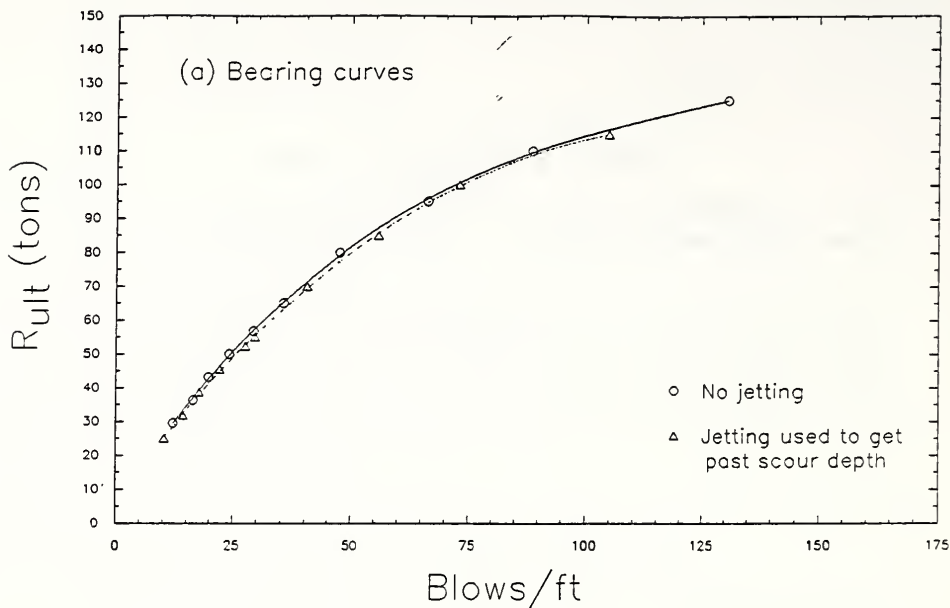


Figure 3.28 Effect of jetting/preboring (E206/TB-2)

## Section 3.2.2 - E206 St. (TB-2) Case00

R <sub>ult</sub> kips	Bl bpf	Ct down	Stroke (ft) up	MinStr I,J ksi	MaxStr I,J ksi	Enthru ft-kip	Bl Rt bpm
143.0	35.5	4.8	4.9	.00( 1, 0)	27.07( 1, 99)	.0	53.4
176.0	47.5	5.2	5.2	.00( 1, 0)	30.77( 1,100)	.0	51.7
209.0	66.3	5.3	5.5	.00( 1, 0)	33.73( 1,101)	.0	50.7
242.0	88.6	5.8	5.7	.00( 1, 0)	36.65( 1,102)	.0	49.2
275.0	130.8	6.0	6.0	.00( 1, 0)	38.66( 1,103)	.0	48.2

## Section 3.2.2 - E206 St. (TB-2) Case07

R <sub>ult</sub> kips	Bl bpf	Ct down	Stroke (ft) up	MinStr I,J ksi	MaxStr I,J ksi	Enthru ft-kip	Bl Rt bpm
121.0	29.6	4.6	4.7	.00( 1, 0)	24.56( 1, 98)	.0	54.6
154.0	40.4	5.0	5.0	.00( 1, 0)	28.67( 1,100)	.0	52.7
187.0	55.8	5.1	5.3	.00( 1, 0)	31.94( 1,100)	.0	51.4
220.0	72.9	5.6	5.6	.00( 1, 0)	35.23( 1,101)	.0	49.8
253.0	104.7	5.9	5.9	.00( 1, 0)	37.52( 1,102)	.0	48.7

### 3.3 SR 14 over Beal Taylor Ditch

Project No:	ST-4402(B)
Contract No:	B-17220
Location:	Allen County (near Fort Wayne), Indiana
Structure:	3-span continuous reinforced concrete slab bridge
Piling done:	May, 1989

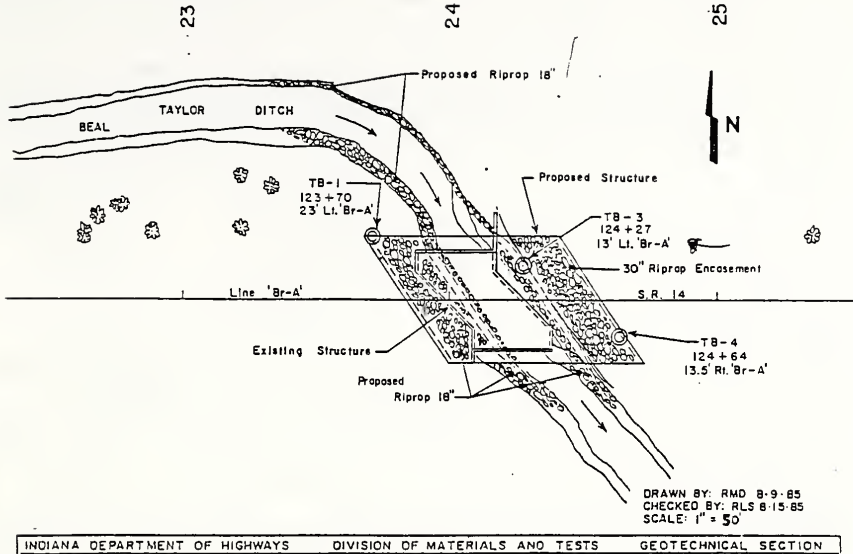
The plan layout of the three test borings (TB-1, TB-3 and TB-4) used to obtain soil profiles is shown in Fig. 3.29(a). Figure 3.29(b) is an elevation view of the bridge structure and shows the positions of the pile bents as well as the minimum pile toe elevations. Fig. 3.30 is a sketch of the generalized subsurface conditions at the site of the bridge structure.

The data from TB-1 is used to develop the estimated shaft friction distribution (Fig. 3.31) bent number 1 (end bent - Sec. 3.3.1) and the data from TB-3 is used for the shaft friction distribution (Fig. 3.36) at bent number 3 (interior bent - Sec. 3.3.2).

At this site the proportion of  $R_{ult}$  being contributed by the friction resistance along the side ( $Q_s$ ) is considered to have been estimated with greater accuracy than the contribution of the resistance at the base of the pile ( $Q_b$ ), hence a negative IPERCS value (this keeps the side resistance constant and varies the end resistance. See Appendix C for an explanation of IPERCS) is used for input to WEAP87. Two sets of  $R_{ult}$  values are used for analysis in the next two sections. The first set uses one constant value for  $Q_{sd}$ , and the next set uses another.

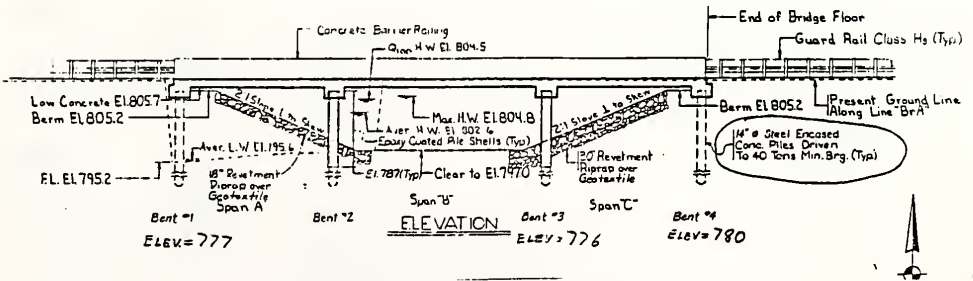
**BORING LOCATION PLAN**

RS -PROJECT No. 4402 ( )  
 STRUCTURE No. 14-02-6129  
 S.R. 14 OVER BEAL TAYLOR  
 DITCH IN ALLEN COUNTY



INDIANA DEPARTMENT OF HIGHWAYS DIVISION OF MATERIALS AND TESTS GEOTECHNICAL SECTION

(a) Plan layout of the three test borings (TB-1, TB-3 and TB-4)



(b) Minimum pile toe elevations at each bent

Figure 3.29 Boring plan and bent location for the SR14 bridge over Beal Taylor Ditch



### 3.3.1 Pile at bent number 1 (End bent)

Ground elevation at TB-1 was 798.5 ft at time of piling. The specified minimum pile tip elevation is 777 ft, and the final pile top elevation required is 806 ft. Based on these considerations a pile length of 29 ft is used with the last 21.5 ft penetrating into the ground. The estimated values of  $Q_b$  and  $Q_{sd}$  are 50 t and 60 t, respectively. These values are obtained based on the bore-hole data from TB-1. The friction distribution profile for input to WEAP87 is shown in Figure 3.31. The expected value of  $R_{ult}$  is 95 tons. Table 3.7 lists the range of ultimate capacity values used for analysis. The first four sets are based on an  $R_{ult}$  of 43.2 t (95 kips) with a constant  $Q_{sd}$  of 20.5 t, and the last four sets use a constant 45 t as the  $Q_{sd}$  value.

Table 3.7  
Range of  $R_{ult}$  : IPERCS = -60%

$R_{ult}$ (tons)	34.1	43.2	52.3	61.4	75	95	115	135
$R_{ult}$ (kips)	75	95	115	135	165	209	253	297
$Q_b$ (tons)	13.6	22.7	31.8	40.9	30	50	70	90
$Q_{sd}$ (tons)	20.5	20.5	20.5	20.5	45	45	45	45

The standard case (Case00) parameters are as follows:

Pile	Type	Thin steel shell		
	Gage	5 (wall thickness = 0.203"; c/s area = 8.8 in <sup>2</sup> )		
	$\phi$	14"		
	Length	29 ft		
Hammer	Type	MKT DE 30		
	Efficiency	0.8		
	Cushion	Area	283.5 in <sup>2</sup>	
		Material	Plywood	
		Thickness	0.75"	
Helmet	Weight	2.02 kips		
Soil Parameters	Quake	Shaft	0.1"	
		Toe	0.1"	
	Damping	Type	Smith (Normal)	

Soil Parameters	Shaft Toe	0.05 s/ft 0.15 s/ft
$R_{ult}$	Table 3.7	
Shaft Friction	As a % of $R_{ult}$ Distribution used	Fixed at 20.5 t and 45 t (IPERCS = -60) Fig. 3.31

Parametric studies are conducted to assess the effects of different parameters. Only one parameter is varied at a time, with the remainder of the data identical to that of the standard case:

Pile	Gage	Case01	7 (wall thickness = 0.179"; c/s area = 7.77 in <sup>2</sup> )
Hammer	Type	Case02	Delmag D 22
Damping	Toe	Case03	0.10 s/ft
		Case04	0.20 s/ft
Quake	Toe & Shaft	Case05	0.05"
	Toe & Shaft	Case06	0.15"

The results of these analyses are given as Figures 3.32 to 3.35. A tabular summary of WEAP87 results (for the second set of  $R_{ult}$  values) follows each figure.

Figure 3.32 shows the results of using a different gage for the shell material. The thinner shell causes an increase in the blow count and the peak stress generated. The increase in blow count is marginal (*i.e.*,  $AF_B = 1.00$ ), however, the increase in stress is about 11% (*i.e.*,  $AF_S = 1.11$ ) and occurs over the entire range of capacities studied. These results indicate that although 7 gage shells would perform satisfactorily at this site under most conditions, there is a risk of damage due to high stresses if driving conditions deteriorate.

In comparison to the blows required by the standard hammer used at the site (a MKT DE 30), using a heavier hammer (*e.g.*, the Delmag D 22) would result in reducing to less than half ( $AF_B = 0.45$ ), the number of blows required to drive the shell to the same ultimate capacities (Fig. 3.33(a)). However, using the heavier hammer results in an increase in stresses induced in the shell (Fig. 3.33(b)). The increase in the peak stress is of the order of 15% ( $AF_S = 1.15$ ) and could cause damage to the shell for high values



of  $R_{ult}$ . These results indicate that a hammer with an energy rating between the two hammers studied here would have been a more judicious choice, primarily in terms of the savings in time with the heavier hammer.

The effect of variation in damping at toe follows a smooth pattern (Fig. 3.34). This observation combined with the trends observed in Chapter 2 leads to the conclusion that adjustment factors of 1.25 and 1.05 for  $AF_B$  and  $AF_S$  respectively, would be appropriate to adjust for variations in damping (*i.e.*, to account for the difference in field values from the values used in the analyzed standard case).

Changing the quake (to 0.15 inch) from the recommended values (0.1 inch), for both toe and shaft, has a small effect (*i.e.*,  $AF_B = 1.06$ ) on the drivability (Fig. 3.35(a)), and results in a marginal reduction (*i.e.*,  $AF_S = 0.97$ ) in peak stresses induced in the shell (Fig. 3.35(b)). A similar effect is observed if the quake is reduced (to 0.05 inch), and the corresponding values of the adjustment factors are 0.94 and 1.03, for  $AF_B$  and  $AF_S$ , respectively.

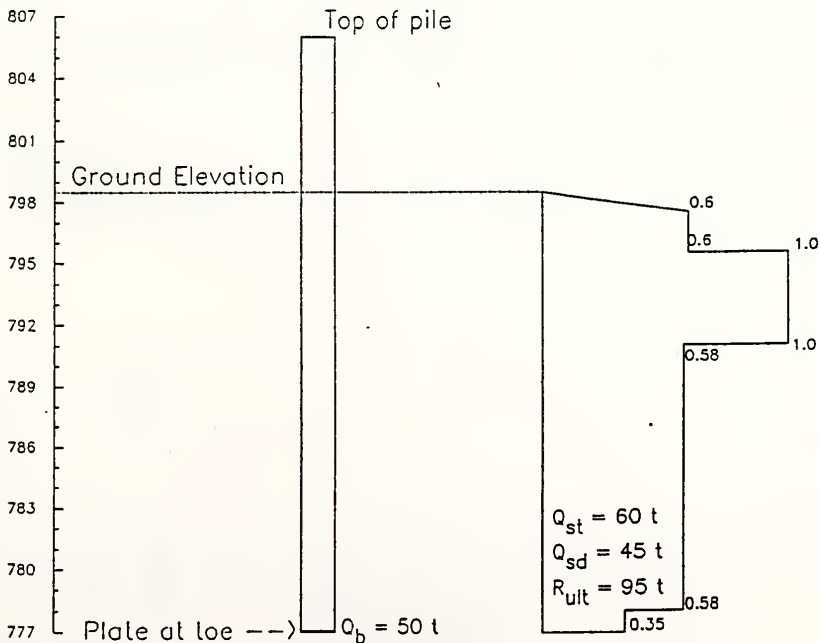


**Figure 3.31** Shaft friction distribution for bent no. 1 at SR 14 over Beal Taylor Ditch

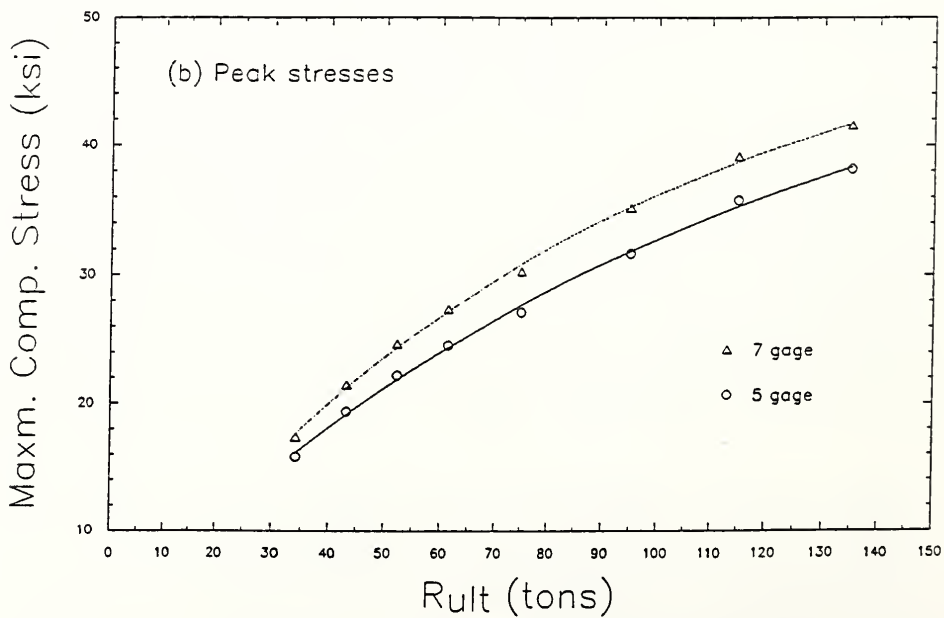
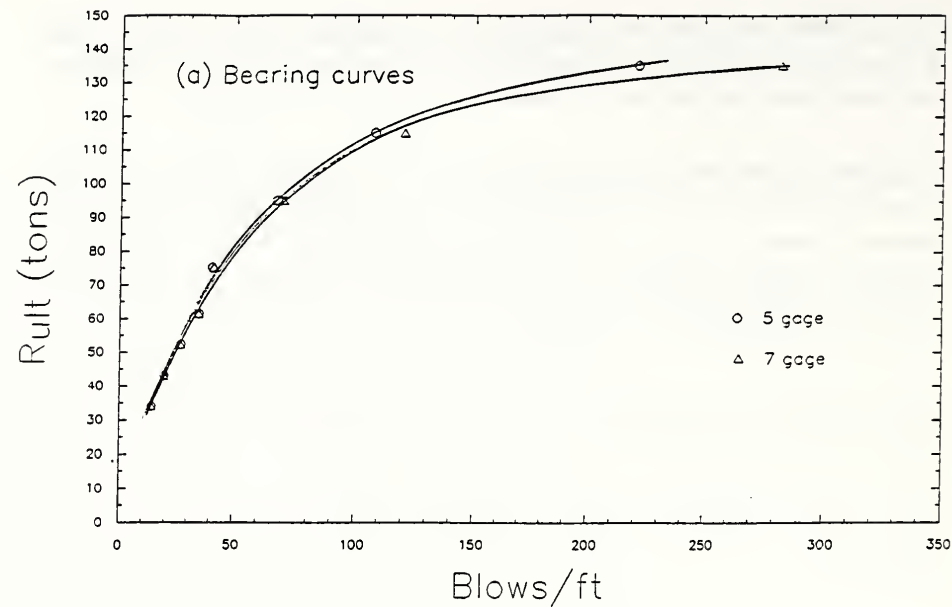


Figure 3.32 Variation in thin shell gage (SR14/TB-1)

## Section 3.3.1 - SR14 (TB-1) Case00

R <sub>ult</sub> kips	Bl bpf	Ct	Stroke (ft) down up	MinStr I,J ksi	MaxStr I,J ksi	Enthru ft-kip	Bl Rt bpm
165.0	40.7	5.1	5.2	.00( 1, 0)	27.08( 1,106)	.0	51.7
209.0	67.6	5.4	5.6	.00( 1, 0)	31.64( 1,109)	.0	50.2
253.0	107.8	6.0	5.9	.00( 1, 0)	35.76( 1,112)	.0	48.2
297.0	221.2	6.3	6.3	.00( 1, 0)	38.15( 1,115)	.0	46.9

## Section 3.3.1 - SR14 (TB-1) Case01

R <sub>ult</sub> kips	Bl bpf	Ct	Stroke (ft) down up	MinStr I,J ksi	MaxStr I,J ksi	Enthru ft-kip	Bl Rt bpm
165.0	41.3	5.1	5.1	.00( 1, 0)	30.25( 1,111)	.0	51.9
209.0	69.9	5.4	5.5	.00( 1, 0)	35.14( 1,114)	.0	50.1
253.0	120.2	6.0	5.9	.00( 1, 0)	39.13( 1,118)	.0	48.2
297.0	282.8	6.2	6.3	.00( 1, 0)	41.51( 1,120)	.0	47.1

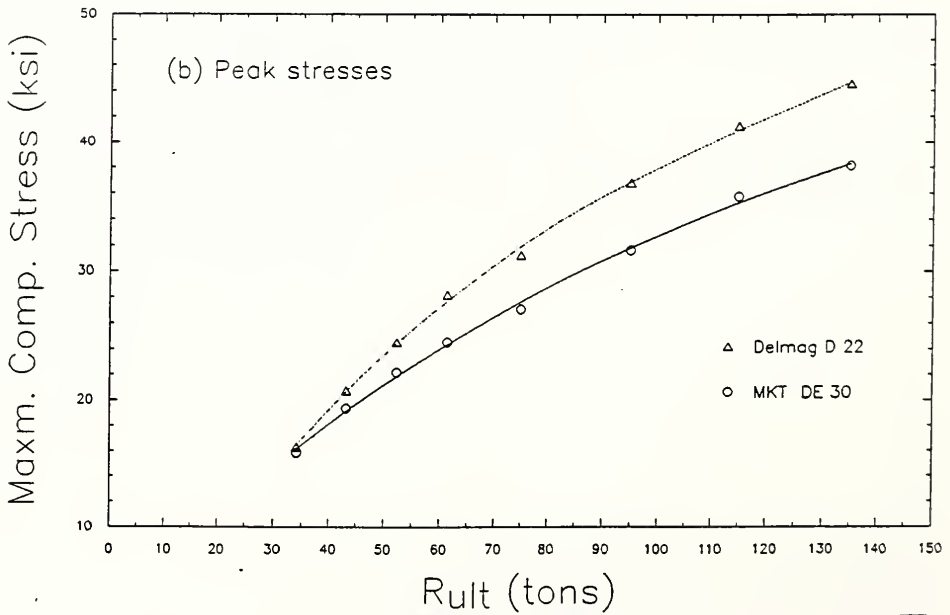
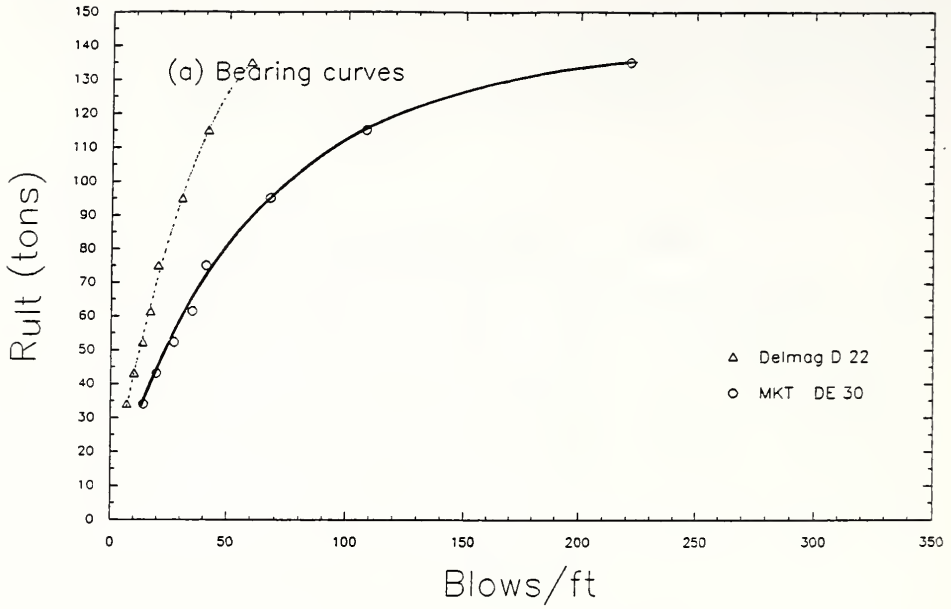


Figure 3.33 Effect of heavier hammer (SR14/TB-1)

## Section 3.3.1 - SR14 (TB-1) Case00

R <sub>ult</sub> kips	Bl bpf	Ct down	Stroke (ft) up	MinStr I,J ksi	MaxStr I,J ksi	Enthru ft-kip	Bl Rt bpm
165.0	40.7	5.1	5.2	.00( 1, 0)	27.08( 1,106)	.0	51.7
209.0	67.6	5.4	5.6	.00( 1, 0)	31.64( 1,109)	.0	50.2
253.0	107.8	6.0	5.9	.00( 1, 0)	35.76( 1,112)	.0	48.2
297.0	221.2	6.3	6.3	.00( 1, 0)	38.15( 1,115)	.0	46.9

## Section 3.3.1 - SR14 (TB-1) Case02

R <sub>ult</sub> kips	Bl bpf	Ct down	Stroke (ft) up	MinStr I,J ksi	MaxStr I,J ksi	Enthru ft-kip	Bl Rt bpm
165.0	20.0	4.0	3.9	.00( 1, 0)	31.26( 1,111)	.0	58.5
209.0	30.3	4.3	4.3	.00( 1, 0)	36.81( 1,114)	.0	56.5
253.0	41.3	4.6	4.6	.00( 1, 0)	41.27( 1,116)	.0	54.6
297.0	59.3	4.8	4.8	.00( 1, 0)	44.56( 1,120)	.0	53.4

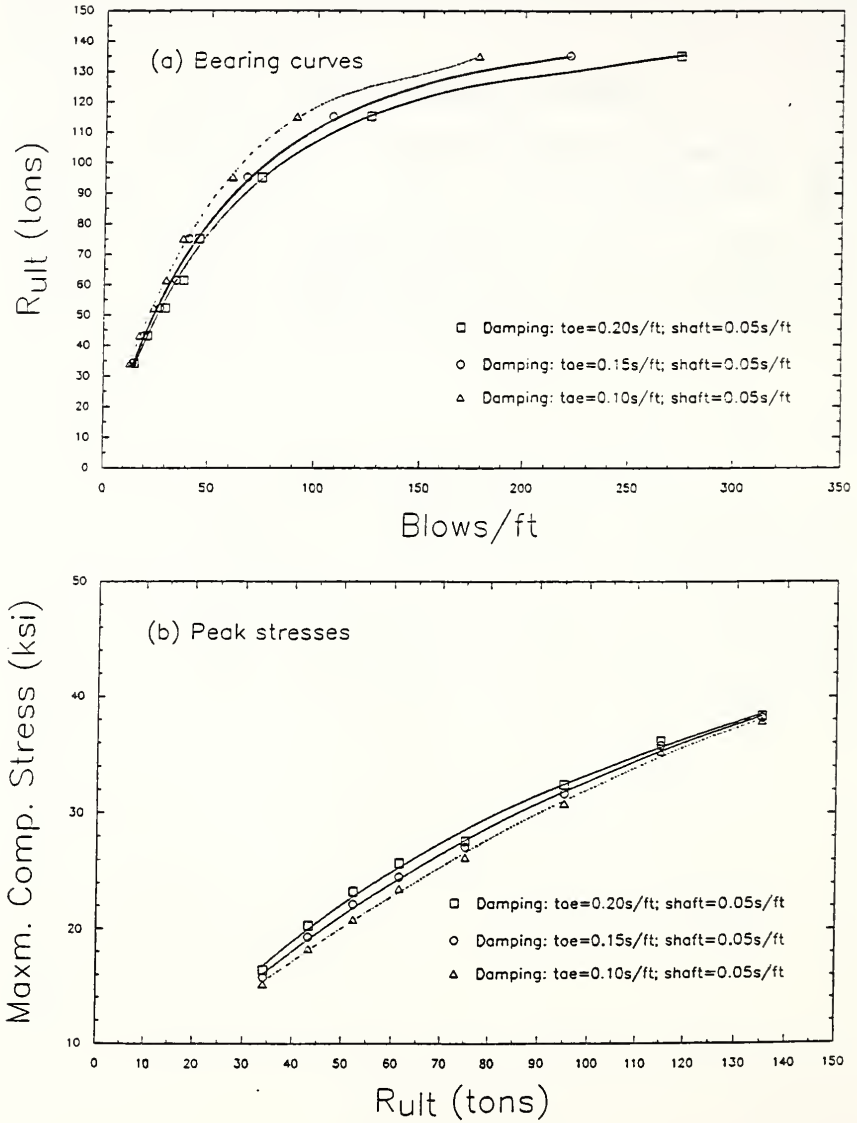


Figure 3.34 Variation in damping at toe (SR14/TB-1)

## Section 3.3.1 - SR14 (TB-1) Case00

R <sub>ult</sub> kips	Bl bpf	Ct	Stroke (ft) down up	MinStr I,J ksi	MaxStr I,J ksi	Enthru ft-kip	Bl Rt bpm
165.0	40.7	5.1	5.2	.00( 1, 0)	27.08( 1,106)	.0	51.7
209.0	67.6	5.4	5.6	.00( 1, 0)	31.64( 1,109)	.0	50.2
253.0	107.8	6.0	5.9	.00( 1, 0)	35.76( 1,112)	.0	48.2
297.0	221.2	6.3	6.3	.00( 1, 0)	38.15( 1,115)	.0	46.9

## Section 3.3.1 - SR14 (TB-1) Case03

R <sub>ult</sub> kips	Bl bpf	Ct	Stroke (ft) down up	MinStr I,J ksi	MaxStr I,J ksi	Enthru ft-kip	Bl Rt bpm
165.0	37.9	5.1	5.1	.00( 1, 0)	26.19( 1,105)	.0	52.0
209.0	60.6	5.3	5.5	.00( 1, 0)	30.78( 1,108)	.0	50.5
253.0	90.6	5.9	5.8	.00( 1, 0)	35.25( 1,112)	.0	48.5
297.0	177.7	6.3	6.3	.00( 1, 0)	37.91( 1,114)	.0	47.1

## Section 3.3.1 - SR14 (TB-1) Case04

R <sub>ult</sub> kips	Bl bpf	Ct	Stroke (ft) down up	MinStr I,J ksi	MaxStr I,J ksi	Enthru ft-kip	Bl Rt bpm
165.0	45.4	5.1	5.3	.00( 1, 0)	27.59( 1,106)	.0	51.7
209.0	74.4	5.5	5.6	.00( 1, 0)	32.41( 1,111)	.0	49.8
253.0	126.0	6.0	6.0	.00( 1, 0)	36.16( 1,113)	.0	48.0
297.0	275.0	6.3	6.4	.00( 1, 0)	38.32( 1,116)	.0	46.9

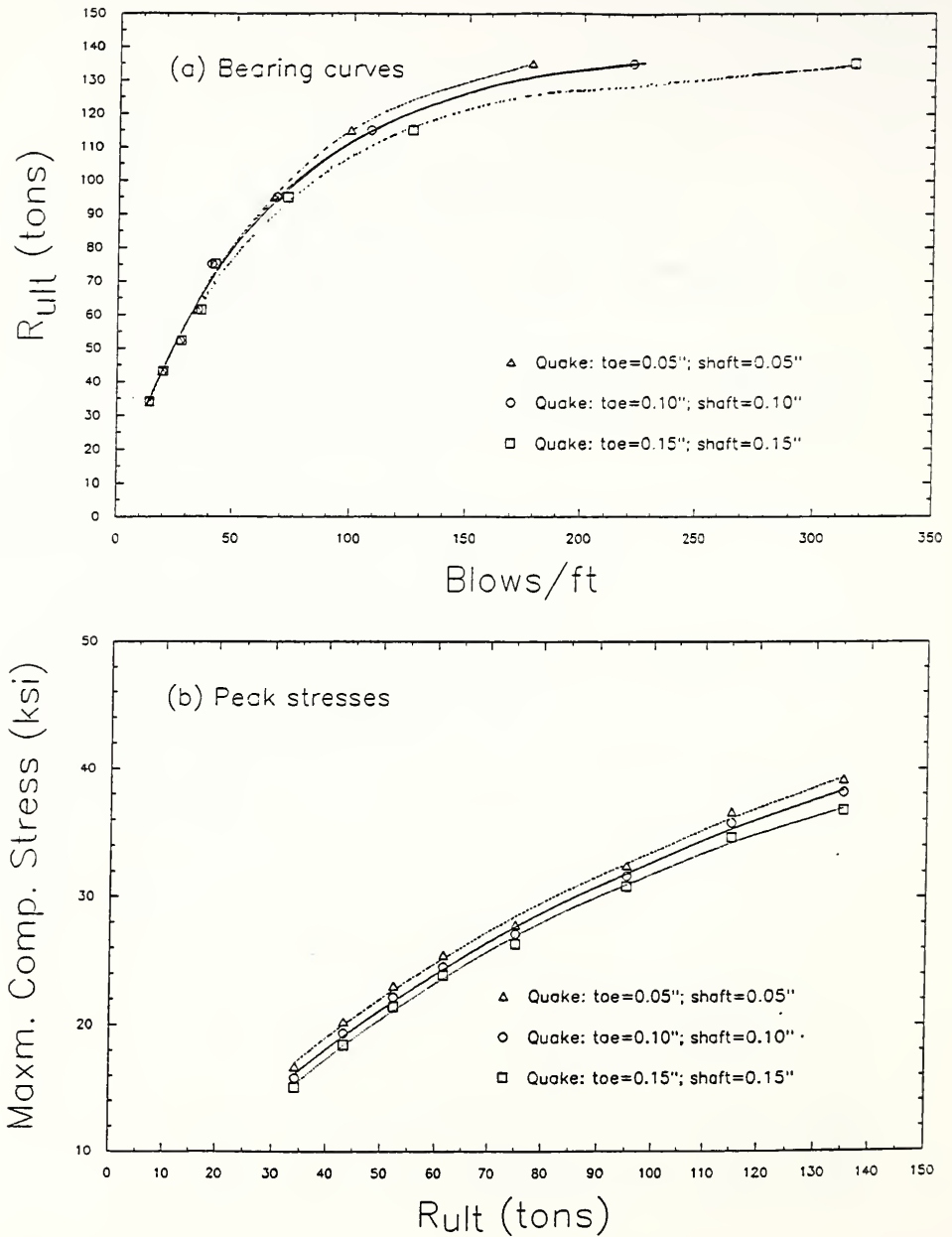


Figure 3.35 Variation in quake (SR14/TB-1)



## Section 3.3.1 - SR14 (TB-1) Case00

R <sub>ult</sub> kips	Bl bpf	Ct down	Stroke (ft) up	MinStr I,J ksi	MaxStr I,J ksi	Enthru ft-kip	Bl Rt bpm
165.0	40.7	5.1	5.2	.00( 1, 0)	27.08( 1,106)	.0	51.7
209.0	67.6	5.4	5.6	.00( 1, 0)	31.64( 1,109)	.0	50.2
253.0	107.8	6.0	5.9	.00( 1, 0)	35.76( 1,112)	.0	48.2
297.0	221.2	6.3	6.3	.00( 1, 0)	38.15( 1,115)	.0	46.9

## Section 3.3.1 - SR14 (TB-1) Case05

R <sub>ult</sub> kips	Bl bpf	Ct down	Stroke (ft) up	MinStr I,J ksi	MaxStr I,J ksi	Enthru ft-kip	Bl Rt bpm
165.0	41.9	5.1	5.1	.00( 1, 0)	27.80( 1,100)	.0	52.2
209.0	66.3	5.4	5.6	.00( 1, 0)	32.43( 1,104)	.0	50.2
253.0	99.2	6.0	6.0	.00( 1, 0)	36.63( 1,107)	.0	48.1
297.0	178.2	6.3	6.4	.00( 1, 0)	39.17( 1,111)	.0	46.8

## Section 3.3.1 - SR14 (TB-1) Case06

R <sub>ult</sub> kips	Bl bpf	Ct down	Stroke (ft) up	MinStr I,J ksi	MaxStr I,J ksi	Enthru ft-kip	Bl Rt bpm
165.0	42.2	5.1	5.1	.00( 1, 0)	26.30( 1,112)	.0	52.0
209.0	72.1	5.4	5.5	.00( 1, 0)	30.82( 1,116)	.0	50.2
253.0	125.6	5.9	5.9	.00( 1, 0)	34.65( 1,117)	.0	48.4
297.0	316.8	6.2	6.3	.00( 1, 0)	36.78( 1,120)	.0	47.2

### 3.3.2 Pile at bent number 3 (interior bent)

This is an interior bent with a ground elevation, at time of piling, equal to 795 ft. The recommended minimum pile tip elevation is 776 ft. A 30 ft length of shell is used. The estimated values of  $Q_b$  and  $Q_s$  are 120 t and 30 t, respectively. These values are obtained based on the bore-hole data from TB-3. Since the subsurface soils are mostly clayey, the dynamic side friction resistance,  $Q_{sd}$ , is the same as  $Q_s$ . The expected value of  $R_{ult}$  is 150 t. Table 3.8 lists the range of ultimate capacity values used for analysis. The first three sets are based on an  $R_{ult}$  of 68.2 t (150 kips) with a constant  $Q_{sd}$  of 14.2 t (31.25 kips), and the last three sets use a constant 31.3 t as the  $Q_{sd}$  value. The friction distribution profile for input to WEAP87 is shown in Figure 3.36.

**Table 3.8**  
Range of  $R_{ult}$  : IPERCS = -25%

$R_{ult}$	(tons)	56.8	68.2	79.5	125	150	175
	(kips)	125	150	175	275	330	385
$Q_b$	(tons)	42.6	54	65.3	93.7	118.7	143.7
$Q_{sd}$	(tons)	14.2	14.2	14.2	31.3	31.3	31.3

The standard case (Case00) parameters are as follows:

Pile	Type	Thin steel shell		
	Gage	5 (wall thickness = 0.203"; c/s area = 8.8 in <sup>2</sup> )		
	$\phi$	14"		
	Length	30 ft		
Hammer	Type	MKT DE 30		
	Efficiency	0.8		
	Cushion	Area	283.5 in <sup>2</sup>	
		Material	Plywood	
		Thickness	0.75"	
Helmet	Weight	2.02 kips		
Soil Parameters	Quake	Shaft	0.1"	
		Toe	0.1"	

	Damping	Type	Smith (Normal)
		Shaft	0.05 s/ft
		Toe	0.15 s/ft
$R_{ult}$	Table 3.8		
Shaft Friction	As a % of $R_{ult}$ Distribution used		Fixed at 14.2 t and 31.3 t (IPERCS = -25) Fig. 3.36

Parametric studies are conducted to assess the effects of different parameters. Only one parameter is varied at a time, with the remainder of the data identical to that of the standard case:

Pile	Gage	Case01	7 (wall thickness= 0.179"; c/s area=7.77 in <sup>2</sup> )
Hammer	Type	Case02	Delmag D 22
Damping	Toe	Case03	0.10 s/ft
		Case04	0.20 s/ft
Quake	Toe & Shaft	Case05	0.05"
	Toe & Shaft	Case06	0.15"

The results of these analyses are given as Figures 3.37 to 3.40. A tabular summary of WEAP87 results (for the second set of  $R_{ult}$  values) follows each figure.

The results show that the standard hammer is inadequate to drive the pile to an ultimate capacity beyond 150 t.

Figure 3.37 shows the effect of using a different gage for the shell material. The thinner shell results in a 10% increase in peak stresses (*i.e.*,  $AF_s = 1.10$ ), and it also reduces the drivability for  $R_{ult}$  values greater than 80 t. The 7 gage shell cannot be driven beyond a capacity of 130 t with a reasonable blow count (for the standard driving system). An adjustment factor of 10% (*i.e.*,  $AF_b = 1.10$ ) must be used for  $R_{ult}$  values between 80 t and 120 t.

Fig. 3.38 shows that using a heavier hammer (the Delmag D 22) results in a large reduction in the number of blows required to achieve comparable bearing capacity. The hammer with the higher rated energy, the Delmag D 22, required only 90 bpf to drive the shell to a capacity of 150 t, whereas the standard MKT DE 30 required more than

700 bpf. Because of the increasing divergence of the bearing curves for the two hammers, a single  $AF_B$  value is difficult to define in this case. Using the heavier hammer also results in a considerable increase in stresses induced in the shell (Fig. 3.38(b)). Using the D 22 hammer causes a 15% to 20% increase (*i.e.*,  $AF_S = 1.18$ ) in the maximum stress, as compared to the MKT DE 30 hammer, for  $R_{ult}$  values from 80 t to 150 t. *These results indicate that a D 22 hammer could have been used for considerable savings in time while driving at this bent if care was taken with other parameters to keep stresses within acceptable limits.*

The effect of variation in damping at toe are shown in Fig. 3.39. An increase/decrease of 0.05 s/ft from the standard value of 0.15 s/ft causes a proportional increase/decrease in the blow count and in the peak stresses generated. The difference in stresses is reduced for high values of  $R_{ult}$  (Fig. 3.39(b)). Again, it is difficult to define one adjustment factor for the range of interest, but  $AF_B$  and  $AF_S$  values of 1.25 and 1.03, respectively are considered appropriate when analyzing expected field driving conditions.

Changing the quake from the recommended values, 0.1" for both toe and shaft, has a small effect on the drivability for  $R_{ult}$  values under 80 t (Fig. 3.40(a)), however, for higher values of the ultimate capacity the blow count increases/decreases to a considerable extent with increase/decrease in the quake (Fig. 3.40(a)). In light of the wide divergence, it is not considered appropriate to define a single value for  $AF_B$ . The change in stresses on the other hand, is marginal and there is a smooth decrease/increase with increase/decrease in the quake (Fig. 3.40(b)). A value of 0.97 for  $AF_S$  is considered acceptable.

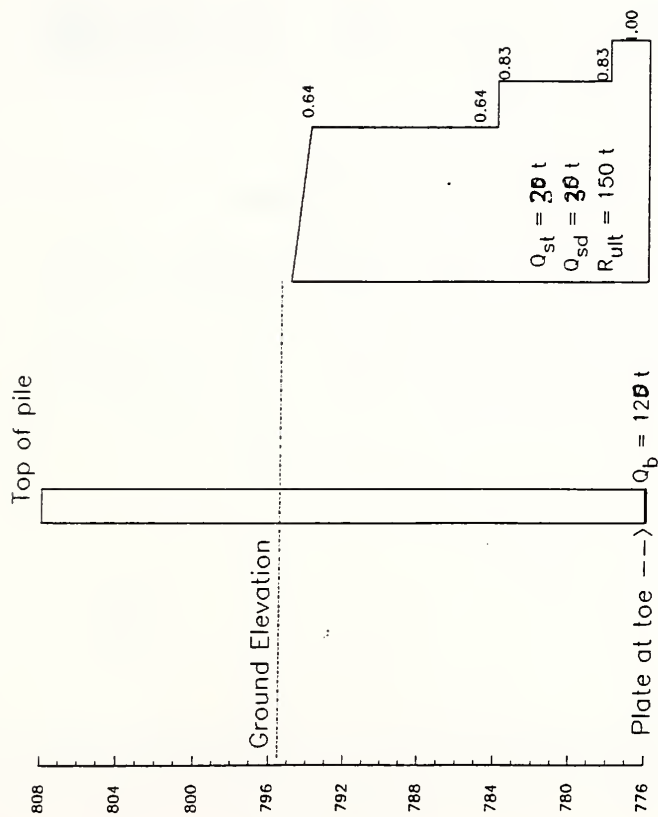


Figure 3.36 Shaft friction distribution for bent no. 3 SR 14 over Beal Taylor Ditch

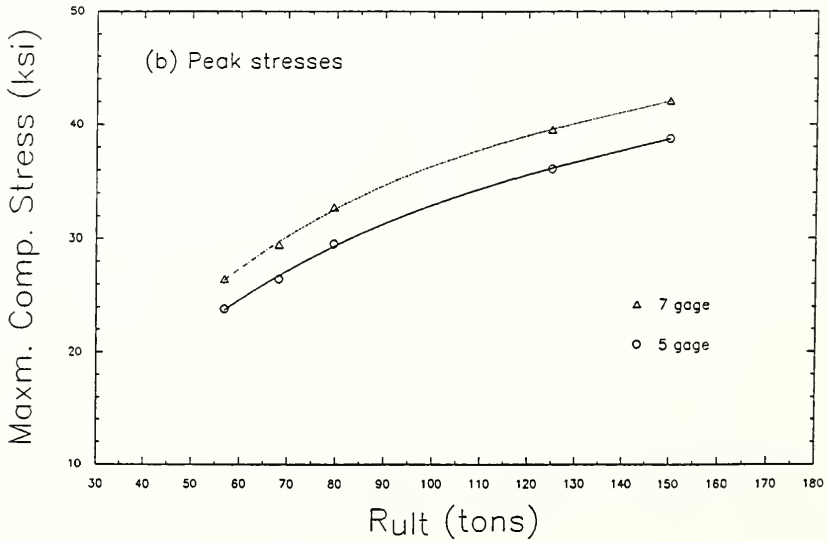
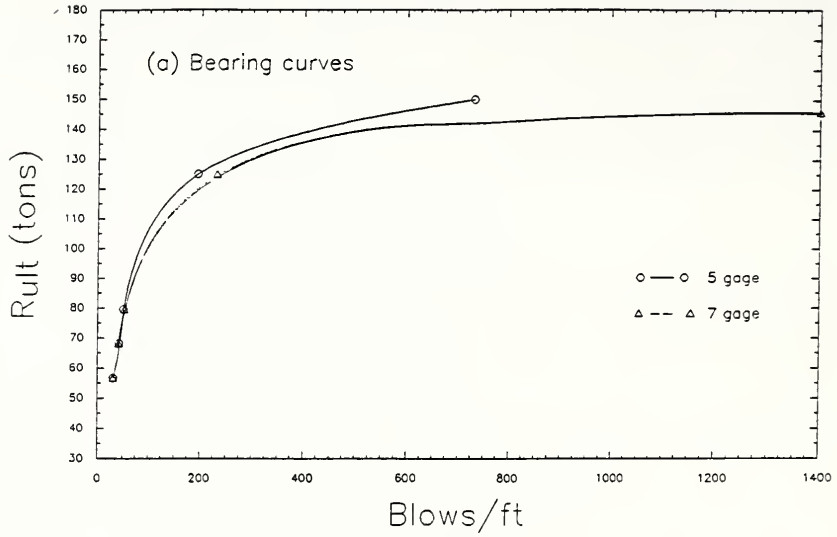


Figure 3.37 Variation in thin shell gage (SR14/TB-3)

## Section 3.3.2 - SR14 (TB-3) Case00

R <sub>ult</sub> kips	Bl bpf	Ct down	Stroke (ft) up	MinStr I,J ksi	MaxStr I,J ksi	Enthru ft-kip	Bl Rt bpm
275.0	194.3	6.0	6.2	.00( 1, 0)	36.10( 1,119)	.0	47.8
330.0	731.5	6.5	6.5	.00( 1, 0)	38.74( 1,121)	.0	46.2
385.0	9999.0	6.8	6.7	.00( 1, 0)	39.93( 1,121)	.0	45.3

## Section 3.3.2 - SR14 (TB-3) Case01

R <sub>ult</sub> kips	Bl bpf	Ct down	Stroke (ft) up	MinStr I,J ksi	MaxStr I,J ksi	Enthru ft-kip	Bl Rt bpm
275.0	231.2	6.0	6.1	.00( 1, 0)	39.51( 1,124)	.0	47.9
330.0	1731.9	6.5	6.5	.00( 1, 0)	42.06( 1,126)	.0	46.2
385.0	9999.0	6.8	6.6	.00( 1, 0)	43.18( 1,125)	.0	45.6

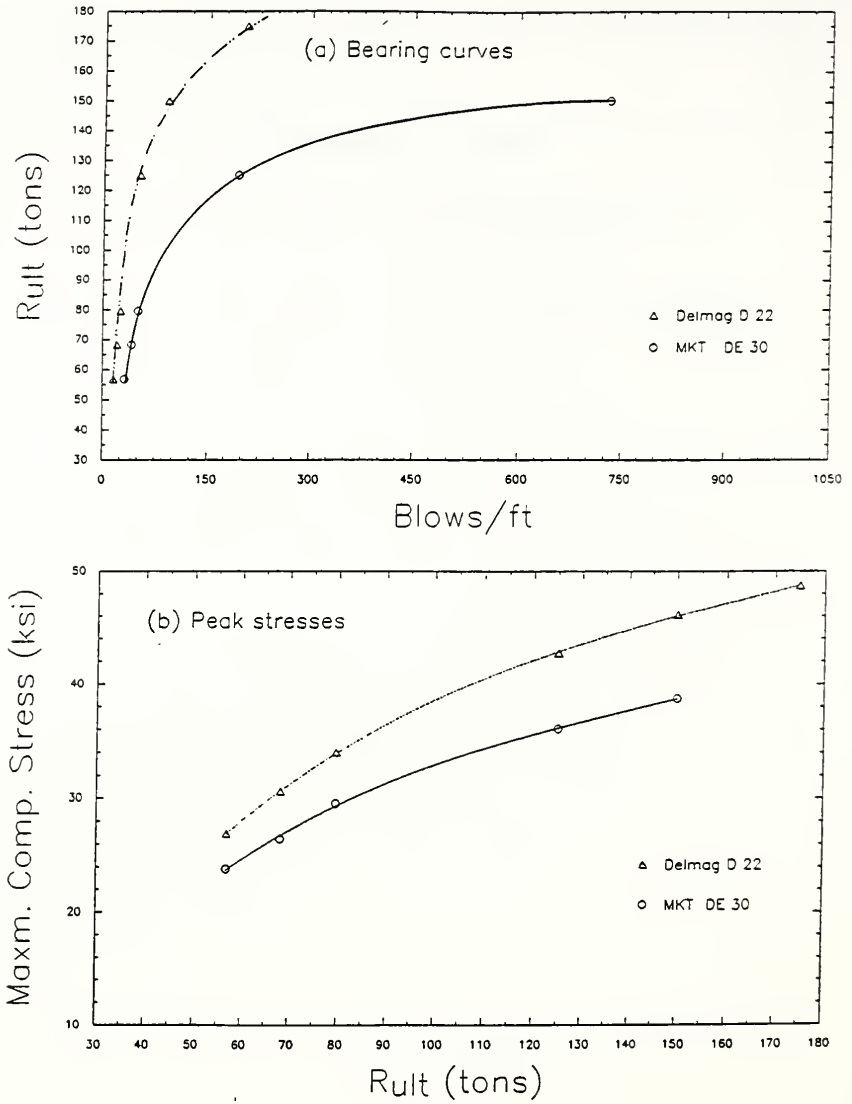


Figure 3.38 Effect of heavier hammer (SR14/TB-3)



## Section 3.3.2 - SR14 (TB-3) Case00

R <sub>ult</sub> kips	Bl Ct bpf	Stroke (ft) down up	MinStr I,J ksi	MaxStr I,J ksi	Enthru ft-kip	Bl Rt bpm
275.0	194.3	6.0 6.2	.00( 1, 0)	36.10( 1,119)	.0	47.8
330.0	731.5	6.5 6.5	.00( 1, 0)	38.74( 1,121)	.0	46.2
385.0	9999.0	6.8 6.7	.00( 1, 0)	39.93( 1,121)	.0	45.3

## Section 3.3.2 - SR14 (TB-3) Case02

R <sub>ult</sub> kips	Bl Ct bpf	Stroke (ft) down up	MinStr I,J ksi	MaxStr I,J ksi	Enthru ft-kip	Bl Rt bpm
275.0	52.3	4.8 4.7	.00( 1, 0)	42.74( 1,124)	.0	53.8
330.0	90.9	4.9 5.0	.00( 1, 0)	46.13( 1,130)	.0	52.6
385.0	205.3	5.0 5.2	.00( 1, 0)	48.67( 1,134)	.0	51.9

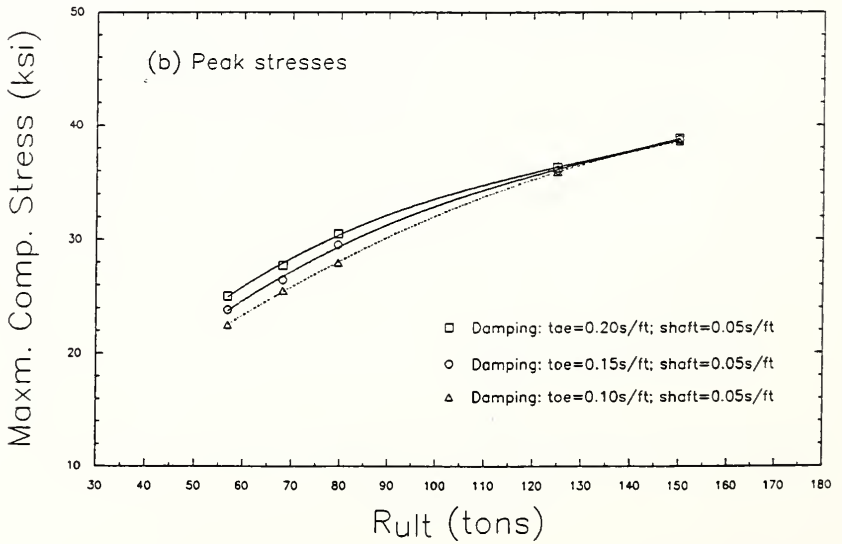
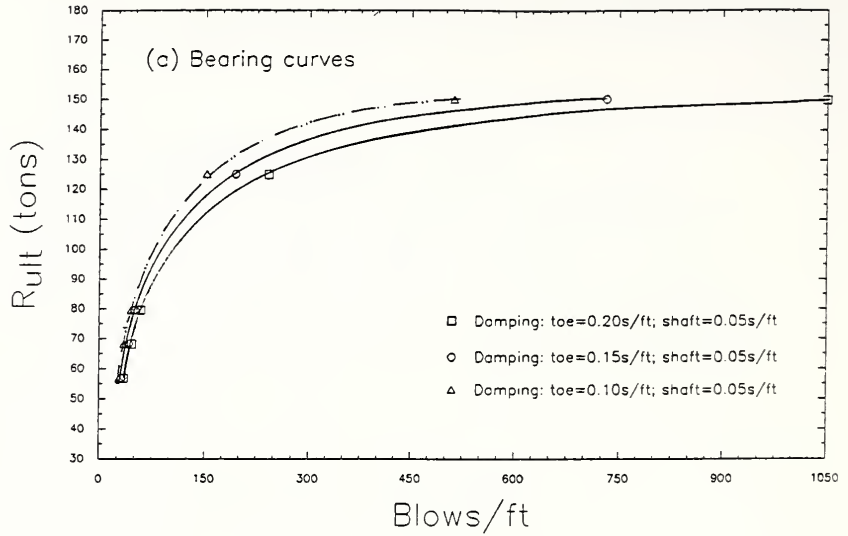


Figure 3.39 Variation in damping at toe (SR14/TB-3)

## Section 3.3.2 - SR14 (TB-3) Case00

R <sub>ult</sub> kips	Bl bpf	Ct down	Stroke (ft) up	MinStr I,J ksi	MaxStr I,J ksi	Enthru ft-kip	Bl Rt bpm
275.0	194.3	6.0	6.2	.00( 1, 0)	36.10( 1,119)	.0	47.8
330.0	731.5	6.5	6.5	.00( 1, 0)	38.74( 1,121)	.0	46.2
385.0	9999.0	6.8	6.7	.00( 1, 0)	39.93( 1,121)	.0	45.3

## Section 3.3.2 - SR14 (TB-3) Case03

R <sub>ult</sub> kips	Bl bpf	Ct down	Stroke (ft) up	MinStr I,J ksi	MaxStr I,J ksi	Enthru ft-kip	Bl Rt bpm
275.0	151.9	6.0	6.1	.00( 1, 0)	35.92( 1,118)	.0	47.9
330.0	512.5	6.5	6.5	.00( 1, 0)	38.58( 1,120)	.0	46.3
385.0	9999.0	6.8	6.8	.00( 1, 0)	39.76( 1,121)	.0	45.3

## Section 3.3.2 - SR14 (TB-3) Case04

R <sub>ult</sub> kips	Bl bpf	Ct down	Stroke (ft) up	MinStr I,J ksi	MaxStr I,J ksi	Enthru ft-kip	Bl Rt bpm
275.0	241.9	6.0	6.2	.00( 1, 0)	36.30( 1,119)	.0	47.7
330.0	1051.3	6.6	6.5	.00( 1, 0)	38.85( 1,121)	.0	46.1
385.0	9999.0	6.9	6.7	.00( 1, 0)	39.98( 1,121)	.0	45.3

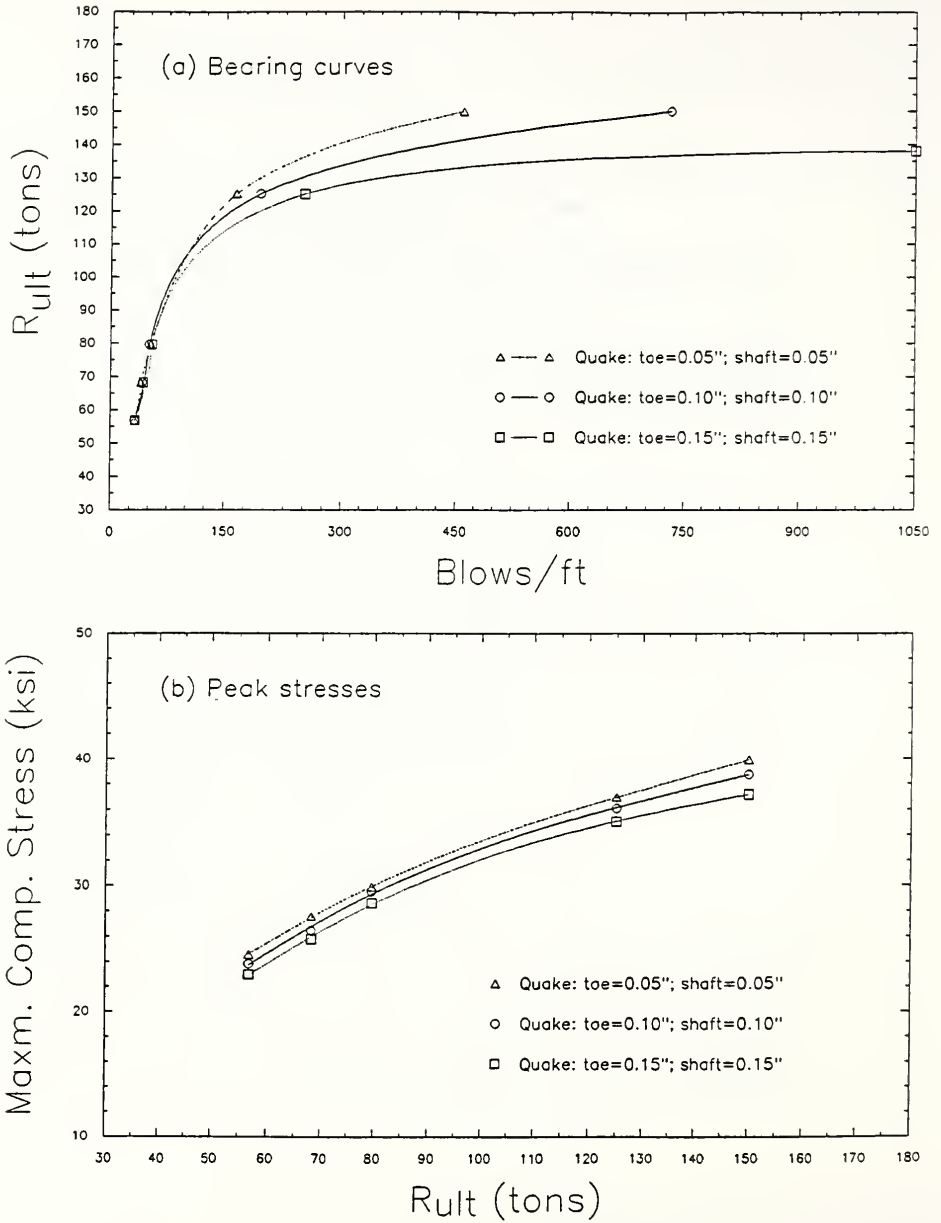


Figure 3.40 Variation in quake (SR14/TB-3)

## Section 3.3.2 - SR14 (TB-3) Case00

R <sub>ult</sub> kips	Bl bpf	Ct	Stroke (ft) down up	MinStr I,J ksi	MaxStr I,J ksi	Enthru ft-kip	Bl Rt bpm
275.0	194.3	6.0	6.2	.00( 1, 0)	36.10( 1,119)	.0	47.8
330.0	731.5	6.5	6.5	.00( 1, 0)	38.74( 1,121)	.0	46.2
385.0	9999.0	6.8	6.7	.00( 1, 0)	39.93( 1,121)	.0	45.3

## Section 3.3.2 - SR14 (TB-3) Case05

R <sub>ult</sub> kips	Bl bpf	Ct	Stroke (ft) down up	MinStr I,J ksi	MaxStr I,J ksi	Enthru ft-kip	Bl Rt bpm
275.0	164.2	6.0	6.2	.00( 1, 0)	36.95( 1,114)	.0	47.7
330.0	458.6	6.6	6.6	.00( 1, 0)	39.90( 1,117)	.0	46.0
385.0	9999.0	6.8	6.8	.00( 1, 0)	41.32( 1,119)	.0	45.1

## Section 3.3.2 - SR14 (TB-3) Case06

R <sub>ult</sub> kips	Bl bpf	Ct	Stroke (ft) down up	MinStr I,J ksi	MaxStr I,J ksi	Enthru ft-kip	Bl Rt bpm
275.0	250.6	6.0	6.1	.00( 1, 0)	35.04( 1,124)	.0	48.0
330.0	2606.6	6.4	6.4	.00( 1, 0)	37.18( 1,124)	.0	46.4
385.0	9999.0	6.7	6.5	.00( 1, 0)	38.27( 1,123)	.0	45.9



## CONCLUSIONS AND RECOMMENDATIONS

### 4.1 Conclusions and Synopsis of Results

Results of the parametric study in Chapter 2 and cases studied in Chapter 3 indicate that the parameter of greatest importance for most projects is the hammer and driving train used in the piling operations. It is necessary to check the adequacy of the strength of a shell to resist stresses caused by the impact of the piling hammer. If bearing graphs are available, as suggested, for a range of parameters for each bent before driving begins, then the appropriate bearing graph can be selected, and an estimate of the likely peak stress obtained, as driving proceeds (as explained in Sections 2.2 and 2.3).

The calculations are not particularly sensitive to the damping constants for the toe and sides of the pile, *i.e.* small changes in these values produce a minor change in the calculated results.

The cases studied in Chapter 3 show that using a heavier hammer such as the Delmag D 22 instead of the more usual D 12 (or the equivalent MKT DE 30) can reduce the blow count by 50%. This does cause an increase in stresses which, although small, must be accounted for. If the available bearing graphs from wave equation analyses indicate that the increase would still keep the driving stresses within safe limits, then the use of a heavier hammer can greatly speed up the driving process. Even if the estimated stresses do approach critical levels, the decrease in cost due to time savings could more than offset the extra cost of using special techniques (such as *insert piles* - explained below) to keep stresses at a safe level.

If at any stage of penetration the stresses are excessive, a heavier hammer may be used, but if greater hammer weights and lesser drops still cause overstressing then using a heavier gage of shell such as 5 gage instead of the usual 7, can result in a decrease in stresses from 10-15%. All other parameters staying the same, this does not make a large difference in the blow count as can be seen in the examples in Chapter 2 and Chapter 3.

Another suggested alternative is the use of an insert pile having a smaller diameter. An insert pile effectively increases the pile c/s area during driving, leading to a reduction in stresses as well as lowering the blow count (similar effect as using a heavier gage of shell). Inserts have the advantage of being reusable and just one or two inserts would be sufficient for an entire site. Once the shell is driven, the insert can be extracted and the concrete poured.

The results also show that the use of jetting (or pre-drilling) to get past material not accounted for in the driving specifications, such as material expected to be lost to scour (or already placed embankment fill), can cause a reduction in the resistance to pile driving of as much as 30% in some cases. To avoid this problem from occurring, the specifications need to be more explicit as explained in Section 1.2 of this report.

The condition of the driving train is another important aspect that needs to be addressed. The efficiency of the hammer is obtained from the manufacturer's rating, but this can decrease as the working parts become worn. The elastic modulus and coefficient of restitution of the packing/cushion may also change from the commencement to the end of driving.

Also, the elastic compression of the ground is usually taken as the elastic modulus under static loading, and this will change as the soil is compacted or is displaced by the pile. Thus further refinements of the calculation procedure need to be made to allow for the changing dynamic characteristics of the hammer-pile-soil system during driving. The wave equation can never give exact values throughout all stages of driving, and its usefulness depends on amassing data on correlations between calculated stress values and observations of driving stress in instrumented piles. This leads to the suggestions in the final section (Section 4.3).

#### 4.2 Suggestions and General Recommendations<sup>15</sup>

Pile foundation design is a trial-and-error procedure whereby pile lengths are selected based on soil properties, determined from exploratory borings and laboratory tests. The pile design is then confirmed, usually on large jobs, using indicator piles, pile test load programs, dynamic monitoring, etc. For routine jobs, the pile design is *most often* confirmed using the production piles themselves.

---

<sup>15</sup> Parts of this section are modified after comments from Short and Williams (1989).



The usual design procedure is to assume that the dynamic resistance of pile to its penetration into the soil is equal to the ultimate static load-bearing capacity, and then to calculate the 'permanent set' in terms of blows per unit penetration distance to develop this resistance, using a hammer of given rated energy. The driving stress is assumed to be the ultimate driving resistance divided by the cross-sectional area of the pile, and this must not exceed the safe working stress on the pile material. The minimum pile tip elevation is usually based on considerations of the depth of scour.

The preceding is not always an appropriate procedure to develop specifications for efficient pile driving, especially thin-shells which are prone to damage due to an excess build-up of stresses which is difficult to anticipate and estimate by the usual design procedures where the 'set' is obtained using dynamic formulae. As a means to overcome these shortcomings, it is suggested that INDOT geotechnical engineers provide detailed analysis of the anticipated driving resistance for various hammer sizes using the wave equation analysis. The results of the analysis can be summarized with a family of curves showing possible upper and lower limit hammer sizes plotted on a capacity *versus* blow count graph as shown in the cases in Chapter 2 and Chapter 3. The information on such plots should be sufficient to allow the selection of a hammer which will be best suited to the conditions at hand. For more extensive control of driving conditions, similar plots can be developed for all other estimated parameters.

In addition to providing more detailed information in the geotechnical investigation report regarding pile hammer size, consideration should be given to specifying construction techniques such as (a) pre-drilling (useful when piles will extend through stratified layers of sands into deeper bearing layers), and pre-jetting (to get past scour depth, or in fine sands where water ponding is not a problem); and (b) specifying minimum efficiency levels and condition of driving train and their monitoring during the driving.

These suggestions could be immediately implemented by the INDOT and would result in savings, both in terms of mitigating damage to shells, and reduction in time spent on driving individual piles.

### 4.3 Suggestions for Future Work

Ultimately, the performance of the pile and driving system cannot be successfully monitored, during driving, without the use of dynamic measurements. Dynamic measurements have proven to be quite successful in determining the wave equation parameters and together with the wave equation analysis, can be used for pile capacity estimation, hammer performance evaluation and checking the pile performance and integrity. The availability of the PDA (pile driving analyzer) makes this fairly straightforward.

Data obtained with a PDA during driving operations should be sent to the person(s) involved with the dynamic analysis in the INDOT design group for comparison with the predictions/ estimations made at the design stage. This would enable adjustment of estimation procedures to allow for better predictions in the future. An earlier report available with INDOT (Darrag, 1987) would be an useful aid to this since one of the stated objectives of that study was:

“To familiarize the IDOH with the state-of-the-art of performing dynamic measurements during pile driving, to briefly illustrate the theoretical background behind their use and to show the potential uses of these measurements.”

At present it may not be feasible for INDOT to monitor all piling projects with a PDA due to the constraints on availability of equipment and technical support, but it must be emphasized that dynamic monitoring must be done as much as possible and the data used as suggested above, since dynamic measurements constitute a very efficient way of monitoring the pile during driving by providing measurements of forces, displacements, velocities, etc., in the pile.

Dynamic measurements can also be used to estimate the pile capacity, the load transfer along the pile shaft, and the load deformation curve that would be obtained from a pile load test. They have also been used to evaluate the efficiency of the driving train under different operating conditions, and finally, the integrity of the pile as well.

In light of the above it is suggested that INDOT acquire the equipment used for dynamic measurements and train the required personnel.

## APPENDICES

## Appendix A: Charts, Plots and Tables used

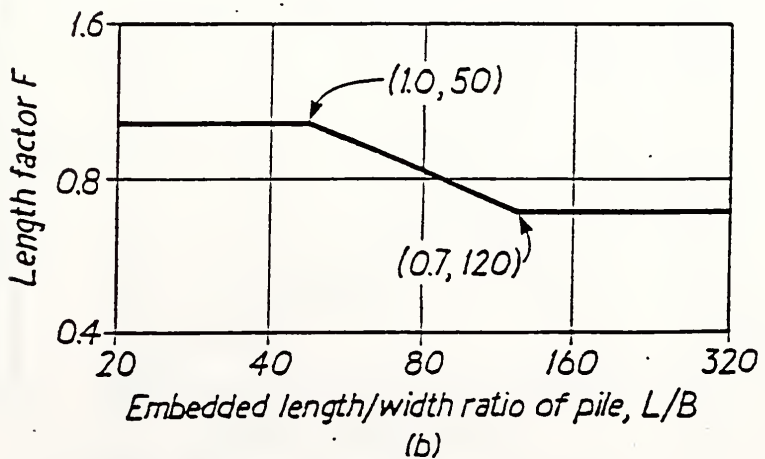
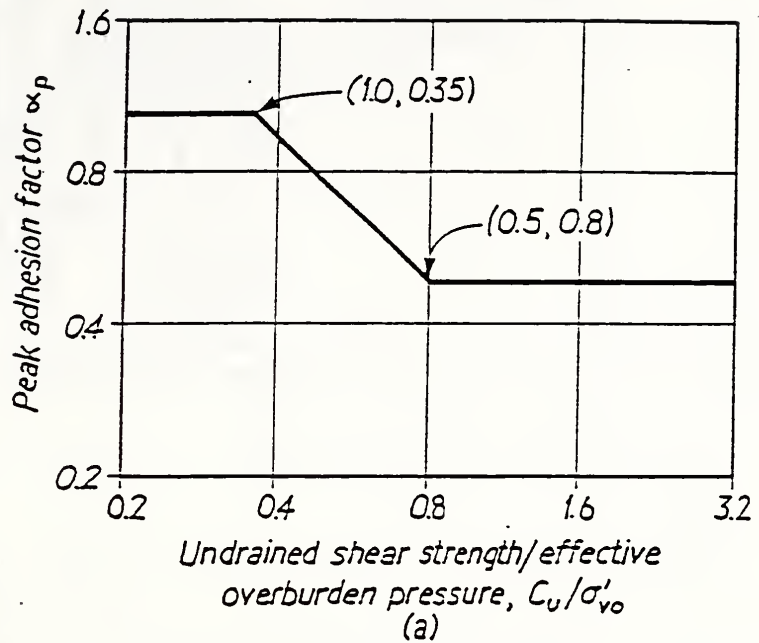
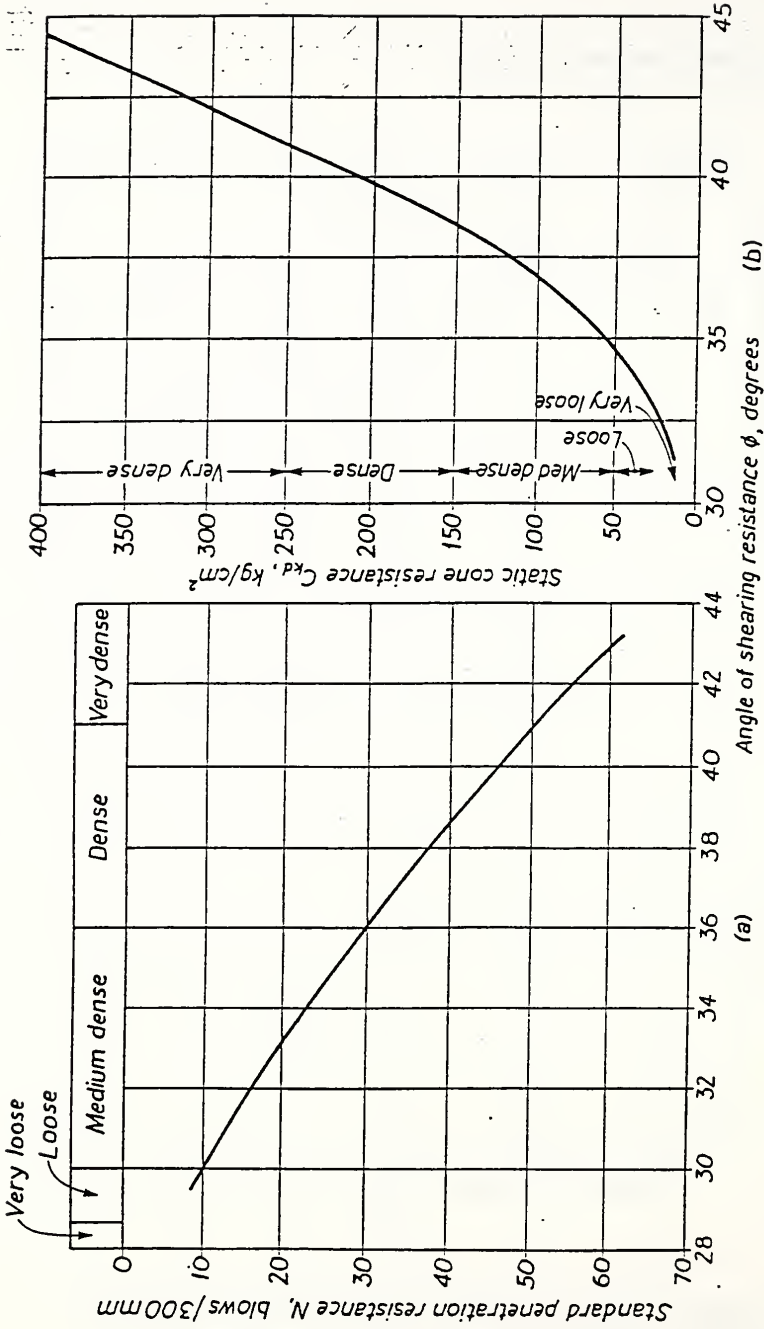
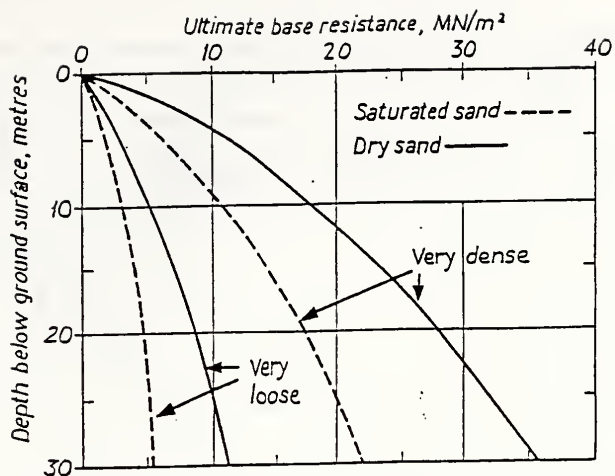


Figure A.1 Adhesion factors for piles driven to deep penetration into clays (after Semple and Rigden, 1984) - (a) Peak adhesion factor vs. shear strength/effective overburden pressure; (b) Length factor

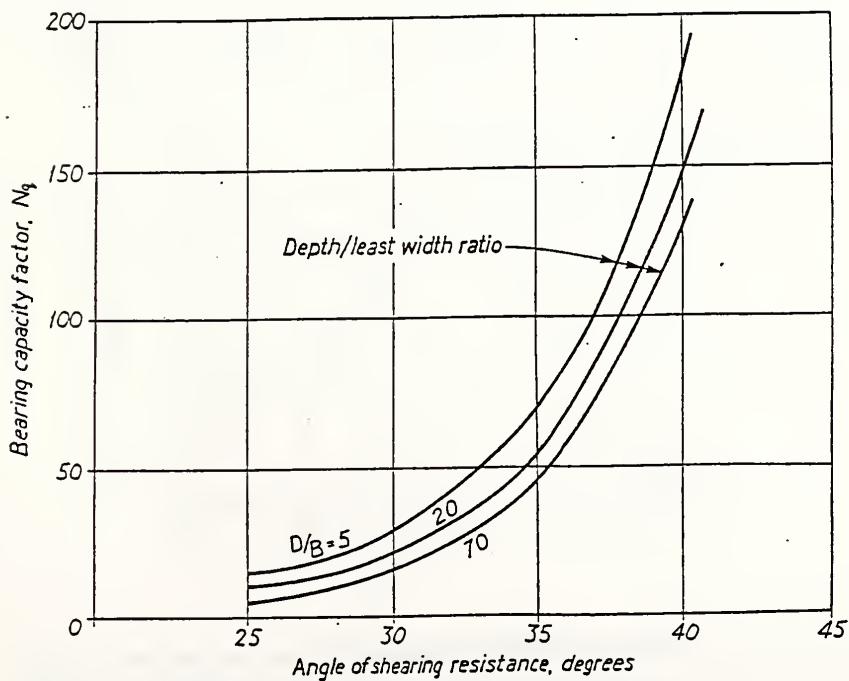


(a) relationship between standard penetration test N-values and angle of shearing resistance (after Peck, Hanson and Thornburn, 1974)  
 (b) relationship between static cone resistance and angle of shearing resistance (after Meyerhof, 1956)

Figure A.2 Determination of angle of shearing resistance of granular soils from in-situ tests



(a) Approximate ultimate base resistance for foundations in sand (after Kulwamy, 1984)



(b) Bearing capacity factors (after Berezantsev, et al., 1961)

Figure A.3

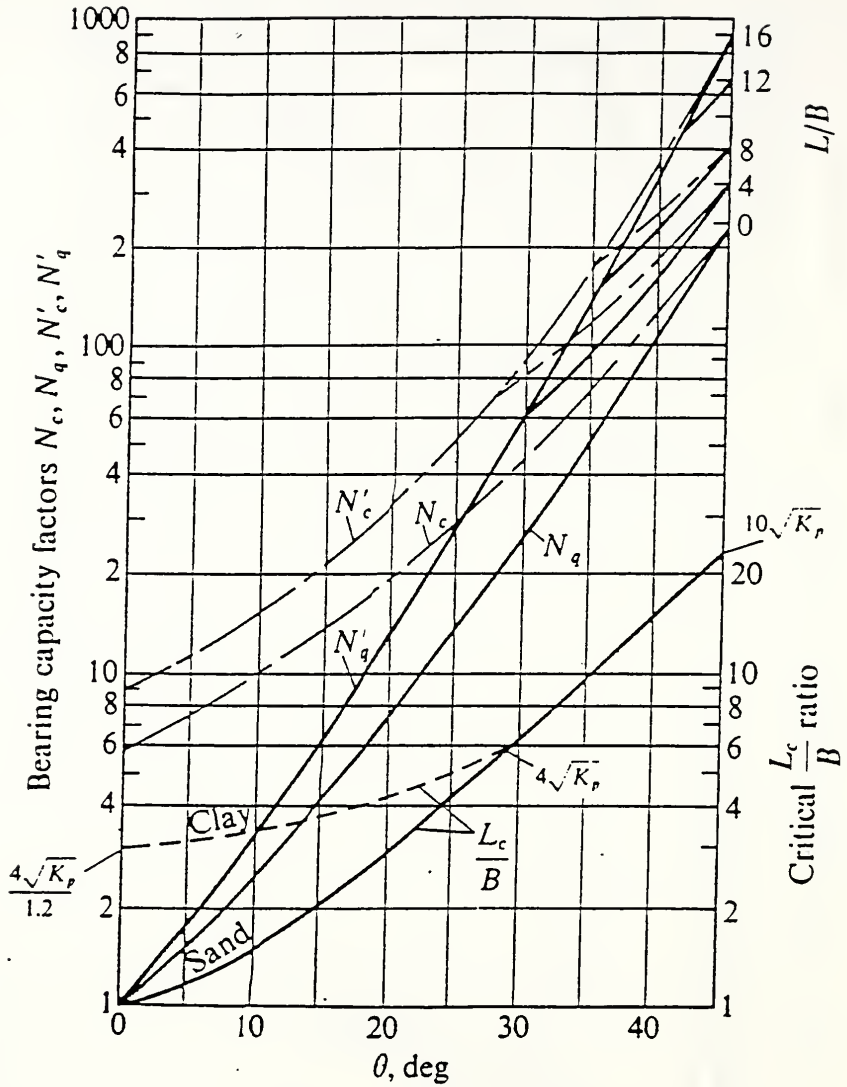


Figure A.4 Bearing-capacity factors for deep foundations  
(after Fig. 16-14 of Bowles, 1982)

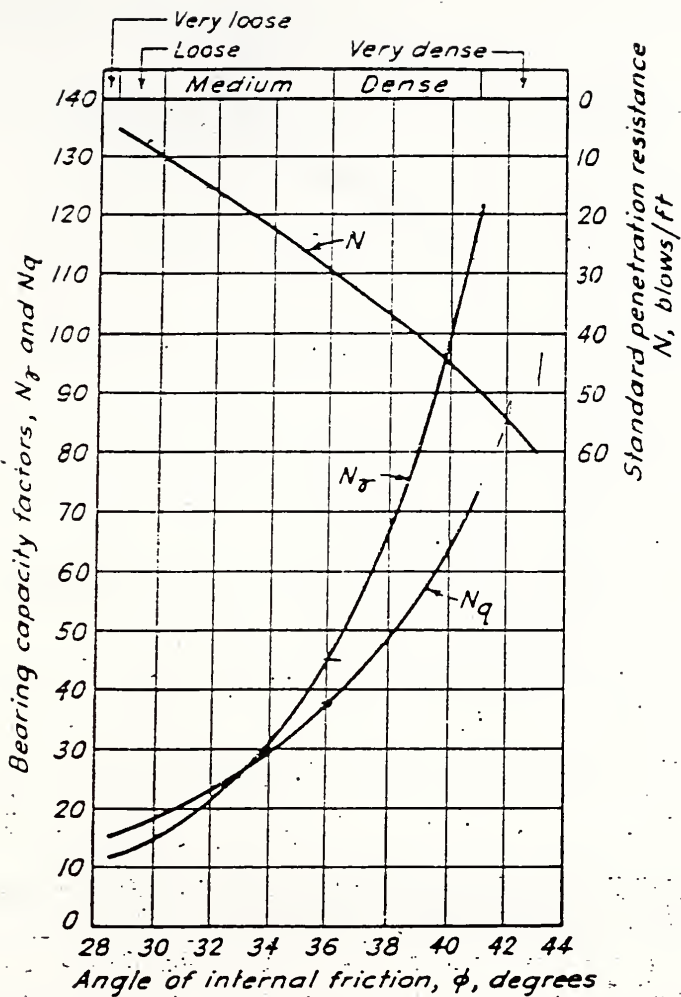


Figure A.5 Curves showing the relationship between bearing-capacity factors and  $\phi$ , as determined by theory, and rough empirical relationship between bearing capacity factors or  $\phi$  and values of standard penetration resistance  $N$  (Fig. 19.5, pp. 310, Peck, Hanson and Thornburn, 1974)



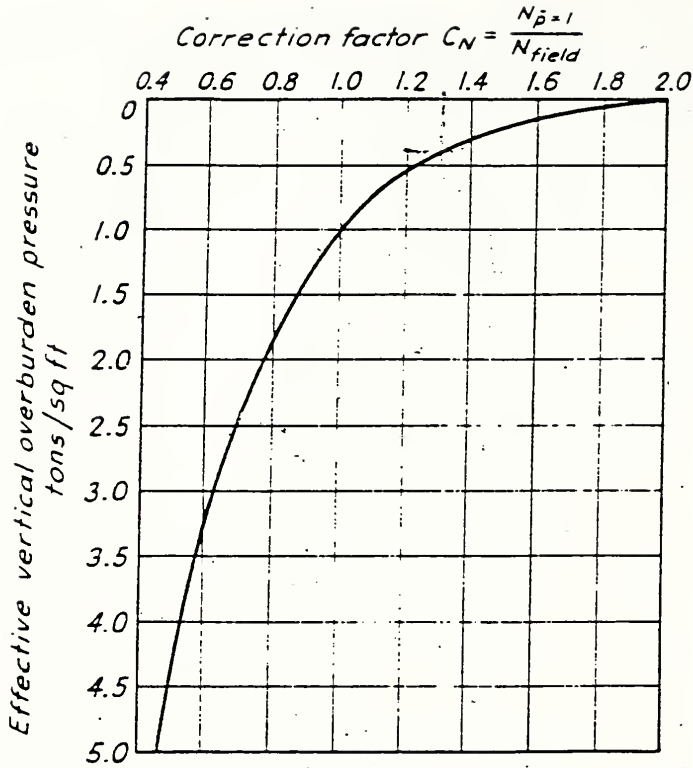


Figure A.6 Chart for correction of  $N$ -values in sand for influence of overburden pressure (reference value of effective overburden pressure is 1 ton/sq. ft.).

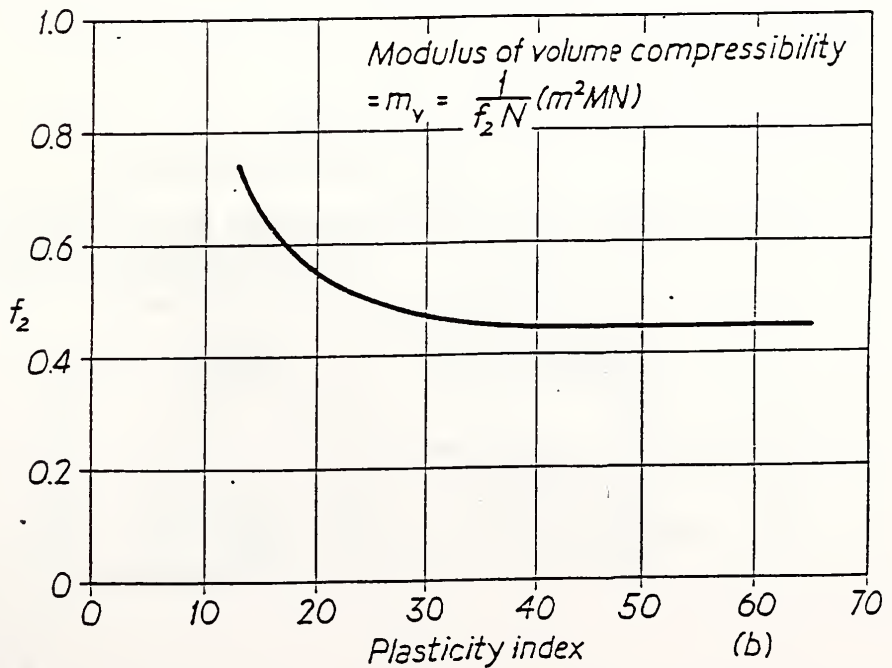
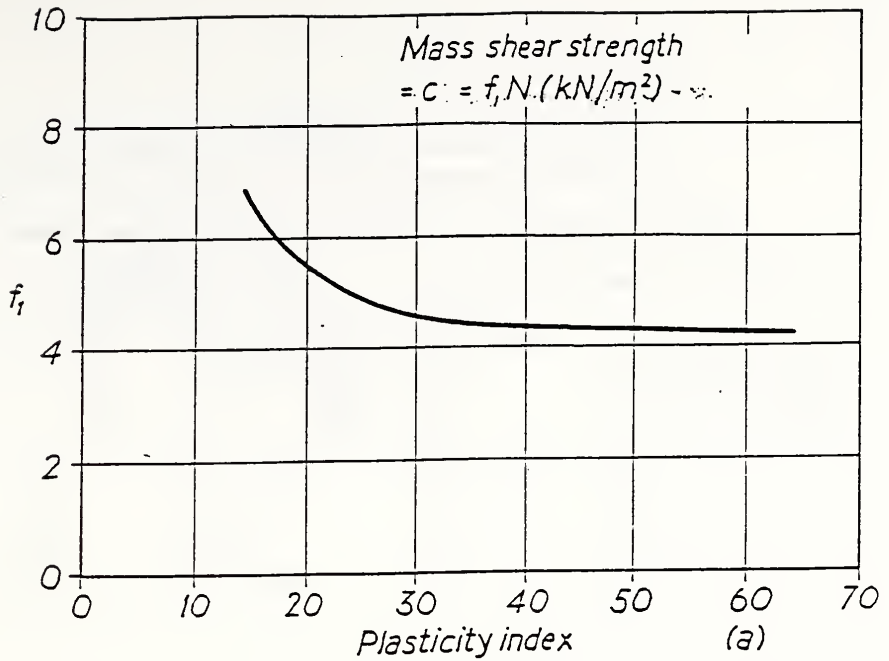


Figure A.7 Relationship between mass shear strength, modulus of volume compressibility, plasticity index and standard penetration test  $N$ -values (after Stroud, 1975).

**Table A.1**  
Values of the angle of pile to soil friction for various interface conditions

Pile/soil interface condition	Angle of pile/soil friction, $\delta$	
	Kulwaly	Broms
Smooth (coated) steel/sand	$0.5\bar{\phi}$ to $0.7\bar{\phi}$	$20^\circ$
Rough (corrugated) steel/sand	$0.7\bar{\phi}$ to $0.9\bar{\phi}$	—
Precast concrete/sand	$0.8\bar{\phi}$ to $1.0\bar{\phi}$	$0.75\bar{\phi}$
Cast-in-place concrete/sand	$1.0\bar{\phi}$	
Timber/sand	$0.8\bar{\phi}$ to $0.9\bar{\phi}$	$0.7\bar{\phi}$

**Table A.2**  
Values of the coefficient of horizontal stress,  $K_h$

Installation method	$K_p/K_u$
Driven piles, large displacement	1 to 2
Driven piles, small displacement	0.75 to 1.25
Bored and cast-in-place piles	0.70 to 1
Jetted piles	0.50 to 0.7

Typical values of  $K_o$  for a normally consolidated sand are:

Relative density	$K_o$
Loose	0.5
Medium-dense	0.45
Dense	0.35

**Table A.3**  
Penetration Resistance and Soil Properties on Basis of the Standard  
Penetration Test (after Table 5.3, p. 114, Peck, Hanson and Thornburn, 1974)

Sands (Fairly Reliable)		Clays (Rather Unreliable)	
Number of Blows per ft, $N$	Relative Density	Number of Blows per ft, $N$	Consistency
0-4	Very loose	Below 2	Very soft
4-10	Loose	2-4	Soft
10-30	Medium	4-8	Medium
30-50	Dense	8-15	Stiff
Over 50	Very dense	15-30	Very stiff
		Over 30	Hard

**Table A.4**  
(after Table 45.2, Terzaghi and Peck, 1967)

*Relation of Consistency of Clay, Number of Blows  $N$  on Sampling Spoon,  
and Unconfined Compressive Strength*

Con- sistency	$q_u$ in tons/ ft <sup>2</sup>					
	Very Soft	Soft	Medium	Stiff	Very Stiff	Hard
$N$	<2	2-4	4-8	8-15	15-30	>30
$q_u$	<0.25	0.25-0.50	0.50-1.00	1.00-2.00	2.00-4.00	>4.00

Table A.5

Empirical values for  $\phi$ ,  $D_r$ , and unit weight of granular soils based on the standard penetration number with corrections for depth and for fine saturated sands. (after Table 3.2, Bowles, 1982)

Description	Very loose	Loose	Medium	Dense	Very dense	
Relative density $D_r$ *	0	0.15	0.35	0.65	0.85	1.00
Standard penetration no. $N$		5-10	8-15	10-40	20-70	> 35
Approx. angle of internal friction $\phi$ †	25-30°	27-32°	30-35°	35-40°	38-43°	
Approx. range of moist unit weight $\gamma$ , pcf (kN/m <sup>3</sup> )	70-100‡ (11-16)	90-115 (14-18)	110-130 (17-20)	110-140 (17-22)	130-150 (20-23)	

\* Depends on  $p_o$  ranging from 70 to 500 kPa. Low value of  $N$  corresponds to lesser  $p_o$ .

† After Meyerhof (1956).  $\phi = 25 + 25D_r$  with more than 5 percent fines and  $\phi = 30 + 25D_r$  with less than 5 percent fines. Use larger values for granular material with 5 percent or less fine sand and silt. See also Eq. (4-10) for estimate of  $\phi$ .

‡ It should be noted that excavated material or material dumped from a truck will weigh 70 to 90 pcf. Material must be quite dense and hard to weigh much over 130 pcf. Values of 105 to 115 pcf for nonsaturated soils are common.

Table A.6

Empirical values for  $q_u$  and consistency of cohesive soils based on the standard penetration number (after Table 3-3, Bowles, 1982).

Consistency	Very soft	Soft	Medium	Stiff	Very stiff	Hard
$q_u$ , ksf (kPa)	0	0.5 (25)	1.0 (50)	2.0 (100)	4.0 (200)	8.0 (400)
$N$ , standard penetration resistance	0	2	4	8	16	32
$\gamma_{sat}$ , pcf (kN/m <sup>3</sup> )		100-120 (16-19)	110-130 (17-20)		120-140 (19-22)	

\* These values should be used as a guide only. Local cohesive samples should be tested, and the relationship between  $N$  and the unconfined compressive strength  $q_u$  established as  $q_u = KN$ .

**Table A.7**  
Influence of various parameters on ultimate driving resistance from wave equation analysis.

<i>Parameter</i>	<i>Effect on <math>R_u</math> for given set as parameter increases</i>
(1) <i>Pile characteristics</i>	
Free-standing length	Very slight increase
Embedded length	Slight increase
Wall thickness (tube pile) or cross-sectional area	Significant increase
Stiffness of pile material	Significant increase
(2) <i>Soil characteristics</i>	
Quake $Q$	Moderate decrease
Damping $J$	Significant decrease
Proportion of tip load	Slight decrease
(3) <i>Hammer and cushion characteristics</i>	
Hammer energy	Significant increase
Hammer efficiency	Significant increase
Cushion stiffness	Significant increase (for higher values of $R_u$ )
Coefficient of restitution of cushion	Moderate increase

**Table A.8**  
Case damping factor  $J_c$  for different soils at the pile toe

Soil	$J_c$
clay	0.60 - 1.10
silty clay or clayey silt	0.40 - 0.70
silt	0.20 - 0.45
silty sand or sandy silt	0.15 - 0.30
sand	0.05 - 0.20



## Appendix B: List of References

- Berezantsev, V.G et al. (1961). Load bearing capacity and deformation of piled foundations. *Proceedings of the 5th International Conference, ISSMFE*, Paris. Volume 2, 11-12.
- Bowles, J.E. (1982). *Foundation analysis and design*, 3rd edition. McGraw-Hill Book Co., N.Y. International Student Edition (1986), McGraw-Hill, Singapore, 816 p.
- Broms, B. (1966). Methods of calculating the ultimate bearing capacity of piles, a summary. *Sols-Soils*. 5(18-19) 21-31.
- Burland, J.B. (1973). Shaft friction of piles in clay. *Ground Engineering*. 6(3) 30-42.
- Dangla, P. and Corté, J -F. (1988). Impedances for pile toe reaction during driving. *Proc. 3rd Intl. Conf. Application of Stress-Wave Theory to Piles*. Edited by B.H. Fellenius. May 25-27, ISSMFE and Canadian Geotech. Soc., May 25-27, Ottawa, Canada, 186-196.
- Darrag, A.A. (1987). Pile capacity prediction using static and dynamic load testing. *FHWA/IN/JHRP-87/1*. Joint Highway Research Project. Purdue Univ., West Lafayette, Ind., 365 p.
- Fleming, W.G.K. and Thorburn, S. (1983). Recent piling advances. In *Piling and Ground Treatment*. Proc. Intl. Conf. advances in piling and ground treatment for foundations. ICE, March 2-2, London, U.K.
- Gendron, G.J. (1970). Pile driving: Hammers and driving methods. *Highway Res. Rec.*, Highway research board. No. 333, 16-22.
- Goble, G.G. and Hauge, K. (1978). Comparative capacity performance of pipe and monotube piles as determined by wave equation analysis. *Piling Research Laboratory, Department of Civil, Env. and Arch. Engrg., Univ. of Colorado*.
- Hery, P. (1983). Residual stress analysis in WEAP. *M. Sc. Thesis*, Department of Civil, Env. and Arch. Engrg., Univ. of Colorado.
- Kulwahy, F.H. (1984). Limiting tip and side resistance, fact or fallacy. *Symposium on analysis and design of pile foundations*, ASCE, San Francisco, *Proceedings*, 80-98.
- Li, J.C., Yao, H -L and Ong, B. (1988). Hammer selection and stress-wave behavior of piles. *Proc. 3rd Intl. Conf. Application of Stress-Wave Theory to Piles*. Edited by B.H. Fellenius. May 25-27, ISSMFE and Canadian Geotech. Soc., May 25-27, Ottawa, Canada, 601-612.



- Meyerhof, G.G. (1951). The ultimate bearing capacity of foundations. *Geotechnique*. 2(4) 301-332.
- Meyerhof, G.G. (1956). Penetration tests and bearing capacity of cohesionless soils. *ASCE, JSMFD*. 82(SM1) 866/1-866/19.
- Meyerhof, G.G. (1976). Bearing capacity and settlement of pile foundations. *Proc. ASCE*. (GT3) 197-228.
- New concept in cushions speeds pile driving project (Anon., 1983). *Better Roads*. 53(11) 30.
- Nordlund, R.L. (1965). Bearing capacity of piles in cohesionless soils. *ASCE, JSMFD*. 91(SM3) 1-35.
- Peck, R.B., Hanson, W.E. and Thornburn, T.H. (1974). *Foundation engineering*, 2nd edition. John Wiley & Sons, Inc., New York. Second Wiley Eastern reprint (1984), Wiley Eastern Limited, New Delhi, India, 514 p.
- Pile hammer selection a function of soil type (Anon., 1974). *Construction methods and equipment*. 56(2) 97-99.
- Poulos, H.G. (1987). Piles and Piling. In *Ground engineer's reference book*, F.G. Bell, ed. Butterworth and Co. Ltd, London, U.K.
- Rausche, F. and Goble, G.G. (1972). Performance of pile driving hammers. *ASCE Jnl. Constr. Div.* 98(2) 201-218.
- Rausche, F., Goble, G.G. and Likins Jr, G.E. (1985). Dynamic determination of pile capacity. *Jnl. Geotech. Engrg.*, ASCE, 111(3) 367-383.
- Rudolph, M.F. and Wroth, C.P. (1982). Recent developments in understanding the axial capacity of piles in clay. *Ground engineering*. 15(7) 17-25.
- Sandhu, B.S. (1982). Predicting driving stresses in piles. *ASCE Jnl. Constr. Div.* 108(4) 485-503.
- Semple, R.M. and Rigden, W.J. (1984). Shaft capacity of driven pipe piles in clay. *Symposium on analysis and design of pile foundations*, ASCE, San Francisco, *Proceedings*, 59-79.
- Short, R.D. and Williams, M.B. (1989). Impact of environmental regulations on pile foundation design and construction using diesel hammers. In *Piling and Deep Foundations*. Proc. Intl. Conf. Piling and Deep Foundations, Vol. I. Edited by J.B.

- Burland and J.M. Mitchell. May 15-18, London, U.K., pp. 293-296. Published by A.A. Balkema, Rotterdam, Netherlands.
- Smith, E.A.L. (1960). Pile driving analysis by the wave equation. *ASCE, JSFMD*. 86(SM4) 35-61.
- Stroud, M.A. (1975). The standard penetration test in insensitive clays. Proceedings of the European Symposium on penetration testing, Stockholm, 1975, Vol. 2, pp. 367-375.
- Terzaghi, K. and Peck, R.B. (1967). *Soil mechanics in engineering practice*, 2nd edition. A Wiley International Edition, John Wiley & Sons, Inc., New York, 729 p.
- Thorburn, S. and MacVicar, R.S.L. (1971) Pile load tests to failure in the Clyde alluvium. *Behaviour of piles, Conf. Proc.*, Sept., ICE, London, U.K., 1-8.
- Tomlinson, M.J. (1957). The adhesion of piles driven in clay soils. *Proceedings, 5th Intl. conf., ISSMFE*, London, Vol. 2, 66-71.
- Tomlinson, M.J. (1971). Some effects of pile driving on skin friction. *Proc. Conference on the Behaviour of Piles*. Institution of Civil Engineers, London, 1971, 107-114.
- Tomlinson, M.J. (1987). *Pile design and construction practice, 3rd edition*. A Viewpoint Publication, Palladian publications ltd., London, England, 378 p.
- Vesic, A.S. (1970). Tests on instrumented piles, Ogeechee River site. *ASCE, JSMFD*. 96(SM2).
- Vesic, A.S. (1977). Design of pile foundations, NCHRP Synthesis 42, *TRB*, Washington, D.C.



### Appendix C: Explanation of the WEAP87 input variable, IPERCS

(i) *IPERCS = negative of estimated  $Q_{sd}$  (as a percent of the first specified  $R_{ult}$  value).* For each subsequent  $R_{ult}$  the amount of load carried in skin friction stays the same and the toe capacity varies with varying  $R_{ult}$ . This option is used when the estimated shaft load carrying capacity is considered to be more accurate.

(ii) *IPERCS = 100 + positive of estimated  $Q_{sd}$  (as a percent of the first specified  $R_{ult}$  value).* For each subsequent  $R_{ult}$  the amount of load carried in end bearing (toe capacity) stays the same and the shaft capacity varies with varying  $R_{ult}$ . This option is used when the estimated toe bearing capacity is considered to be more accurate.

(iii) *IPERCS = Shaft capacity as a percent of  $R_{ult}$ .* The percentage stays the same for all cases. Both shaft capacity and toe capacity are varied. This option is used most often.

In all three of these cases the shape of the shaft friction distribution does not vary with differing values of  $R_{ult}$ , since WEAP87 is not very sensitive to the actual shape of the distribution as well as the fact that relative magnitudes are more easily determinable, when looking at layered soils, than the actual magnitude.

In the present example the second option is never used since the bulk of the load capacity comes from the friction resistance at the shaft-soil interface. The third option is used most often for (a) the standard case and most of the variations thereof, with IPERCS set to 80% ( $55/70 \approx 0.8$ ) for input to WEAP87; and (b) the bulk of the cases in Chapter 3.





COVER DESIGN BY ALDO GIORGINI